Analysis of receptor-receptor interactions and their implications on the formation of signaling competent TRAIL receptor clusters

Vorgelegt von

Simon Paul Neumann

aus Stuttgart

Hiermit erkläre ich, dass die vorliegende Arbeit von mir selbständig und nur unter Verwendung der darin angegebenen Hilfsmittel angefertigt wurde.

I hereby assure that I performed the presented work independently and without further help or any other materials than stated.

Stuttgart, 25. März 2013

Simon Neumann

Table of contents

Abbreviations

2-ME	β-mercaptoethanol
°C	degree Celsius
aa	amino acid
AIF	apoptosis-inducing factor
ALPS	autoimmune lymphoproliferative syndrome
Amp	ampicillin
Apaf-1	apoptotic protease activating factor 1
APS	ammonium persulfate
ATP	adenosine triphosphate
Bad	Bcl-2-associated death promoter
Bcl-2	B-cell lymphoma 2
BH3	Bcl-2 homology domain 3
Bid	BH3 interacting domain death agonist
BIR	baculoviral IAP repeat
bp	base pairs
BSA	bovine serum albumin
BS^3	bis(sulfosuccinimidyl)suberate
CAD	caspase-activate DNAse
CARD	caspase activation recruitment domain
CD	cluster of differentiation
cDNA	complementary DNA
cFLIP	cellular FLICE-like inhibitory protein
CHX	cycloheximide
cIAP	cellular inhibitor of apoptosis
CIP	calf intestinal phosphatase
CRD	cysteine-rich domain
dATP	deoxyadenosine triphosphate
DC	dendritic cell
DcR2	decoy receptor 2
DD	death domain

DED	death effector domain
ddH$_2$O	bidistilled water
DIABLO	direct IAP-binding protein with low isoelectric point
DISC	death-inducing signaling complex
DMSO	dimethyl sulfoxide
DNA	deoxyribonucleic acid
DNAse	deoxyribonuclease
dNTP	deoxyribonucleotide triphosphate
DR	death receptor
DTT	dithiothreitol
ECD	extracellular domain
ECL	enhanced chemiluminescence
EDTA	ethylene di-amine tetra acetic acid
e.g.	*exempli gratia* (for example)
eGFP	enhanced green fluorescent protein
EGTA	ethylene glycol tetraacetic acid
ERK	Extracellular signal-regulated kinase
et al.	*et alii* (and others)
FACS	fluorescence activated cell sorting
FADD	Fas-associated protein with death domain
Fas	FS-7 cell-associated surface antigen
FasL	FS-7 cell-associated surface antigen ligand
FCS	fetal calf serum
FITC	fluorescein isothiocyanate
FP	fluorescent protein
g	gram
g	gravitational acceleration
GPI	glycosylphosphatidylinositol
h	hour
HEK	human embryonic kidney
HRP	horse radish peroxidase

HVEM	herpes virus entry mediator
IAP	inhibitor of apoptosis protein
ICAD	inhibitor of caspase-activated DNAse
i.e.	*id est* (that is)
IFN	interferon
Ig	immunoglobulin
IgG	immunoglobulin G
IgM	immunoglobulin M
IκBα	nuclear factor kappa-light-chain-enhancer of activated B cells inhibitor α
IKK	IκB kinase
IMAC	Immobilized metal affinity chromatography
JNK	c-Jun N-terminal kinase
K	Kelvin
kDa	kilo Dalton
K_d	dissociation constant
KOD	*Thermococcus kodakaraensis*
k_{off}	dissociation rate
k_{on}	association rate
l	liter
LB	Lysogeny broth
LPS	lipopolysaccharide
LTα	lymphotoxin α
M	molar
mA	milliampere
MAPK	mitogen-activated protein kinase
mTRAIL	membrane-bound TRAIL
MF	murine embryonic fibroblast
MFI	mean fluorescence intensity
mg	milligram (10^{-3} g)
min	minute
ml	milliliter (10^{-3} l)
mM	millimolar (10^{-3} M)

MW	molecular weight
NEMO	NFκB essential modulator
NFκB	nuclear factor 'kappa-light-chain-enhancer' of activated B cells
ng	nanogram (10^{-9} g)
NIK	NFκB-inducing kinase
Ni-NTA	nickel nitrilotriacetic acid
NK	natural killer
nm	nanometer (10^{-9} m)
nM	nanomolar (10^{-9} M)
OD	optical density
Opti-MEM	Opti-MEM I Reduced Serum Medium
OPG	osteoprotegerin (TNFRSF11B)
ORF	open reading frame
PAA	polyacrylamide
PAGE	polyacrylamide gel electrophoresis
PARP	poly (ADP-ribose) polymerase
PBA	PBS containing BSA and sodium azide
PBS	phosphate-buffered saline
PBS-T	PBS containing Tween-20
PCD	programmed cell death
PCR	polymerase chain reaction
PFA	paraformaldehyde
PI3K	phosphatidylinositol 3-kinase
PIDD	p53-induced protein with a death domain
PIP	Phosphatidylinositol phosphate
PKB/Akt	protein kinase B
PLAD	pre-ligand binding assembly domain
PRAS40	proline-rich Akt substrate of 40 kDa
QCM	quartz crystal microbalance
RAIDD	RIP-associated protein with a death domain
RANK	receptor activator of nuclear factor κ B

RANKL	receptor activator of nuclear factor κ B ligand
Rel	reticuloendotheliosis oncogene
RFU	Relative fluorescence units
RING	Really Interesting New Gene
RIP1	receptor interacting protein 1
rpm	revolutions per minute
RPMI1640	Roswell Park Memorial Institute medium 1640
RSK	ribosomal S6 kinase
RT	room temperature
s	second
scTRAIL	single-chain TRAIL
SD	standard deviation
SDS	sodium dodecyl sulfate
SDS-Page	SDS-polyacrylamide gel electrophoresis
SEM	standard error of the mean
Smac	second mitochondria-derived activator of caspases
SOC^{++}	Super Optimal broth with Catabolite repression
SPR	surface plasmon resonance
sTNF	soluble human recombinant TNF
sTRAIL	Soluble human recombinant TRAIL, FLAG-tagged
sTRAILR1	soluble TRAIL receptor 1
sTRAILR4	soluble TRAIL receptor 4
TACE	TNF-α converting enzyme
TAE	Tris-acetate borate
TBS	Tris-buffered saline
TEMED	N,N,N′,N′-tetramethylethyl-diamine
TM	transmembrane
TNF	tumor necrosis factor

TNFR1	tumor necrosis factor receptor 1 (TNFRSF1A)
TNFR2	tumor necrosis factor receptor 2 (TNFRSF1B)
TRADD	TNF receptor type-1 associated death domain protein
TRAF	TNF receptor-associated factor
TRAIL	TNF-related apoptosis-inducing ligand (TNFSF10, APO2L)
TRAILR	TRAIL receptor
TRAILR1	TRAIL receptor 1 (DR4, TNFRSF10A)
TRAILR2	TRAIL receptor 2 (DR5, TNFRSF10B)
TRAILR3	TRAIL receptor 3 (DcR1, TNFRSF10C)
TRAILR4	TRAIL receptor 4 (DcR2, TNFRSF10D)
Tris	Tris-(hydroxymethyl)-aminomethane
TWEAK	TNF-like weak inducer of apoptosis
U	units
UV	ultraviolet
V	volt
v/v	volume/volume
w/v	weight/volume
wt	wild type
XIAP	X-linked inhibitor of apoptosis protein
zVAD-fmk	N-Benzyloxycarbonyl-valyl-alanyl-aspartyl-[O-methyl]-fluoromethylketone
µg	microgram (10^{-6} g)
µl	microliter (10^{-6} l)
µM	micromolar (10^{-6} M)

Summary

The cytokine tumor necrosis factor-related apoptosis-inducing ligand (TRAIL) and its associated receptors constitute an elaborate signaling system fulfilling important functions in regulation of the immune system and in tumor surveillance. Two TRAIL membrane receptors, receptor 1 (TRAILR1) and receptor 2 (TRAILR2), possess an intracellular death domain. Activation of these receptors can lead to apoptosis in TRAIL susceptible cells, but also non-apoptotic signals can be induced. Two additional TRAIL receptors, TRAILR3 and TRAILR4, are generally referred to as decoy receptors. TRAILR3 is linked to the plasma membrane via a glycosylphosphatidylinositol anchor, hence it is devoid of intracellular and transmembrane domains and thus most likely incapable of signal transduction. The intracellular domain of TRAILR4 contains merely a partial death domain consensus motif, therefore it is often referred to as a truncated death domain. Signaling capabilities of TRAILR4 are likely contextual and cell type-dependent, furthermore TRAILR4 can exclusively transduce non-apoptotic signals. Expression of either of the decoy receptors has been shown to reduce sensitivity to TRAIL-induced apoptosis. However, the underlying molecular mechanisms, in particular concerning TRAILR4, remain vaguely defined. Alike other members of the tumor necrosis factor receptor superfamily, TRAIL receptors contain a pre-ligand binding assembly domain (PLAD) in their extracellular domain which mediates receptor-receptor interactions. However, the outcome of TRAIL receptor oligomerization, that is the stoichiometry of the formed complexes as well as the issue whether the PLAD mediates only homotypic or also heterotypic interactions, remained inconclusive until now.

Accordingly, different techniques for the investigation of protein-protein interactions were applied in order to study ligand-independent oligomerization of TRAIL receptors 1, 2 and 4. Interactions of these TRAIL receptors in all six possible combinations were demonstrated through fluorescence resonance energy transfer. The stoichiometry of the resulting TRAIL receptor complexes was clarified through chemical crosslinking experiments. Homophilic interaction of the death receptor TRAILR2, as well as heterophilic interactions between the two death receptors or between either of the death receptors and the decoy receptor TRAILR4 resulted in the formation of dimeric complexes. Subsequent biochemical assays and biosensor measurements performed with the soluble extracellular domains of TRAILR1 and

TRAILR4 confirmed that ligand-independent dimerization is an intrinsic capability of the extracellular domains of TRAIL receptors.

The implications of the demonstrated receptor-receptor interactions on TRAIL-induced signal transduction were investigated in cellular models expressing TRAILR1 and either wild type or a truncated, non-signaling variant of TRAILR4. The apoptotic effects of TRAIL were significantly reduced in presence of TRAILR4 and this reduction was directly correlated to the expression level of receptor 4. Not only inhibition of proapoptotic signaling could be demonstrated, but also reduced activation of the transcription factor NFκB, assessed by analyzing the phosphorylation of its inhibitor IκBα. Accordingly, TRAILR4 exerted a general inhibitory function on signaling by TRAILR1 in the studied cellular model. The inhibitory capacity of TRAILR4 could be clearly attributed to signaling-independent mechanisms. This could be demonstrated through the capacity of the truncated non-signaling receptor variant to interfere with TRAIL-mediated signaling to a comparable extent as the wild type receptor. The reduced cellular sensitivity to the apoptotic effects of TRAIL manifested itself already at the level of procaspase-8 processing, indicating that TRAILR4 impedes proapoptotic signaling early in the extrinsic apoptosis pathway. As a molecular mechanism underlying this, I propose the reduction of signaling competent death receptor dimers through PLAD-mediated formation of mixed receptor complexes. Furthermore, no intracellular signaling pathways emanating from TRAILR4, neither constitutive nor ligand-induced, could be identified in the studied cellular system.

The reported experimental findings were integrated into a model explaining the capability of TRAILR4 to interfere with apoptosis induction by TRAIL death receptors through ligand-independent receptor pre-assembly. Moreover, the proposed model affirms the necessity to take account of TRAILR4 expression in matters of TRAIL-based tumor therapy.

Zusammenfassung

Das Zytokin Tumornekrosefaktor-verwandter Apoptose-induzierender Ligand (*tumor necrosis factor-related apoptosis-inducing ligand*, TRAIL) und die zugehörigen Rezeptoren bilden ein kompliziertes Signalisierungssystem, dem wichtige Funktionen in der Regulation des Immunsystems und im Schutz vor Tumoren zukommen. Zwei TRAIL Membranrezeptoren, Rezeptor 1 (TRAILR1) und Rezeptor 2 (TRAILR2), besitzen eine intrazelluläre Todesdomäne. Aktivierung dieser Rezeptoren kann in TRAIL sensitiven Zellen zu Apoptose führen, jedoch können auch nicht-apoptotische Signale ausgelöst werden. Zwei weitere TRAIL Rezeptoren, TRAILR3 und TRAILR4, werden generell als Köderrezeptoren (*decoy receptors*) bezeichnet. TRAILR3 ist über einen Glykosylphosphatidylinositol-Anker mit der Plasmamembran verbunden, folglich besitzt er weder eine intrazelluläre, noch eine transmembranäre Domäne und kann daher wahrscheinlich keine intrazellulären Signale auslösen. Die intrazelluläre Domäne von TRAILR4 enthält lediglich ein partielles Todesdomänen Konsensusmotives, daher wird sie oft als verkürzte Todesdomäne bezeichnet. Die Fähigkeit von TRAILR4 intrazelluläre Signale auszulösen ist vermutlich vom Zelltyp und dem zellulären Kontext abhängig, des Weiteren ist die Signaltransduktion via TRAILR4 auf nicht-apoptotische Signale beschränkt. Es konnte gezeigt werden, dass beide Köderrezeptoren die Sensitivität von Zellen gegenüber TRAIL vermittelter Apoptose verringern können, allerdings sind die zugrundeliegenden molekularen Mechanismen, insbesondere im Fall von TRAILR4, unklar. Wie auch andere Mitglieder der Superfamilie der Tumornekrosefaktor Rezeptoren besitzen TRAIL Rezeptoren eine Assemblierungsdomäne (*pre-ligand binding assembly domain*, PLAD) in ihrer extrazellulären Domäne, die Rezeptor-Rezeptor Interaktionen vermittelt. Allerdings ist das Resultat der TRAIL Rezeptor Oligomerisierung, also die Stöchiometrie der gebildeten Komplexe sowie die Frage ob die PLAD nur homotypische oder auch heterotypische Interaktionen vermittelt, bis heute nur unvollständig geklärt.

Daher wurden verschiedene Techniken zur Untersuchung von Protein-Protein Interaktionen angewendet, um die Ligand-unabhängige Oligomerisierung der TRAIL Rezeptoren 1, 2 und 4 zu analysieren. Interaktionen dieser drei Rezeptoren in allen sechs möglichen Kombinationen konnten durch Fluoreszenz-Resonanzenergietransfer nachgewiesen werden. Die Stöchiometrie der

resultierenden Komplexe wurde durch Verwendung eines chemisch quervernetzenden Agens aufgeklärt. Homophile Interaktion von Molekülen des Todesrezeptors TRAILR2, heterophile Interaktionen zwischen beiden Todesrezeptoren sowie zwischen einem der Todesrezeptoren und dem Köderrezeptor TRAILR4 resultierten in der Bildung von dimeren Rezeptor Komplexen. Nachfolgende biochemische Untersuchungen und Biosensor Messungen unter Verwendung der löslichen extrazellulären Domänen von TRAILR1 und TRAILR4 bestätigten, dass die Ligand-unabhängige Dimerisierung eine intrinsische Fähigkeit der extrazellulären Domänen von TRAIL Rezeptoren ist.

Die Auswirkungen der nachgewiesenen Rezeptor-Rezeptor Interaktionen auf die TRAIL vermittelte Signaltransduktion wurden anschließend in zellulären Modellen untersucht, die TRAILR1 und entweder Wildtyp oder eine verkürzte nicht-signalisierende Variante von TRAILR4 exprimierten. In Gegenwart von TRAILR4 waren die apoptotischen Effekte von TRAIL signifikant reduziert und es konnte gezeigt werden, dass das Ausmaß dieser Reduktion direkt mit dem Expressionsniveau von TRAILR4 korrelierte. Nicht nur proapoptotische Signale wurden gehemmt, auch die Aktivierung des Transkriptionsfaktors NFκB (nachgewiesen durch Analyse der Phosphorylierung des Inhibitors IκBα) war in Gegenwart von TRAILR4 vermindert. Folglich übt TRAILR4 eine allgemeine hemmende Wirkung auf die Signalisierung durch TRAILR1 aus. Die verkürzte, nicht-signalisierende Rezeptorvariante interferierte in vergleichbarem Ausmaß wie der Wildtyp Rezeptor mit der TRAIL-vermittelten Signaltransduktion. Daher konnte die inhibitorische Eigenschaft von TRAILR4 eindeutig signalisierungs-unabhängigen Mechanismen zugeschrieben werden. Die verminderte zelluläre Sensitivität gegenüber den apoptotischen Effekten von TRAIL manifestierte sich bereits auf der Ebene der Procaspase-8 Spaltung, was daraufhin deutet, dass TRAILR4 an einem frühen Punkt im extrinsischen apoptotischen Signalweg die proapoptotische Signalisierung hemmt. Als zugrundeliegenden molekularen Mechanismus schlage ich eine Reduzierung der signalisierungsfähigen dimeren Todesrezeptorkomplexe durch PLAD-vermittelte Ausbildung von gemischten Rezeptorkomplexen vor. Des Weiteren konnten in dem untersuchten zellulären System keine von TRAILR4 (weder konstitutiv noch Ligand-abhängig) ausgehenden Signalwege identifiziert werden.

Die gezeigten experimentellen Ergebnisse können in einem Modell zusammengefasst werden, dass aufzeigt wie TRAILR4 durch Ligand-unabhängige

Oligomerisierung die apoptotische und nicht-apoptotische Signaltransduktion durch Todesrezeptoren hemmt. Darüber hinaus zeigt das vorgeschlagene Modell auf, weshalb die Expression von TRAILR4 in Zusammenhang mit TRAIL-basierten Ansätzen zur Tumor-Therapie berücksichtigt werden sollte.

1. Introduction

1.1. Programmed cell death

Programmed cell death (PCD) is an elementary process in development and tissue homeostasis of multicellular organisms. In vertebrates a multitude of cells undergo PCD, ranging from early steps as inner cell mass differentiation in blastocysts to maintenance of tissue homeostasis in adult organisms (Hardy et al., 1989). Studies in various organisms, including analyses of human diseases, have shown different reasons for cells to be eliminated in a physiological context. During development, PCD plays a crucial part in forming and deletion of structures. Well-known examples in higher vertebrates would be the shaping of digits through deletion of interdigital webs or the removal of evolutionary relics or structures that are only required in one sex, like the Wolffian duct in female or the Müllerian duct in male mammals (Jacobson et al., 1997). In many developing tissues and organs, e.g. in the mammalian central nervous system, cells are overproduced and cell number is subsequently adjusted by induction of PCD in surplus cells. In adult organisms also elimination of potentially harmful or unwanted cells is mediated by PCD. Virally infected cells or cells bearing DNA defects are removed, as well as autoreactive B and T lymphocytes or cells that somehow escaped correct cell cycle regulation (Fuchs and Steller, 2011). The finding that mice bearing deficiencies in key components of programmed cell death are often viable and show only small developmental defects points towards a high functional redundancy in PCD, and also to the existence of different alternative pathways of cell death induction (Yuan and Kroemer, 2010).

1.1.1. Apoptosis

The term apoptosis was introduced by Kerr and colleagues in 1972 (Kerr et al., 1972). It describes a tightly regulated process of cell death with distinct morphological changes, differing from those of necrosis or other types of cell death. Cell shrinkage, chromatin condensation and fragmentation of the nucleus, membrane blebbing and finally cellular disintegration into apoptotic bodies are characteristic for apoptotic cell death. Molecular changes, like internucleosomal DNA cleavage and altered

distribution of phosphatidylserine between the inner and outer leaflet of the plasma membrane are additional apoptotic markers.

Apoptosis can be initiated by two major pathways, the intrinsic and the extrinsic pathway. The extrinsic pathway is induced through extracellular stimuli and is transduced via cell surface receptors, so-called death receptors. Arising from within the cell, the intrinsic pathway is initiated by intracellular stimuli, e.g. DNA damage or reactive oxygen species (Degterev et al., 2003). Both pathways converge at the activation of a set of aspartate-specific cysteine proteases (caspases), the short prodomain effector caspases (caspase-3, -6 and -7) which are the key executioners of the apoptotic program. The group of effector caspases is complemented by the long prodomain initiator caspases, which contain one of two protein-protein interaction motifs: the death effector domain (DED, caspases-8 and -10) or the caspase activation and recruitment domain (CARD, among others caspase-9). They exert their activity through the proteolytic cleavage of specific substrates, resulting in most cases in inactivation, yet frequently also in activation of the target (Hengartner, 2000). Caspases are found in the cell as inactive zymogens (procaspases), which can be proteolytically cleaved by previously activated caspases at specific sites, resulting in activation. This caspase cascade mechanism is the driving force for the final activation of the three short prodomain (effector) caspases, caspase-3, -6 and -7. Substrates inactivated by effector caspases include proteins with functions necessary for cell survival, like DNA repair (poly (ADP-ribose) polymerase, PARP), cell cycle (cyclins), apoptosis regulators (typically inhibitors like Bcl-2, XIAP or cIAP1), cytoskeletal and structural proteins (actin, tubulin, lamins) and kinases (e.g. protein kinase B/Akt) (Fischer et al., 2003). In addition, effector caspases also mediate the activation of detrimental factors like caspase-activated DNAse (CAD), through cleavage of its inhibitor ICAD (Nagata, 2000). Membrane blebbing is finally induced through caspase-mediated cleavage of the negative regulatory subunit of PAK2, a member of the p21-activated protein kinase family (Rudel and Bokoch, 1997).

Initiator caspases are activated at two distinct structures, depending on the type of apoptotic pathway. Triggering of the extrinsic pathway relies on the stimulation of death receptors (e.g. CD95/Fas, TRAIL receptors 1 and 2) by their ligands (Figure 1). Activated death receptors recruit the intracellular adapter protein Fas-associated protein with death domain (FADD) to their death domain (DD), either directly or via

the previously recruited adapter-protein TNF receptor type-1 associated death domain protein (TRADD). FADD, which contains both a DD and a DED, can in-turn recruit procaspase-8 (or -10) via homotypic interaction of the DED, hence forming the death-inducing signaling complex, DISC (Kischkel et al., 1995; Degterev and Yuan, 2008). The induced high local concentration of procaspase-8 renders the low intrinsic protease activity of this zymogen sufficient to mutually cleave and activate each other (Salvesen and Dixit, 1999; Boatright and Salvesen, 2003). Several steps are necessary to achieve full activation of caspase-8. Subsequent to dimerization, two cleavage events lead to the generation of mature caspase-8. The limited enzymatic activity of procaspase-8 dimers is sufficient to cleave adjacent procaspase-8 molecules in the region separating the large and small subunit. The resulting conformational change then renders the linker between the large subunit and the prodomain prone to further cleavage. Mature caspase-8 (a complex of two p18/p10 heterodimers) is released from the DISC into the cytoplasm (Chang et al., 2003). Active caspase-8 can then cleave procaspase-3, hence inducing the caspase cascade. In contrast to the initiator caspases, the effector caspases-3 and -7 occur in the cytoplasm as inactive dimeric zymogens. They are activated through cleavage within their interdomain linker mediated by an active initiator caspase (Boatright and Salvesen, 2003). In so-called type I cells the level of mature caspase-8 generated at the DISC is sufficient to induce cell death through direct activation of the effector caspases-3 and -7. Yet in type II cells, amplification of the apoptotic signal through involvement of the mitochondria is necessary (Scaffidi et al., 1998). Therefore, caspase-8 cleaves Bid, a BH3-only protein of the Bcl-2 family. The resulting truncated Bid (tBid) then translocates to the mitochondria as an integral membrane protein where it induces the polymerization of proapoptotic Bcl-2 family members Bax and/or Bak in the mitochondrial outer membrane (Martinou and Youle, 2011; Czabotar et al., 2013). The thereby formed pores allow the release of proapoptotic factors (among others cytochrome c, second mitochondria-derived activator of apoptosis (Smac) and apoptosis-inducing factor (AIF)) from the mitochondrial intermembrane space, hence connecting the extrinsic to the intrinsic apoptotic pathway (Gross et al., 1999). All BH3-only members of the Bcl-2 family (e.g. Bid, Bim/Bod, Bad and Puma) have proapoptotic functions. Bid, and probably also Bim, can directly exert their functions through activation of Bax and Bak. The other BH3-only proteins function predominantly through binding to antiapoptotic proteins of the

Bcl-2 family (Chipuk et al., 2010). The remaining Bcl-2 family members can be grouped into antiapoptotic Bcl-2-like proteins (e.g. Bcl-2, Bcl-x_L) and proapoptotic Bax-like proteins (e.g. Bax, Bak). Bcl-2-like antiapoptotic proteins contribute to the conservation of mitochondrial integrity by direct binding to Bax and Bak (Youle and Strasser, 2008).

Caspase-9 is the initiator caspase of the intrinsic mitochondrial apoptosis pathway. The scaffold for procaspase-9 activation is the apoptosome, a heptameric cytosolic complex. Assembly of the apoptosome requires cytochrome c, which upon its release from the mitochondria, binds to the WD40 domains of Apaf-1. This activates Apaf-1, which then assumes an open conformation. The subsequent binding of dATP or ATP to the nucleotide-binding domain induces the multimerization of Apaf-1 (Li et al., 1997). Multiple procaspase-9 molecules are subsequently recruited by homotypic interactions between the CARDs and the local accumulation promotes the formation of procaspase-9 dimers. Dimerization of procaspase-9 is sufficient for activation of the enzymatic activity, yet it is accompanied by autocatalytic cleavage into a large and a small caspase-9 subunit (Adams and Cory, 2002; Würstle et al., 2012).

Both activation and enzymatic activity of caspases can be regulated at various levels through the action of regulatory and inhibitory proteins. Activation of procaspase-8 or -10 at the DISC can be blocked by the cellular FLICE-like inhibitory protein (cFLIP). cFLIP is a capase-8 like protein, featuring two DEDs, yet lacking a functional catalytic site. Three different splice variants of cFLIP, namely $cFLIP_S$, $cFLIP_L$ and $cFLIP_R$, have been described at the protein level (Budd et al., 2006). The two short splice variants, $cFLIP_S$ and $cFLIP_R$, can be recruited into the DISC via interaction of the DEDs and inhibit procaspase-8 activation, probably by competitive binding to FADD (Golks et al., 2005). The long splice variant $cFLIP_L$ has also been shown to be recruited into the DISC where it forms heterodimers with procaspase-8. Whereas the two shorter cFLIP splice variants completely inhibit the autocatalytic activation of procaspase-8 in a dominant negative manner, $cFLIP_L$ allows the first cleavage step and is in turn also cleaved by caspase-8 (Krueger et al., 2001). Therefore, under physiological conditions, $cFLIP_L$ most likely acts as an activator of procaspase-8 at the DISC. However, this partial activation of caspase-8 does not result in apoptosis induction, yet in the formation of a membrane-localized heterodimer with reduced enzymatic activity and a limited substrate spectrum (Micheau et al., 2002).

Activation of caspases as well as their enzymatic activity can be inhibited by certain members of the inhibitor of apoptosis protein (IAP) family. These IAPs target the effector caspases caspase-3 and -7, as well as the initiator caspase-9 (Shi, 2002). XIAP is the only IAP capable to block active caspases. The mechanism by which XIAP inhibits active caspase-3 and -7 is direct interaction via its second baculoviral IAP repeat (BIR) domain (Scott et al., 2005). XIAP predominantly binds to the effector caspases-3 and -7, while binding to caspase-9 is considerably weaker (Eckelman et al., 2006). Furthermore, it features a RING domain with E3 ligase activity at its carboxyl-terminus. Hence an additional mechanism through which XIAP can regulate apoptotic signaling is targeting of proteins for ubiquitination. E3 ligase activity of XIAP is not only involved in apoptotic signaling through ubiquitination of caspases, Smac or AIF, yet also in other signaling pathways, like the transcription factor NFκB or the mitogen-activated protein kinase c-Jun N-terminal kinase (Wilkinson et al., 2008; Galban and Duckett, 2010). Binding of cIAP1 and cIAP2, additional mammalian IAPs involved in regulation of cell survival, to active caspases is insufficient to inhibit their enzymatic activity (Eckelman and Salvesen, 2006). However, similar to XIAP, cIAP1 and cIAP2 harbor a RING domain providing them with E3 ubiquitin ligase activity. Hence these IAPs are presumably capable to neutralize active caspases through ubiquitination, targeting them for proteasomal degradation (Bader and Steller, 2009; Vucic et al., 2011). IAP activity can in turn be restricted through inhibition by Smac/DIABLO, Omi/HtrA2 (Du et al., 2000; Verhagen et al., 2000; Verhagen et al., 2002) and through proteolytic degradation by active caspases (Deveraux et al., 1999; Guicciardi et al., 2011).
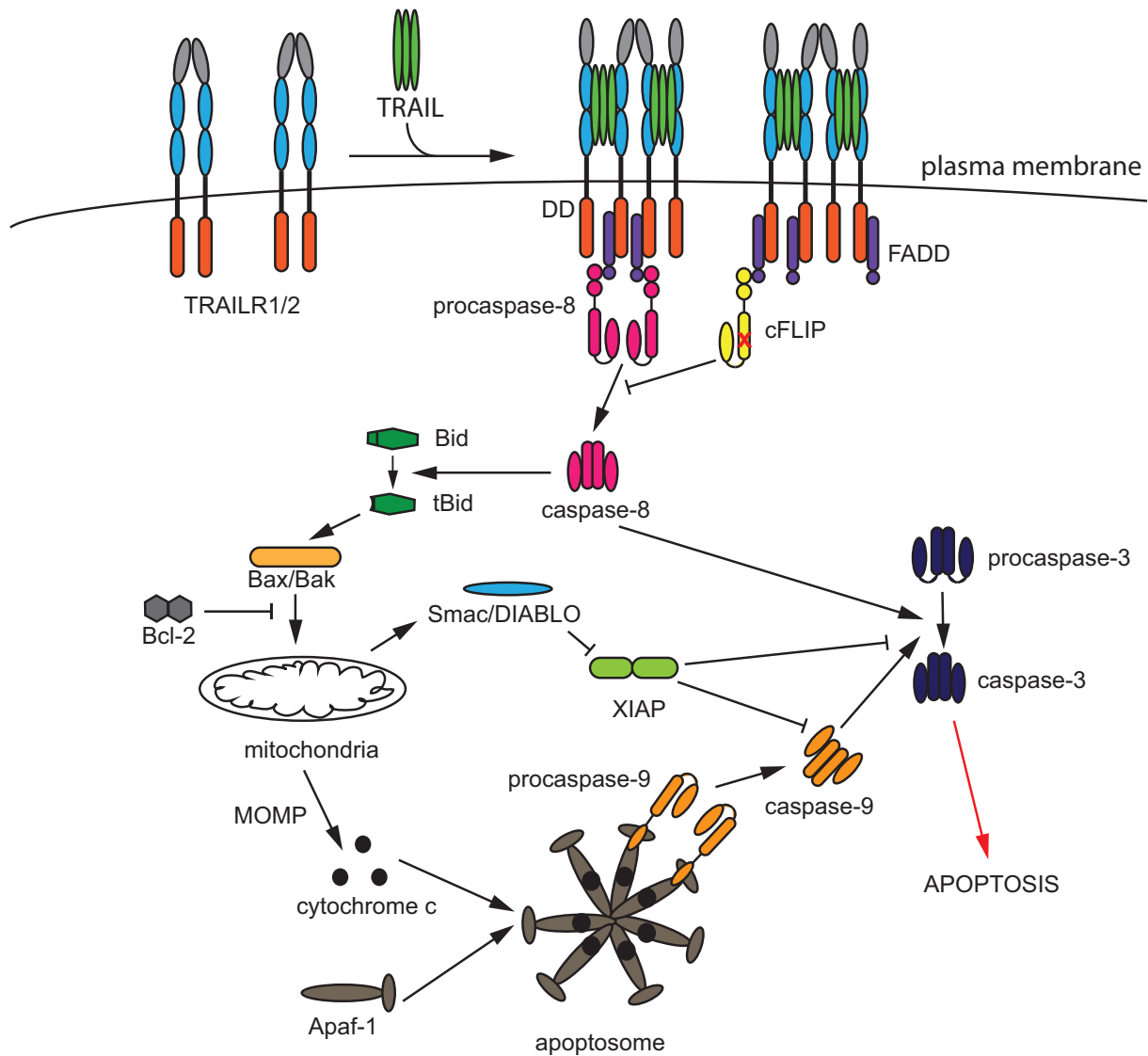
Figure 1: TRAIL-induced apoptotic signaling pathway. Activation of the death receptors TRAILR1 and/or TRAILR2 induces formation of the DISC. FADD is recruited via homotypic interactions to the DD of activated receptors. Procaspase-8 (or-10) in turn binds to the DED of FADD and is autoproteolytically activated. Mature caspase-8 can then directly cleave and activate procaspase-3 leading to execution of the apoptotic program (in type I cells) or activate a mitochondrial amplification loop through cleavage of the BH3-only protein Bid (in type II cells). Truncated Bid then induces polymerization of Bax and/or Bak resulting in mitochondrial outer membrane permeabilization (MOMP) and release of cytochrome c (and other proapoptotic factors) from the mitochondrial intermembrane space inducing formation of the apoptosome, the scaffold for procaspase-9 activation. Caspase-9 then cleaves procaspase-3, completing the mitochondrial amplification loop and triggering apoptosis.

1.1.2. Necroptosis

Apoptosis was long considered to be the only type of regulated cell death in development, homeostasis and disease. Necrotic cell death, on the other hand, was thought to solely represent an uncontrollable and unregulated occurrence. Evidence for the existence of a pathway of regulated necrosis had been accumulating for several years before the term necroptosis was introduced for its description (Degterev et al., 2005). The exact molecular mechanisms of necroptosis have only begun to unravel, yet many participating processes and molecules have already been described (Vandenabeele et al., 2010). Activation of death receptors, including CD95/Fas, TNFR1, TRAILR1 and TRAILR2, can induce necroptosis under certain conditions (Holler et al., 2000). Death receptor-mediated necroptosis can occur in certain cell lines and primary cells when transcription and/or translation are inhibited or under conditions where caspase activation is blocked (Fiers et al., 1996; Vercammen et al., 1998). Necroptosis induction by death receptors is dependent on the kinase activity of receptor interacting proteins 1 and 3 (RIP1/3) which cooperate with FADD and caspase-8 to form the necrosome, a signaling complex heavily regulated by ubiquitination and phosphorylation of RIP1 and RIP3 (Cho et al., 2009; Declercq et al., 2009). Execution of necroptosis is a complicated process involving the production of reactive oxygen species through different mechanisms, depletion of cytoplasmic ATP and permeabilization of the mitochondrial membrane leading to the release of cytotoxic proteins, like AIF1, into the cytosol. All these processes culminate in the active disintegration of lysosomal, mitochondrial and plasma membranes and finally cell death (Vandenabeele et al., 2010; Delavallee et al., 2011).

1.2. Tumor necrosis factor ligand/receptor superfamily

The tumor necrosis factor (TNF) superfamily consists to date of 19 ligands and 29 receptors. It was named after its most prominent member, TNF. Many ligands and receptors of the TNF superfamily show pro-inflammatory activity, among others through activation of the transcription factor NFκB. Others exhibit proliferative activities or play a role in differentiation. Some TNF superfamily members are also tightly involved in apoptosis induction (Aggarwal et al., 2012). Initial discovery of TNF was due to its antitumoral effects (Carswell et al., 1975). Since then, TNF and many additional superfamily members have been linked to various pathophysiological conditions including autoimmune, neurological and metabolic diseases, as well as cancer (Aggarwal, 2003). Accordingly, both antagonists and agonists of TNF superfamily members have been developed and are currently being examined for their beneficial effects for the treatment of various diseases and malignancies (Kontermann et al., 2009; Gerspach et al., 2011). TNF ligands are mostly expressed as type II transmembrane proteins. They feature a characteristic TNF homology domain at the carboxyl-terminus and assemble as non-covalently linked homotrimeric complexes. Trimerization of the protomers is required for receptor-binding and hence also for the induction of intracellular signals. Soluble forms of the ligands are generated through proteolytic cleavage by distinct proteases and/or alternative splicing. Receptor members of the TNF superfamily can be characterized by the presence of up to six cysteine-rich domains (CRDs) in their extracellular amino-terminal parts. Typically, two of these CRDs, which are all arranged in tandem repeats, constitute the ligand binding site (Bodmer et al., 2002). Several receptors of the TNF superfamily can be found on the plasma membrane in pre-arranged oligomeric complexes. This oligomerization has been shown to be mediated by the pre-ligand binding assembly domain (PLAD), which localizes to the most membrane-distal cysteine-rich domain, the CRD1 (Chan et al., 2000; Siegel et al., 2000).

1.3. TNF-related apoptosis-inducing ligand

Tumor necrosis factor-related apoptosis-inducing ligand (TRAIL, Apo2L) is a more recently discovered member of the TNF superfamily. TRAIL was independently identified by two groups when searching in an expressed sequence tag library for sequences homologous to conserved parts of ligand members of the TNF

superfamily. The TRAIL cDNA was successfully cloned and the ligand's capability to induce apoptosis in susceptible cells was demonstrated (Wiley et al., 1995; Pitti et al., 1996). Interestingly, most TRAIL susceptible cell lines were shown to be tumor-derived or virally transformed, whereas normal cells were generally insensitive to the cytotoxic effects of TRAIL (Pitti et al., 1996; Walczak et al., 1999).

1.3.1. Structure and function of TRAIL and its receptors

In TRAIL producing cells, the ligand is expressed as a type II transmembrane protein. It features a short amino-terminal cytoplasmic and a long extracellular carboxyl-terminal domain. Similar to other members of the TNF superfamily the extracellular domains of TRAIL protomers associate at hydrophobic interfaces to form compact homotrimers. Unique for TRAIL is a zinc-binding site at the trimer interface. The coordination of a Zn^{2+}-ion by three free cysteine residues (one from each TRAIL protomer) is indispensible for the structure and stability of TRAIL, hence also for its bioactivity (Hymowitz et al., 2000). Limited proteolysis of membrane-bound TRAIL by cysteine proteases has been suggested as mechanism to generate the soluble form of the ligand (Mariani and Krammer, 1998).

The family of human TRAIL receptors is composed of five different members (see Figure 2). One of them, osteoprotegerin (OPG) is a soluble, dimeric TNF receptor homologue which inhibits osteoclastogenesis and increases bone density *in vivo* (Schneeweis et al., 2005). OPG exerts this function by competing with receptor activator of nuclear factor κB (RANK) for binding of the ligand RANKL (Nelson et al., 2012). As binding of OPG to RANKL occurs with higher affinity than binding to TRAIL (Emery et al., 1998), it is still a matter of discussion whether OPG actually plays a significant role in TRAIL signaling. However, recent studies implicate a function of OPG as a soluble decoy receptor for TRAIL (De Toni et al., 2008; Lane et al., 2012).

Three of the remaining four human TRAIL receptors are type I transmembrane proteins. They show the typical structure of TNF receptor superfamily members with their extracellular parts consisting of cysteine-rich domains (CRDs). The two membrane-proximal CRDs, CRD 2 and 3, constitute the ligand binding site. The most membrane-distal CRD1 is actually only a partial CRD, lacking two of the usually three cysteine bonds (Kimberley and Screaton, 2004). It is assumed that this partial CRD harbors the PLAD in all TRAIL receptors (Chan, 2007). TRAIL receptor 1 (TRAILR1, DR4) and TRAIL receptor 2 (TRAILR2, DR5) were the first two TRAIL receptors to be

identified (MacFarlane et al., 1997; Pan et al., 1997b; Walczak et al., 1997). They share an overall homology of 58% in the amino acid sequence. The highest degree of conservation can be found in the intracellular death domain (DD). The DD is composed of approximately 90 amino acid residues which fold to a characteristic structure of six α-helices. This domain mediates homotypic interactions with FADD, a DD containing protein. FADD can in-turn interact with DED-only proteins, thus demonstrating a crucial role of these domains in the formation of the apoptosis promoting DISC (Park et al., 2007a; Dickens et al., 2012b).

TRAIL receptor 3 (TRAILR3, DcR1) is an exception in the group of TRAIL cell surface receptors. It is devoid of any intracellular and transmembrane domains. Instead, it is tethered to the plasma membrane via a glycosylphosphatidylinositol (GPI) anchor (Degli-Esposti et al., 1997b; Pan et al., 1997a). Signaling of TRAILR3 has so far not been studied experimentally. However the complete absence of transmembrane and intracellular domains indicates that its capabilities are most likely only minimal, although direct signaling via its GPI anchor cannot be excluded (Kimberley and Screaton, 2004). Expression of TRAILR3 renders cells less susceptible to TRAIL-mediated apoptosis induction. Accordingly, a decoy function was proposed for TRAILR3, stating that it competes with the DRs for TRAIL binding (Degli-Esposti et al., 1997b). The finding that TRAILR3 does not bind TRAIL with higher affinity than the death receptors (Truneh et al., 2000) has somewhat challenged the function of TRAILR3 as decoy. An alternative hypothesis to explain the apoptosis-inhibiting effect of TRAILR3 is the formation of mixed receptor complexes. This interpretation is being rendered unlikely by the presumption that the GPI anchor mediates the localization of TRAILR3 in membrane domains distinct from those the DRs are localized in (Kimberley and Screaton, 2004; Mérino et al., 2006).

TRAIL receptor 4 (TRAILR4, DcR2) is again a type I transmembrane protein. Its intracellular domain closely resembles that of TRAILR1 and TRAILR2, albeit being considerably smaller. Accordingly, the intracellular domain of TRAILR4 is often referred to as truncated DD (Degli-Esposti et al., 1997a; Marsters et al., 1997; Pan et al., 1998). Due to the incomplete DD, binding of ligand to TRAILR4 does not induce apoptosis. Non-apoptotic signaling capacities of this receptor are relatively undefined and have been only poorly characterized. There is evidence that TRAILR4 is capable to activate the transcription factor NFκB (Degli-Esposti et al., 1997a; Hu et al., 1999), although other studies were unable to reproduce these results (Marsters et al., 1997;

Harper et al., 2001). Similar to TRAILR3, expression of TRAILR4 renders cells less susceptible to TRAIL-induced apoptosis (Marsters et al., 1997). In addition to the above mentioned decoy mechanism, the formation of mixed receptor complexes, both ligand-mediated (Mérino et al., 2006) and ligand-independent (Clancy et al., 2005), has been described with partially contradictory findings. Accordingly, the definite molecular mechanism of TRAILR4 action could not be conclusively demonstrated to date.
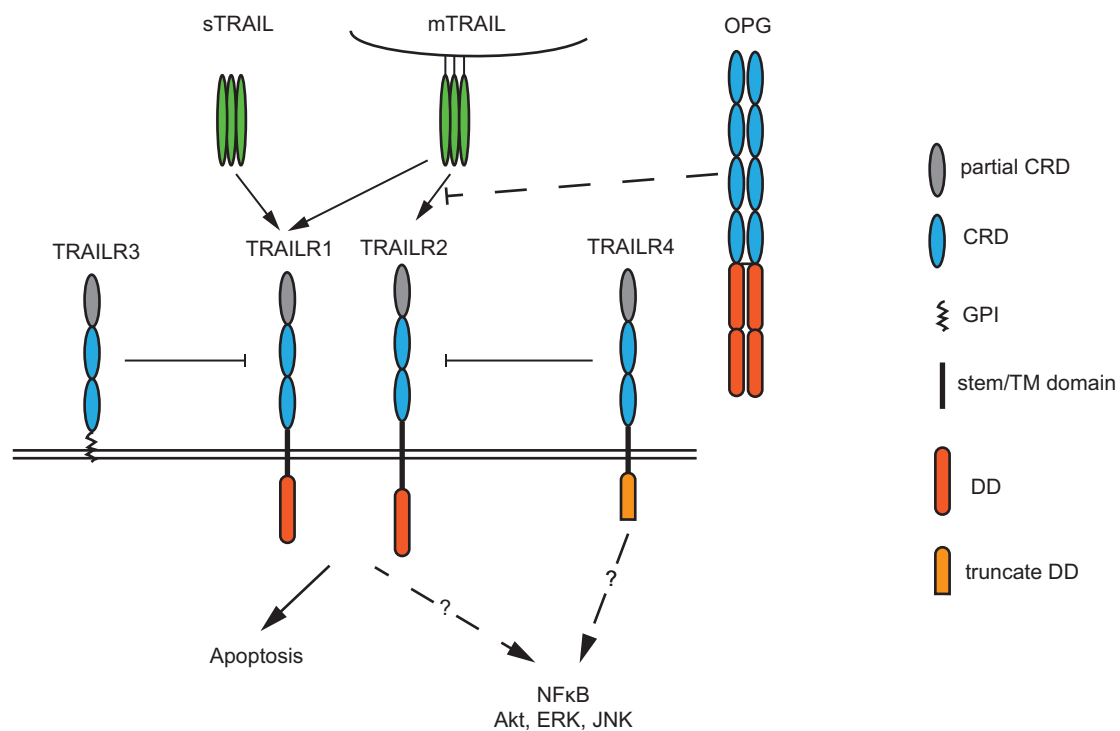
Figure 2: Schematic illustration of the structure and function of TRAIL receptors. TRAIL receptors 1, 2 and 4 are expressed as type I transmembrane proteins. The extracellular part of these receptors is composed of two complete and one partial CRD. The amino-terminal partial CRD has been proposed to harbor the PLAD, while the two membrane proximal CRDs form the ligand binding site. TRAILR3 is similar to the other TRAIL receptors in its ECD, yet it is attached to the plasma membrane via a GPI anchor. TRAILR3 and TRAILR4 exert an inhibitory effect on signaling by the death receptors TRAILR1 and TRAILR2. While TRAILR1 can be fully activated by both soluble TRAIL (sTRAIL) and the membrane-bound form of the ligand (mTRAIL), TRAILR2 responds only to binding of mTRAIL. For TRAILR3 and TRAILR4 a differential response to binding of sTRAIL or mTRAIL is not known. OPG is a soluble TNF receptor homologue that self-associates to form a disulfide-linked dimer. It consists of four amino-terminal CRDs and two DD-related domains. OPG can bind TRAIL and has been shown to act as a decoy receptor under certain circumstances.

1.3.2. TRAIL-induced intracellular signaling

Originally, the members of the TNF receptor superfamily were considered to occur on the plasma membrane as monomers. Trimerization of these receptors mediated through their cognate ligand was the prevailing model to describe the initiation of intracellular signaling in the TNF superfamily. Yet, as accumulating evidence supports the notion that at least some of these receptors are pre-assembled on the cell surface (Chan, 2007), the ligand-induced trimerization model has become obsolete. It is now generally accepted that the formation of organized high molecular weight complexes by the combined action of receptor-receptor and ligand-receptor interactions is necessary for signal transduction by TNF receptor superfamily members (Siegel et al., 2004; Henkler et al., 2005; Wagner et al., 2007; Branschädel et al., 2010; Valley et al., 2012).

Binding of the ligand TRAIL to TRAILR1 or TRAILR2 principally results in transduction of proapoptotic signals. However, the final outcome of death receptor activation is strongly dependent on the cellular status and the cell type. Activation of TRAILR1 can be achieved by binding of the soluble or membrane-bound form of its ligand. In contrast, the soluble ligand is insufficient to induce significant signaling via TRAILR2, which requires membrane-bound TRAIL or secondarily crosslinked soluble TRAIL for full activation (Wajant et al., 2001). Distinct functions for the two DRs could so far not be demonstrated, though TRAILR2 had been described to induce a stronger apoptotic response (Kelley et al., 2005). Yet in different cellular systems this response could be dominated by either receptor (Lemke et al., 2010; van Geelen et al., 2011). The observed differences could be based on distinct affinities to the ligand (Truneh et al., 2000), or post-translational modifications of receptors, e.g. palmitoylation of TRAILR1 targeting it to localize to membrane microdomains, which results in more efficient signaling (Rossin et al., 2009). Recently, also a role of the receptors' transmembrane domain in the regulation of apoptotic signaling capacity was proposed (Neumann et al., 2012).

Ligand binding to TRAILR1 and TRAILR2 drives the clustering of the death receptors into high molecular weight complexes and induces the formation of the DISC. The TRAIL DISC consists of the death domains of the receptors, the adapter protein FADD, which interacts with the DDs of the receptors and in turn recruits the initiator caspase-8 (and/or caspase-10) through homophilic interactions of the DEDs (Kischkel et al., 2000; Kischkel et al., 2001). The different splice variants of cFLIP can

also be recruited by FADD into the DISC *in lieu* of initiator caspases, leading either to reduced procaspase cleavage (mediated by the short cFLIP splice variants) or to the generation of a DISC resident caspase-8/cFLIP$_L$ heterodimer with reduced enzymatic activity (Boatright et al., 2004). Activation of initiator caspases at the DISC occurs through proximity-induced formation of procaspase dimers and limited proteolysis. The activated subunits, forming a complex of two p18/p10 heterodimers, are subsequently released into the cytoplasm. Mature caspase-8 can further either directly induce the caspase cascade through proteolytic processing of effector procaspases (in type I cells) or via the mitochondrial amplification loop through cleavage of the BH3-only protein Bid. Polyubiquitination of caspase-8 has been proposed as a mechanism to facilitate full activation of the initiator caspase. Caspase-8 can be ubiquitinated by a cullin3-based E3 ligase. Subsequent association with the ubiquitin-binding protein p62/sequestosome-1 leads to the translocation of polyubiquitinated caspase-8 into intracellular ubiquitin-rich foci, hence increasing its local concentration and leading to more efficient activation (Jin et al., 2009).

Subsequent to formation of the DISC, TRAIL induces the formation of a second, intracellular, complex termed complex II. Albeit complex II retains some components of the DISC, i.e. caspase-8 and FADD, it is distinct from this complex. RIP1, TRADD and/or TRAF2, NEMO and/or IKKα and caspase-10 are additionally recruited into complex II (Varfolomeev et al., 2005; Jin and El-Deiry, 2006). RIP1 can then activate the IKK complex, which in turn phosphorylates and thereby induces the proteolytic degradation of IκB proteins, leading to the activation of the transcription factor NFκB. Recently, a RIP1-independent, but FADD- and caspase-8-dependent pathway of TRAIL-mediated NFκB activation in Jurkat cells, a T cell lymphoma line, was described (Grunert et al., 2012). Whether this represents an alternative or cell type specific mechanism of NFκB activation has not yet been clarified. Additional signaling pathways activated in response to ligand binding to TRAILR1 and TRAILR2 include kinase pathways, like protein kinase B (PKB)/Akt and mitogen-activated protein kinases (MAPK) like c-Jun NH$_2$-terminal kinase (JNK), extracellular signal-regulated kinase (ERK) and p38-MAPK (Falschlehner et al., 2007). Analogous to activation of the transcription factor NFκB, these kinase pathways are involved in various cellular processes, including proliferation, differentiation and inflammation, but also apoptosis. JNK and p38-MAPK are activated at complex II in a similar way as NFκB

(Varfolomeev et al., 2005), while the molecular mechanisms leading to activation of ERK and PKB/Akt pathways are not completely understood. In addition, the physiological relevance of TRAIL-mediated activation of these kinase cascades remains to be elucidated (Lin et al., 2000; Secchiero et al., 2003).

As previously mentioned, signaling capabilities of TRAILR4 remain only poorly defined. Signal transduction by this receptor is likely cell type-dependent. This notion is supported by the fact that some studies show TRAILR4-mediated NFκB activation while others were unable to demonstrate the activation of this transcription factor. Recently, constitutive (i.e. ligand-independent) Akt phosphorylation has been shown to be induced by TRAILR4 (Lalaoui et al., 2011), however the physiological implications of this observation remain undefined.

1.3.3. TRAIL in physiology and pathophysiology

TRAIL and its receptors exert important functions in regulation of the immune system, especially in T cell homeostasis and the transition from innate to adaptive immunity. Moreover, TRAIL is involved in killing of cells infected with certain viruses and in immune surveillance against tumors and metastases.

Detection of TRAIL expression in various cells of the adaptive and innate immune systems was the first evidence for an immunological role of TRAIL and TRAIL receptors. Interestingly, TRAIL expression on monocytes and macrophages is upregulated in response to lipopolysaccharide or IFN-γ stimulation (Ehrlich et al., 2003), while IFN-γ can induce cell surface expression of TRAIL in dendritic (DC) and natural killer (NK) cells (Fanger et al., 1999). Membrane-bound TRAIL is one of the effector mechanisms enabling NK cell-mediated killing of tumor cells *in vitro* and *in vivo* (Takeda et al., 2001). Involvement of TRAIL and CD95L/FasL in T helper cell response was shown in *in vitro* experiments. Stimulation of differentiated T helper cells with anti-CD3 antibody induced an upregulation of CD95L in T helper 1 cells, while T helper 2 cells were induced to express TRAIL on the plasma membrane. T helper 2 cells are then also rendered resistant to TRAIL-induced apoptosis, presumably through an increased expression of cFLIP (Zhang et al., 2003).

Homeostasis of a certain subset of CD8-positive T cells, so-called helpless CD8-positive cells which were primed in absence of CD4-positive T cells, was suggested to be regulated by a TRAIL-dependent mechanism. Generally, helpless CD8-positive T cells are unable to undergo a second round of clonal expansion upon restimulation

with their matching antigen (Shedlock et al., 2003). Helpless CD8-positive T cells generally undergo activation-induced cell death upon secondary stimulation. Yet TRAIL-deficient helpless CD8-positive T cells were capable of expanding a second time, hence elimination of this T cell subset by TRAIL was suggested (Janssen et al., 2005).

Killing of virally infected cells by TRAIL is dependent on the production of type I and type II interferons. Virally infected cells show higher cell surface expression of TRAILR1 and TRAILR2 and produce IFN-α and IFN-β. These type I interferons, in combination with autocrine stimulation by IFN-γ, activate cytotoxic T lymphocytes to express increased amounts of membrane-bound TRAIL, hence enabling them to efficiently eradicate virally infected cells through a TRAIL-dependent mechanism (Falschlehner et al., 2009).

Evidence for a tumor suppressive function of endogenous TRAIL was first gathered by Sedger and colleagues who reported that a syngeneic tumor transplant showed enhanced growth in TRAIL double-knockout mice (Sedger et al., 1999). Later, TRAIL-mediated killing of metastasizing breast and renal carcinoma cells by activated NK cells was demonstrated (Smyth et al., 2001; Takeda et al., 2001). Furthermore, exogenously administered recombinant TRAIL has been shown to be capable of inducing apoptosis in tumor xenografts (Ashkenazi et al., 1999; Walczak et al., 1999). However, resistance of many primary tumors to TRAIL-based therapy poses considerable problems (Koschny et al., 2007). Numerous studies have shown that TRAIL resistance can occur at various levels in the signaling pathway. Expression of the decoy receptors TRAILR3 and TRAILR4 was proposed to be responsible for TRAIL resistance, yet no direct correlation between TRAIL susceptibility and decoy receptor expression could be found despite the fact that these receptors can serve as prognostic markers in certain types of tumors (Granci et al., 2008; Ganten et al., 2009). *In vitro* experiments showed that OPG can prevent TRAIL binding to death receptors, hence inducing TRAIL resistance (Lane et al., 2012). Moreover, high expression levels of antiapoptotic proteins can account for resistance in cancer cells. Expression of cFLIP was shown to be upregulated in human ovarian cancer samples (Horak et al., 2005) and cFLIP knock-down sensitized melanoma cells to TRAIL-induced apoptosis (Geserick et al., 2007). IAP family members, especially XIAP which is capable to directly inhibit the activity of caspase-3, -7 and -9, are important factors that can cause TRAIL resistance in cancer cells (Takahashi et al., 1998;

Deveraux et al., 1999; Schimmer et al., 2004). Finally, overexpression of antiapoptotic members of the Bcl-2 family has also been shown to impair efficient TRAIL treatment (Fulda et al., 2002). Major attempts to control the problems caused by TRAIL resistance include strategies for TRAIL-based antitumor therapies in combination with classical chemotherapeutic compounds, proteasome or kinase inhibitors or IAP antagonists (Hellwig and Rehm, 2012; Zhang et al., 2012).

1.4. The transcription factor NFκB

Besides activation of the apoptotic program, induction of the nuclear factor of κB transcription factors (NFκB) is the best characterized cellular response to TRAIL receptor activation. NFκB is well known for its role in immune and inflammatory responses (Hayden et al., 2006). Yet also additional physiological and pathological processes are under the control of this transcription factor family. The group of NFκB transcription factors is composed of five different subunits which are active as dimers. RelA (p65), RelB, c-Rel, p50 and p52 feature a Rel homology domain at the amino-terminus which is responsible for DNA binding and subunit dimerization (Gilmore, 2006). NFκB dimers are sequestered in the cytoplasm of unstimulated cells by inhibitors masking their nuclear localization sequence. This is achieved by binding of one of three typical inhibitor of κB (IκB) proteins (IκBα, IκBβ or IκBε) or by intramolecular binding of an inhibitory domain of the p52 or p50 precursors (p100 or p105, respectively). These different mechanisms for retaining NFκB in an inactive state are linked to two distinct pathways for its activation (Scheidereit, 2006; Hayden and Ghosh, 2008).

The alternative or non-canonical pathway is characterized by proteasomal processing of p100 to p52 thus liberating p52 containing NFκB dimers from the inhibitory effect, enabling them to translocate into the nucleus where they can induce transcription of their target genes. Activation of the non-canonical pathway relies on the activity of the protein kinase NFκB-inducing kinase (NIK) in response to a limited number of stimuli. NIK phosphorylates IKKα which then phosphorylates p100 and thus triggers its ubiquitination and partial proteasomal degradation (Gilmore, 2006).

Activation of the canonical, or classical, NFκB pathway occurs in response to all physiological NFκB-inducing stimuli, including most ligands of the TNF superfamily. It involves stimulation of the kinase activity of the IKK (IκB kinase) complex, which consists of IKKα, IKKβ and the regulatory component IKKγ (also called NFκB

essential modulator, NEMO). The activated IKK complex phosphorylates IκB proteins and thus triggers their ubiquitination and proteasomal degradation (Scheidereit, 2006; Wajant and Scheurich, 2011). The freed NFκB dimers can then translocate into the nucleus where they induce transcription of their target genes. The best characterized NFκB dimer is the p50/p65 complex. This heterodimer is mostly bound to IκBα and nuclear p50/p65 induces (among others) the expression of its own inhibitor IκBα, thus establishing a negative regulation loop (Hayden and Ghosh, 2008).

1.4.1. NFκB and cell death

Generally, NFκB induces the expression of genes encoding antiapoptotic or antioxidant proteins, hence exerting cytoprotective effects. Nonetheless, under certain circumstances and cellular contexts it can sensitize cells to death-inducing stimuli or even exhibit direct proapoptotic functions. Activation of gene expression is the predominant mechanism how NFκB executes its protective activity, accordingly the transcription of several different gene products which block the extrinsic and/or intrinsic pathway of apoptosis is induced upon NFκB activation (Kucharczak et al., 2003). Also expression of cFLIP, an inhibitor of DR-induced apoptosis, has been shown to be regulated by NFκB (Kreuz et al., 2001; Micheau et al., 2001). Other important target genes of NFκB include the antiapoptotic members of the Bcl-2 family, IAPs, the TRAIL decoy receptor TRAILR3 and the zinc-finger protein A20, which blocks both NFκB activation and TNF-induced cell death by means of its E3 ligase and deubiquitinase activities (Dutta et al., 2006). Transcriptional repression of genes encoding for components of the extrinsic apoptosis pathway (TRAILR1, TRAILR2 and caspase-8) is an additional mechanism for apoptosis inhibition by NFκB (Chen et al., 2003).

Despite the predominance of antiapoptotic effects, activation of NFκB can be linked to or can even be required for the process of apoptosis or other types of induced cell death. Proapoptotic target genes include several DRs and death ligands, Bax, the tumor suppressor p53 as well as Bcl-x$_s$, an alternatively spliced proapoptotic form of Bcl-x$_L$ (Chen et al., 2003; Kucharczak et al., 2003). Apoptosis as a result of endoplasmic reticulum stress can be induced through NFκB-dependent upregulation of TNF expression. In combination with impaired TNF-mediated JNK and NFκB activation, a potent cytotoxic effect is induced (Hu et al., 2006).

In a recent study, NFκB has been shown to influence TRAIL and CD95L/FasL-mediated apoptosis in glioblastoma cells by facilitating formation of the DISC (Jennewein et al., 2012). On the other hand, several publications have suggested that TRAIL-resistance can be mediated by NFκB (Plantivaux et al., 2009). Accordingly, activation of NFκB elicits a multitude of effects which can both impair and promote cell death, showing that the final outcome of NFκB activation is likely strongly contextual, cell type- and stimulus-dependent (Radhakrishnan and Kamalakaran, 2006).

1.5. Aim of the work

The presented work had two major aims. The first one was the investigation of receptor-receptor interactions of the three human TRAIL receptors that are expressed as type I transmembrane proteins. Several members of the TNF receptor superfamily exist on the cell membrane as pre-assembled oligomers. This was demonstrated for Fas, TNFR1 and TNFR2, as well as TRAIL receptors. Interestingly, for TRAIL receptors the formation of heteromers has been described, too. However, conflicting results concerning this ligand-independent pre-assembly of TRAIL receptors can be found in literature. In addition, no reports describing the stoichiometry of TRAIL receptor homo- and heteromers have been made. Accordingly, topic of the first part of this work was the study of ligand-independent interactions of TRAIL receptors using different approaches and the elucidation of the stoichiometry of pre-assembled oligomers. The intention of this part of the study was to expand the understanding of the elaborate TRAIL system, as ligand-independent complex formation could potentially affect the efficient transduction of proapoptotic signals. This aspect is of particular significance in the context of TRAIL-based therapeutic approaches for tumor treatment. Inferring from the finding that expression of TRAILR4 can be of prognostic significance in certain tumor types, a detailed understanding of the consequence of receptor-receptor interaction is crucial. Therefore, a cellular model to investigate the influence of the decoy receptor TRAILR4 on signaling by TRAILR1 was established. Using this cellular model, distinct differences in TRAIL-induced cytotoxicity, progression of the apoptotic program and also non-apoptotic signaling were demonstrated. In order to conceive the molecular mechanisms that could mediate the observed effects, a truncated variant of TRAILR4 was generated and used in the established cellular model to

exclude signaling-dependent mechanisms. Furthermore, as signal transduction by TRAILR4 is only incompletely understood, and could further impede transduction of proapoptotic signals, an antibody array was used to screen for intracellular signaling pathways that are affected by activation of TRAILR4.

2. Material & Methods

2.1. Materials

2.1.1. Instruments and laboratory equipment

Balances	Kern ALJ120-4, Kern & Sohn GmbH, Balingen-Frommern, Germany and Precision Standard, OHAUS Co., Parsippany, New Jersey, USA
Centrifuges	Centrifuge 5415R and Centrifuge 5810R, Eppendorf, Hamburg, Germany and Heraeus Multifuge 3 L-R; Heraeus, Thermo Fisher Scientific, Ulm, Germany
Cryoboxes	Cryo 1 °C Freezing Containers; NALGENE, Thermo Fisher Scientific, Ulm, Germany
Electroblotting system	Semi-dry blotting chamber, Phase, Lübeck, Germany
Electrophoresis chambers	Phase, Lübeck, Germany
Film developing machine	Agfa Curix60, Agfa HealthCare GmbH, Cologne, Germany
Flow cytometer	Cytomics FC 500, Beckman Coulter, Krefeld, Germany and FACSVantage SE+FACSDiVa Option, BD Biosciences, Heidelberg, Germany
Freezer	Liebherr profi-line (-20 °C), Liebherr-International Deutschland GmbH, Biberach a. d. Riss, Germany and NuAire -85 °C ultra-low freezer, Plymouth, Minnesota, USA
Gel documentation	Biostep GmbH, Jahnsdorf, Germany
Heat block	HBT-1-131, Haep Labor Consult, Bovenden, Germany
Incubator (eukaryotic cells)	CO_2 Incubator, Zapf, Sarstedt, Germany
Incubator (prokaryotic cells)	Nuaire, Plymouth, Minnesota, USA
LI-COR Odyssey	LI-COR Biotechnology GmbH, Bad Homburg, Germany
Magnetic stirrer	Ikamag RCT basic, IKA-Werke GmbH & Co. KG, Staufen, Germany

Microscopes	Olympus CKX41; Olympus Deutschland GmbH, Hamburg, Germany and Zeiss LSM710, Carl Zeiss MicroImaging GmbH, Jena, Germany
PCR cycler	Mastercycler Gradient, Eppendorf AG, Hamburg, Germany
Peristaltic pump	P1; GE Healthcare Europe GmbH, Freiburg, Germany
pH meter	pH 530; Wissenschaftlich-Technische Werkstätten GmbH, Weilheim, Germany
Pipets	Eppendorf Research Family, Eppendorf AG, Hamburg, Germany
Photometer	BioPhotometer, Eppendorf AG, Hamburg, Germany and NanoDrop ND-100, Thermo Fisher Scientific, Ulm, Germany
Plate reader	Infinite 200, Tecan, Männedorf, Switzerland
Power supplies	Electrophoresis Power Supply EPS 301 and EPS 601, Amersham Pharmacia Biotech; GE Healthcare Europe GmbH, Freiburg, Germany
Quartz crystal microbalance	Attana A100 C-Fast system; Attana AB, Stockholm, Sweden
Sonicator	Sonoplus HD; Bandelin electronics GmbH, Berlin, Germany
Thermomixer	Thermomixer compact, Eppendorf AG, Hamburg, Germany
Vortexer	VF2; Janke & Kunkel, IKA-Werke GmbH & Co. KG, Staufen, Germany
Water bath	Julabo GmbH, Seelbach, Germany
Water purification	Destamat Bi 18 E; Heraeus, Thermo Fisher Scientific, Ulm, Germany
Workbenches	Mobilien 90, Varolab GmbH, Gießen, Germany and Biological Safety Cabinet Class I, Nuaire, Plymouth, Minnesota, USA

2.1.2. Consumables

15/50 ml tubes, sterile	CELLSTAR; Greiner bio-one, Frickenhausen, Germany
Blotting membrane	Protran BA85; Whatman, Schleicher & Schüll, Dassel, Germany
Blotting paper, 3 mm	Whatman, Schleicher & Schüll, Dassel, Germany
Cell culture flasks and plates	CELLSTAR; Greiner bio-one, Frickenhausen, Germany
Counting chamber	Neubauer counting chamber, Marienfeld, Lauda-Königshofen, Germany
Cover slips	#1; 18×18 mm; Menzel-Gläser, Braunschweig, Germany
Cryovials, 1 ml	CELLSTAR; Greiner bio-one, Frickenhausen, Germany
Dialysis tubes	D-Tube Dialyzer Maxi MWCO 6-8 kDa; Merck, Darmstadt, Germany
Filters, bottle-top, 0.2 µm	Zap Cap-S; Whatman, Schleicher & Schüll, Dassel, Germany
Flow cytometry tubes	Polystyrene tubes, round bottom; Greiner bio-one, Frickenhausen, Germany
IMAC columns	HisTrap FF, 1 ml, GE Healthcare Europe GmbH, Freiburg, Germany
Low non-specific binding (LNB) carboxyl-sensorchips	Attana AB, Stockholm, Sweden
Microreaction tubes, 0.2, 0.5, 1.5, 2.0 ml	Eppendorf AG, Hamburg, Germany
Microscopy slides	SuperFrost; Menzel-Gläser, Braunschweig, Germany
Pipets	CELLSTAR, Greiner bio-one, Frickenhausen, Germany
Pipet tips	Greiner bio-one, Frickenhausen, Germany

Sterilin plates, square   Sterilin, Thermo Fisher Scientific, Ulm,
                                                 Germany

Syringe filters   Acrodisc Syringe filter with 0.2 µm HT
                                                 Tuffryn membrane; Pall corporation, Ann
                                                 Arbor, Michigan, USA

X-ray film   CEA, Stagnas, Sweden

2.1.3. Chemicals and reagents

Acetic acid (glacial)   Carl Roth GmbH & Co., Karlsruhe,
                                                 Germany

Acrylamide (Rotiphorese Gel 30)   Carl Roth GmbH & Co., Karlsruhe,
                                                 Germany

Agar   Carl Roth GmbH & Co., Karlsruhe,
                                                 Germany

Agarose   Carl Roth GmbH & Co., Karlsruhe,
                                                 Germany

Ammonium persulfate (APS)   Carl Roth GmbH & Co., Karlsruhe,
                                                 Germany

Ampicillin   Sigma-Aldrich Chemie GmbH,
                                                 Taufkirchen, Germany

Blocking reagent   Roche Diagnostics, Mannheim,
                                                 Germany

Bovine serum albumin (BSA)   Sigma-Aldrich Chemie GmbH,
                                                 Taufkirchen, Germany

Bis(sulfosuccinimidyl)suberate (BS^3)   Pierce Protein Research Products,
                                                 Thermo Fisher Scientific, Ulm, Germany

Bromphenol blue   Serva Electrophoresis GmbH,
                                                 Heidelberg, Germany

$CaCl_2$ Carl Roth GmbH & Co., Karlsruhe,
                                                 Germany

Complete Protease Inhibitor Cocktail   Roche Diagnostics, Mannheim,
                                                 Germany

Crystal violet   Carl Roth GmbH & Co., Karlsruhe,
                                                 Germany

Cycloheximide (CHX)   Sigma-Aldrich Chemie GmbH,
                                                 Taufkirchen, Germany

Dimethylsulfoxide (DMSO)   Carl Roth GmbH & Co., Karlsruhe,
                                                 Germany

Dithiothreitol (DTT)   Carl Roth GmbH & Co., Karlsruhe,
                                                 Germany

Eosine	Carl Roth GmbH & Co., Karlsruhe, Germany
Ethanol	Carl Roth GmbH & Co., Karlsruhe, Germany
Ethidiumbromide (EtBr) solution	Carl Roth GmbH & Co., Karlsruhe, Germany
Ethylene-diamine tetraacetic acid (EDTA)	Carl Roth GmbH & Co., Karlsruhe, Germany
Ethylene glycol tetraacetic acid (EGTA)	Carl Roth GmbH & Co., Karlsruhe, Germany
Fluoromount G	Southern Biotechnology Associates Inc., Birmingham, Alabama, USA
Glycine	Carl Roth GmbH & Co., Karlsruhe, Germany
HCl (37% v/v)	Carl Roth GmbH & Co., Karlsruhe, Germany
Imidazole	Carl Roth GmbH & Co., Karlsruhe, Germany
Isopropanol (isopropyl alcohol)	Carl Roth GmbH & Co., Karlsruhe, Germany
Kanamycin	Applichem GmbH, Darmstadt, Germany
KH_2PO_4	Carl Roth GmbH & Co., Karlsruhe, Germany
KCl	Carl Roth GmbH & Co., Karlsruhe, Germany
Methanol	Carl Roth GmbH & Co., Karlsruhe, Germany
$MgCl_2$	Carl Roth GmbH & Co., Karlsruhe, Germany
Milk powder, non-fat	Carl Roth GmbH & Co., Karlsruhe, Germany
NaF	Sigma-Aldrich Chemie GmbH, Taufkirchen, Germany
NaOH	Carl Roth GmbH & Co., Karlsruhe, Germany
Nonidet P 40 (NP-40)	Sigma-Aldrich Chemie GmbH, Taufkirchen, Germany
Paraformaldehyde (PFA)	Carl Roth GmbH & Co., Karlsruhe, Germany
Phenylmethylsulphonyl fluoride (PMSF)	Sigma-Aldrich Chemie GmbH, Taufkirchen, Germany

PhosSTOP	Roche Diagnostics, Mannheim, Germany
Ponceau S	Carl Roth GmbH & Co., Karlsruhe, Germany
Protein G Sepharose	GE Healthcare Europe GmbH, Freiburg, Germany
Puromycin	Applichem GmbH, Darmstadt, Germany
Sodium azide (NaN$_3$)	Carl Roth GmbH & Co., Karlsruhe, Germany
Sodium deoxycholate	Carl Roth GmbH & Co., Karlsruhe, Germany
Sodiumdodecylsulfate (SDS)	Carl Roth GmbH & Co., Karlsruhe, Germany
Sodium pyrophosphate	Sigma-Aldrich Chemie GmbH, Taufkirchen, Germany
Tetramethylethylenediamine (TEMED)	Carl Roth GmbH & Co., Karlsruhe, Germany
Triton X-100	Carl Roth GmbH & Co., Karlsruhe, Germany
Tris-(hydroxymethyl)-aminomethane (Tris)	Carl Roth GmbH & Co., Karlsruhe, Germany
Trypton	Carl Roth GmbH & Co., Karlsruhe, Germany
Tween-20	Carl Roth GmbH & Co., Karlsruhe, Germany
Xylene cyanol	Carl Roth GmbH & Co., Karlsruhe, Germany
Yeast extract	Carl Roth GmbH & Co., Karlsruhe, Germany
Zeocin	Life Technologies, Invitrogen, Karlsruhe, Germany
zVAD-fmk	Bachem AG, Bubendorf, Switzerland
β -glycerophosphate	Sigma-Aldrich Chemie GmbH, Taufkirchen, Germany
β-Mercaptoethanol (2-ME)	Carl Roth GmbH & Co., Karlsruhe, Germany

2.1.4. Buffers and solutions

4x SDS sample buffer	40 mM Tris/HCl, pH 8.0, 0.4 mM EDTA, 140 mM SDS, 4.4 M glycerine, 0.4% (w/v) bromphenol blue
6x DNA sample buffer	1 mM EDTA, 50% (v/v) glycerine, 0.025% (w/v) bromphenol blue, 0.025% xylene cyanol
Binding buffer (IMAC)	50 mM sodium phosphate buffer, 20 mM imidazol, 300 mM NaCl, pH 8.0
Crystal violet solution	0.5% (w/v) crystal violet, 20% (v/v) methanol
Elution buffer (IMAC)	50 mM sodium phosphate buffer, 500 mM imidazol, 300 mM NaCl, pH 8.3
Lysis buffer (immunoprecipitation)	50 mM Tris-HCl, 150 mM NaCl, 1 mM EGTA, 1% (v/v) NP-40, 0.25% (w/v) sodium deoxycholate, pH 7.4
Lysis buffer (whole cell extracts)	20 mM Tris-HCl, 150 mM NaCl, 1mM Na_2EDTA, 1mM EGTA, 1% (v/v) Triton X-100, 2.5 mM sodium pyrophosphate 1mM β-glycerophosphate,1 mM NaF, pH 7.5
PBA	PBS + 0.05% (w/v) BSA + 0.02% (w/v) NaN_3
Phosphate buffered saline (PBS)	2.67 mM KCl, 1.47 mM KH_2PO_4, 137.9 mM NaCl, 8.06 mM Na_2HPO_4, pH 7.2
Ponceau S solution	0.1% (w/v) Ponceau S, 5% acetic acid (glacial) in ddH_2O
SDS-PAGE running buffer	50 mM Tris-HCl, 380 mM glycine, 4 mM SDS, pH 8.3
Separating gel buffer (SDS-Page)	375 mM Tris-HCl (pH 8.8), 3.75 mM SDS
Stacking gel buffer (SDS-Page)	125 mM Tris-HCl (pH 6.8), 3.75 mM SDS
TAE buffer (agarose gel electrophoresis)	40 mM Tris, pH 8.3, 0.11% (v/v) acetate, 50 mM EDTA

TBA	TBS + 0.05% (w/v) BSA + 0.02% (w/v) NaN$_3$
Tris buffered saline (TBS)	20 mM Tris-HCl, 150 mM NaCl, pH 7.4
Transfer buffer (western blotting)	192 mM glycine, 25 mM Tris, 20% (v/v) methanol, pH 8.3
Wash buffer (IMAC)	50 mM sodium phosphate buffer, 20 mM imidazol, 300 mM NaCl, pH 8.0
Wash buffer (immunoprecipitation)	50 mM Tris-HCl, 150 mM NaCl, 1mM EGTA, pH 7.4

2.1.5. Bacterial strains

Subcloning Efficiency DH5α Competent Cells (Life Technologies, Invitrogen, Karlsruhe, Germany)

Genotype: F- Φ80*lac*ZΔM15 Δ(*lac*ZYA-*arg*F)U169 *rec*A1 *end*A1 *hsd*R17(r$_{k-}$, m$_{k+}$) *pho*A *sup*E44 *thi*-1 *gyr*A96 *rel*A1 λ-

2.1.6. Cell lines

HEK293T	HEK293 cells constitutively expressing the simian virus 40 (SV40) large T antigen, American Type Culture Collection, Rockville, Maryland , USA
HEK293T sTRAILR1	HEK293T cells stably expressing the soluble extracellular domains of human TRAILR1
HEL293T sTRAILR4	HEK293T cells stably expressing the soluble extracellular domains of human TRAILR4
HeLa	Human cervix carcinoma cell line, American Type Culture Collection, Rockville, Maryland , USA
HeLa R4	HeLa cells stably expressing human TRAILR4
HeLa R4+	HeLa cells stably expressing human TRAILR4 at high levels
HeLa R4ΔC	HeLa cells stably expressing truncated human TRAILR4 fused to eGFP

MF TNFR1$^{-/-}$/TNFR2$^{-/-}$(MF)	Simian virus 40 large T immortalized murine embryonic fibroblasts from TNFR1/TNFR2 double knockout mice (Daniela Männel, University of Regensburg, Germany)
MF R1ΔC-3FLAG / R2ΔC-GFP	MF stably expressing FLAG-tagged truncated human TRAILR1 and truncated human TRAILR2 fused to eGFP
MF R1ΔC-3FLAG / R4ΔC-GFP	MF stably expressing FLAG-tagged truncated human TRAILR1 and truncated human TRAILR4 fused to eGFP
MF R2ΔC-FLAG	MF stably expressing FLAG-tagged truncated human TRAILR2
MF R2ΔC-FLAG / R2ΔC-GFP	MF stably expressing FLAG-tagged truncated human TRAILR2 and truncated human TRAILR2 fused to eGFP
MF R2ΔC-FLAG / R4ΔC-GFP	MF stably expressing FLAG-tagged truncated human TRAILR2 and truncated human TRAILR4 fused to eGFP

2.1.7. Media and supplements

2.1.7.1. Cell culture media, supplements and reagents

10× Trypsin/EDTA	Life Technologies, Gibco, Karlsruhe, Germany
DMEM	Life Technologies, Gibco, Karlsruhe, Germany
Eosine solution	6 mM eosine, 90% (v/v)PBS, 10% (v/v) FCS, 0.02% (w/v) NaN$_3$
Fetal calf serum (FCS)	FCS Standard Quality, EU approved, heat inactivated, PAN Biotech GmbH, Aidenbach, Germany
Freezing medium	90% (v/v) FCS, 10% (v/v) DMSO
HEK293T culture medium	DMEM + 2 mM L-glutamine + 5% FCS

HEK293T selection medium	DMEM + 2 mM L-glutamine + 5% FCS + 4 µg/ml puromycin
HEK293T transfection and expression medium	Opti-MEM, Life Technologies, Gibco, Karlsruhe, Germany
HeLa culture medium	RPMI 1640 + 2 mM L-glutamine + 5% FCS
HeLa selection medium	RPMI 1640 + 2 mM L-glutamine + 5% FCS + 4 µg/ml puromycin or 200 µg/ml Zeocin
MF culture medium	RPMI 1640 + 2 mM L-glutamine + 5% FCS
MF selection medium	RPMI 1640 + 2 mM L-glutamine + 5% FCS + 2 µg/ml puromycin and/or 200 µg/ml Zeocin
Opti-MEM	Life Technologies, Gibco, Karlsruhe, Germany
Penicillin/Streptomycin, 100x	10^4 U/ml penicillin, 10^4 µg/ml streptomycin; Life Technologies, Gibco, Karlsruhe, Germany
RPMI 1640	Life Technologies, Gibco, Karlsruhe, Germany

2.1.7.2. Bacterial media

Liquid broth (LB) medium	0.5% (w/v) yeast extract, 1% (w/v) tryptone, 1% (w/v) NaCl, pH 7.0
LB_{Amp} medium	LB medium + 100 µg/ml ampicilline
LB_{Amp} agar plates	LB_{Amp} medium + 1.5% agar
LB_{Kan} medium	LB medium + 50 µg/ml kanamycin
LB_{Kan} agar plates	LB_{Kan} medium + 1.5% agar
SOC^{++} medium	2% trypton (w/v), 0.5% yeast extract (w/v), 10 mM NaCl, 2.5 mM KCl, 20 mM glucose, 10 mM $MgCl_2$, pH 7.0

2.1.8. Kits

Amine coupling kit	Attana AB, Stockholm, Sweden
Bradford reagent	Bio-Rad Laboratories GmbH, Munich, Germany
Effectene transfection reagent	QIAGEN, Düsseldorf, Germany
Lipofectamine 2000 reagent	Life Technologies, Invitrogen, Karlsruhe, Germany
NucleoBond Xtra Midi	Macherey-Nagel GmbH, Düren, Germany
NucleoSpin Extract II	Macherey-Nagel GmbH, Düren, Germany
NucleoSpin Plasmid	Macherey-Nagel GmbH, Düren, Germany
PathScan Intracellular Signaling Array, Fluorescent readout	Cell Signaling Technology, Danvers, Massachusetts, USA
PCR reagents	KOD HotStart DNA Polymerase Kit containing KOD HotStart DNA Polymerase, 10× PCR buffer, $MgSO_4$ (25 mM) and dNTP mix (2 mM each), Novagen Toyobo, EMD Milipore, Merck, Darmstadt, Germany
SuperSignal West Dura Extended Duration ECL Substrate	Pierce Protein Research Products, Thermo Fisher Scientific, Ulm, Germany
SuperSignal West Pico ECL Substrate	Pierce Protein Research Products, Thermo Fisher Scientific, Ulm, Germany

2.1.9. DNA and protein markers

1 kb DNA Ladder	Life Technologies, Invitrogen, Karlsruhe, Germany
Protein marker, prestained	ColorPlus Prestained Protein Marker, Broad Range (7-175 kDa), New England Biolabs GmbH, Frankfurt am Main, Germany
Protein marker, unstained	PageRuler Unstained Protein Ladder, Fermentas GmbH, St. Leon-Roth, Germany

2.1.10.   Enzymes

Alkaline phosphatase, calf intestinal (CIP)	New England Biolabs GmbH, Frankfurt, Germany
KOD Hot Start DNA Polymerase	Novagen Toyobo, EMD Milipore, Merck, Darmstadt, Germany
T4 DNA Ligase	New England Biolabs GmbH, Frankfurt, Germany

2.1.11.   Restriction enzymes

*Age*I	New England Biolabs GmbH, Frankfurt, Germany
*Bam*HI-HF	New England Biolabs GmbH, Frankfurt, Germany
*Eco*RI	New England Biolabs GmbH, Frankfurt, Germany
*Eco*RI-HF	New England Biolabs GmbH, Frankfurt, Germany
*Eco*RV-HF	New England Biolabs GmbH, Frankfurt, Germany
*Hind*III-HF	New England Biolabs GmbH, Frankfurt, Germany
*Not*I	New England Biolabs GmbH, Frankfurt, Germany
*Sac*I	New England Biolabs GmbH, Frankfurt, Germany
*Xba*I	New England Biolabs GmbH, Frankfurt, Germany
*Xba*I-HF	New England Biolabs GmbH, Frankfurt, Germany

2.1.12.   Cytokines and ligands

sTNF   Soluble recombinant tumor necrosis factor ($2{\times}10^7$ U/mg) provided by Knoll AG, Ludwigshafen, Germany

sTRAIL   Soluble recombinant FLAG-tagged human TRAIL, Enzo Life Sciences, Lörrach, Germany

scTRAIL   Single-chain TRAIL (Schneider et al., 2010), kindly provided by N. Pollak, University of Stuttgart

2.1.13.   Antibodies

2.1.13.1.   Primary antibodies

antibody	name	species	distributor
anti-Akt	40D4	mouse	Cell Signaling Technology, Danvers, Massachusetts, USA
anti-phospho-Akt (Ser473)	D9E	rabbit	Cell Signaling Technology, Danvers, Massachusetts, USA
anti-DYKDDDDK tag	#2368	rabbit	Cell Signaling Technology, Danvers, Massachusetts, USA
anti-FLAG	M2	mouse	Sigma-Aldrich GmbH, Taufkirchen, Germany
anti-GFP	7.1/13.1	mouse	Roche Diagnostics, Mannheim, Germany
anti-IκBα	L35A5	mouse	Cell Signaling Technology, Danvers, Massachusetts, USA
anti-phospho- IκBα (Ser32/26)	5A5	mouse	Cell Signaling Technology, Danvers, Massachusetts, USA
anti-tubulin-α	DM1A	mouse	NeoMarkers, ThermoFisher Scientific, Waltham, Massachusetts, USA
anti-TRAILR1 (FACS)	MAB6347	mouse	R&D Systems, Wiesbaden, Germany
anti-TRAILR1	N-19	goat	Santa Cruz Biotechnology, Santa Cruz, California, USA
anti-TRAILR2 (FACS)	MAB6311	mouse	R&D Systems, Wiesbaden, Germany
anti-TRAILR2	#3696	rabbit	Cell Signaling Technology, Danvers, Massachusetts, USA

anti-TRAILR3 (FACS)	MAB6302	mouse	R&D Systems, Wiesbaden, Germany
anti-TRAILR4 (FACS)	MAB633	mouse	R&D Systems, Wiesbaden, Germany
IgG$_1$ isotype control	MOPC-21	mouse	BD Pharmingen, Heidelberg , Germany
IgG$_{2B}$ isotype control	27-35	mouse	BD Pharmingen, Heidelberg , Germany

2.1.13.2.   Conjugated secondary antibodies

antibody	conjugate	distributor
anti-goat IgG	horse radish peroxidase (HRP)	Santa Cruz Biotechnology, Santa Cruz, California, USA
anti-mouse IgG + IgM (H+L)	fluorescein isothiocyanate (FITC)	Dianova, Hamburg, Germany
anti-mouse IgG + IgM (H+L)	horse radish peroxidase (HRP)	Dianova, Hamburg, Germany
anti-mouse IgG (H+L)	IRDye 800 CW	LI-COR Biotechnology GmbH, Bad Homburg, Germany
anti-mouse IgG + IgM (H+L)	phycoerythrin (PE)	Dianova, Hamburg, Germany
anti-rabbit IgG (H+L)	horse radish peroxidase (HRP)	Dianova, Hamburg, Germany

2.1.14.   Oligonucleotides

Oligonucleotides were purchased from Thermo Hybaid, Schwerte, Germany.

3FLAG for	5'-TTGATAAAGCTTGGATCCGAATTCGATTACAAAGACGATG ACGATAAAGATTACAAAGACGATGACGATAAA-3'
3FLAG rev	5'-ATTATCTAGATCTTTATTTATCGTCATCGTCTTTGTAATCT TTATCGTCATCGTCTTTGTAATCTTTATCGTCATCGTC-3'
pCR3 for	5'-ATAGGGAGACCCAAGCTTGCCACC-3'
R1ΔCF for	5'-ATTCTAGGATCCATGGCGCCACC-3'
R1ΔCF rev	5'-ATTAGAATTCGTCCATGCACTTGGGGTCCC-3'

R2ΔCF for   5'-TAGGATCCATGGAACAACGGGGACAGAACGCC-3'

R2 ΔCF rev   5'-TATCTAGATTACTTATCGTCGTCATCCTTGTAATCACCTT
                   TCAGGTAAGGAAGGACTTTCTTCCACAG-3'

R1ΔCFP rev   5'-ATTAGGATCCCTGTCCATGCACTTGGGGTCCC-3'

R2ΔCFP rev   5'-ATAAGGATCCCGGCCTTTCAGGTAAGGAAGGAC-3'

R4ΔCFP for   5'-CCGCTCGAGCCTCAGACAGTGGTTCAAAG-3'

R4ΔCFP rev   5'-TGAACCGCGGACCACCTGAGCAGATGCCTTT-3'

2.1.15.   Plasmids

pBluescript SK+	Stratagene, Agilent Technologies, Waldbronn, Germany
pBluescript SK+ 3FLAG	pBluescript SK+ containing a sequence encoding three FLAG-tags 5' to a STOP codon.
pBluescript SK+ R1ΔC-3FLAG	pBluescript SK+ vector containing the gene sequence of a truncated human TRAILR1 in frame to the sequence encoding three FLAG-tags at the 3'-end.
pCDNA3.1+	Life Technologies, Invitrogen, Karlsruhe, Germany
pCDNA3.1+ R2ΔC-GFP	pCDNA3.1+ vector containing the gene sequence of a truncated human TRAILR2-eGFP fusion protein
pCDNA3.1+Zeo R4ΔC-GFP	pCDNA3.1+ vector containing the gene sequence of a truncated human TRAILR2-eGFP fusion protein
pEF PGKpuroA (v18)	A. Strasser, The Walter and Eliza Hall Institute of Medical Research, Melbourne, Australia
pCR3 DR4	pCR3 vector containing the gene sequence of a human wild type TRAILR1, kindly provided by H. Wajant, University of Würzburg.
pCR3 DR5	pCR3) vector containing the gene sequence of a human wild type TRAILR2, kindly provided by H. Wajant, University of Würzburg
pEF PGKpuroA (v18) TRAILR4	pEF PGKpuroA (v18) vector containing the gene sequence of a human wild type TRAILR4.

pEF PGKpuropA (v18) R1ΔC-3FLAG	pEF PGKpuroA (v18) vector containing the gene sequence of a truncated human TRAILR1 in frame to the sequence encoding three FLAG-tags at the 3'-end.
pEF PGKpuropA R2ΔC-FLAG	pEF PGKpuroA (v18) vector containing the gene sequence of a truncated human TRAILR2 in frame to the sequence encoding a FLAG-tag at the 3'-end.
pEGFP-N1	Clontech Laboratories, Mountain View, California, USA
pEGFP-N2 TNFR1-ex+TM	pEGFP-N2 vector containing the gene sequence of truncated human TNFR1 in frame to the eGFP ORF (Gerken et al., 2010).
pEGFP-N1 R1ΔC	pEGFP-N1 vector containing the gene sequence of truncated human TRAILR1 in frame to the eGFP ORF.
pEGFP-N1 R2ΔC	pEGFP-N1 vector containing the gene sequence of truncated human TRAILR2 in frame to the eGFP ORF.
pEGFP-N1 R4ΔC	pEGFP-N1 vector containing the gene sequence of truncated human TRAILR4 in frame to the eGFP ORF.
pIRES-puro3	Clontech Laboratories, Mountain View, California, USA
pMA-T	GENEART standard vector: Life Technologies, Invitrogen, Karlsruhe, Germany
pMA-T sTRAILR1	pMA-T vector containing the gene sequence of the soluble extracellular and stem-domain of human TRAILR1 in frame to the sequence encoding a myc- and 6× His-tag at the 3'-end, optimized for expression in human cell lines.
pMA-T sTRAILR4	pMA-T vector containing the gene sequence of the soluble extracellular and stem-domain of human TRAILR4 in frame to the sequence encoding a myc- and 6× His-tag at the 3'-end, optimized for expression in human cell lines.
pmCherry-N1	Clontech Laboratories, Mountain View, California, USA
pmCherry-N1 R1ΔC	pmCherry-N1 vector containing the gene sequence of truncated human TRAILR1 in frame to the mCherry ORF.
pmCherry-N1 R2ΔC	pmCherry-N1 vector containing the gene sequence of truncated human TRAILR2 in frame to the mCherry ORF.

| pmCherry-N1 R4ΔC | pmCherry-N1 vector containing the gene sequence of truncated human TRAILR4 in frame to the mCherry ORF. |
| pSecTag | Vector for the expression of secreted recombinant proteins in mammalian cells. Life Technologies, Invitrogen, Karlsruhe, Germany. |

2.1.16.   Software

argusX1	Biostep, Jahnsdorf, Germany
Attache Office Evaluation Software (Version 3.3.4)	Attana AB, Stockholm, Sweden
Clone Manager 7.04	Scientific & Educational Software, Cary, North Carolina, USA
Fiji	A distribution of ImageJ (Schindelin et al., 2012).
FlowJo 7.6.1	Tree Star Inc., Ashland, Oregon, USA
FRET_Plotter	MATLAB Compiler-generated standalone application to calculate qualitative false-colored FRET images from acceptor photobleaching data, programmed and kindly provided by F. Neugart, University of Stuttgart.
GraphPad Prism 4.03	GraphPad, La Jolla, California, USA
R	A language and environment for statistical computing and graphics (R Development Core Team, 2012).
ZEN 2010 black (LSM software)	Carl Zeiss MicroImaging GmbH, Jena, Germany

2.2. Methods

2.2.1. Cell culture

Mammalian cells were cultivated in DMEM or RPMI1640 medium containing 2 mM L-glutamine supplemented with 5% (v/v) of heat-inactivated fetal calf serum (FCS) and kept in an incubator buffered with 5% CO_2 at 37 °C and 96% relative humidity. For harvesting, culture medium was aspirated, cells were washed with PBS and treated with trypsin/EDTA (0.5 and 0.2 mg/ml, respectively) for about 3 min at 37 °C. As soon as the cells began to detach, trypsin was inactivated by addition of 8 ml of medium and cells were resuspended. Cell number was determined using a Neubauer counting chamber. Beforehand, an aliquot of cells was stained using eosin to stain dead cells. For long term storage about 3×10^6 cells were collected by centrifugation (400 g, 5 min), resuspended in 0.8 ml of freezing medium and transferred into sterile cryovials. To ensure a constant cooling rate when freezing, cryovials were placed in cryoboxes filled with isopropyl alcohol. The cryoboxes containing the vials were then placed in a -80 °C freezer. After 24 to 72 hours, cryovials were removed from the cryoboxes and stored in the vapor phase of liquid nitrogen.

2.2.2. Transfection and generation of stable cell lines

2.2.2.1. Establishment of MF expressing human TRAIL receptor variants

For the generation of cell lines stably overexpressing truncated variants of human TRAIL receptors, 3×10^5 MF$^{-/-}$ cells per well were seeded in 6-well plates and grown overnight. The following day culture medium was replaced by 2 ml of Opti-MEM and cells were further incubated at 37 °C. 8 µl of Lipofectamine 2000 and 2 µg of plasmid DNA were diluted in 250 µl Opti-MEM each and incubated at 20°C - 25 °C for 5 min. Both dilutions were combined and incubated for a further 30 min. The transfection mixture was added drop-wise and cells were returned to the incubator for 6 h. Medium was replaced by standard culture medium and cells were incubated at 37 °C overnight (i.e. for 16 - 18 h). Stably transfected cells were selected using selection medium. After two to three weeks cells were sorted by fluorescence activated cell sorting. Cell sorting was performed two to three times per cell line in total.

In order to obtain MF cells stably expressing two different TRAIL receptor variants, cells were engineered to stably express one receptor variant. Subsequently, this cell

line was transfected with the second variant encoded by an expression plasmid carrying a different selection marker. Cells were again selected for two to three weeks using selection medium containing both antibiotics and subjected to cell sorting to achieve stable expression of both recombinant receptors.

2.2.2.2. Generation of HeLa cells expressing human TRAILR4 and a truncated variant thereof

HeLa cells (3×10^5 per well) were seeded in 6-well plates and incubated overnight. The following day medium was replaced by 1.6 ml fresh culture medium. Transfection was performed using Effectene transfection reagent according to manufacturer's instructions. The transfection mixture consisted of 0.5 µg DNA, 4 µl of enhancer and 12 µl of Effectene in 100 µl Buffer EC. Transfection complexes were diluted to a total volume of 700 µl using standard cell culture medium. Diluted complexes were added to the cells. After 24 h medium was replaced by appropriate selection medium. Selection was performed for two to four weeks. Cells were sorted two to four times by flow cytometry to obtain a homogenous cell population.

2.2.2.3. Establishment of HEK293T cells stably expressing soluble ECDs of TRAILR1 and TRAILR4

HEK293T cells (8×10^5 per well) were seeded in 6-well plates and incubated overnight. The following day the culture medium was replaced by 2 ml of Opti-MEM and cells were further incubated at 37 °C. 8 µl of Lipofectamine 2000 and 2 µg of plasmid DNA were diluted in 250 µl Opti-MEM each and incubated for 5 min. Both dilutions were combined and incubated for a further 30 min at 20 - 25 °C. The transfection mixture was added drop-wise and cells were returned to the incubator for 6 h. Medium was replaced by standard culture medium and cells were incubated at 37 °C overnight. Stably transfected cells were selected using selection medium.

2.2.2.4. Limiting dilution

Single cell clones from a pool of stably transfected HEK293T sTRAILR1 and HEK293T sTRAILR4 cells were obtained by limiting dilution. Therefore cells were harvested, the concentration was determined using a Neubauer counting chamber and the cell suspension was diluted to a density of 10 cells per ml in selection medium. 100 µl of cell suspension were transferred into each well of a 96-well tissue

culture plate. Plates were incubated for several weeks at 37 °C, 5% CO_2 and 96% relative humidity and checked regularly for individual clones. Clones that had grown dense enough were transferred to 12-well plates and protein expression was checked by western blot analysis of the cell culture supernatant. Clones showing the best production were further expanded and used for larger scale protein production.

2.2.2.5. Transient transfection

To obtain $MF^{-/-}$ cells transiently expressing truncated variants of human TRAIL receptors fused to eGFP or mCherry, 1.5×10^5 cells were seeded on 18×18 mm coverslips and grown overnight. The following day medium was replaced by 0.5 ml of Opti-MEM and cells were transfected using Lipofectamine 2000. 0.5 μg of plasmid DNA encoding the receptor-eGFP fusion-protein and 0.25 μg plasmid DNA encoding the receptor-mCherry fusion protein were combined in 50 μl of Opti-MEM. Lipofectamine 2000 (3 μl) was diluted in 50 μl Opti-MEM. After 5 min incubation both dilutions were combined and incubated for 30 min at 20 – 25 °C. The transfection complexes were added drop-wise and the cells were incubated for 6 h at 37 °C. Transfection medium was removed by aspiration and 1 ml of culture medium was added. After 24 hours cells were washed with PBS and fixed for 15 min at 20 - 25 °C using 4% PFA in PBS.

2.2.3. Production and purification of soluble TRAIL receptors

Single cell clones from HEK293T sTRAILR1 and HEK293T sTRAILR4 were expanded into large tissue culture flasks (175 cm^2) and grown until they reached 90% confluency. Cells were then washed with PBS and 25 ml of Opti-MEM were added to each flask. Cells were incubated for three days before the supernatant was collected and fresh Opti-MEM was added. Supernatants were pooled, centrifuged at 4000 *g* for 10 min and stored at 4 °C.

Recombinant proteins were purified by immobilized metal affinity chromatography (IMAC). HisTrap FF columns were prepared as recommended by the manufacturer. Supernatants and buffers were added onto the column using a peristaltic pump at a flow rate of 1 ml/min. Supernatants were supplemented with 20 mM imidazole to decrease unspecific binding to the column and to adjust the pH value. After loading, the column was washed three times with 5 ml of wash buffer. Bound proteins were eluted in 10 fractions of 500 μl elution buffer each. Fractions were analyzed by SDS-

Page and silver staining. The fractions containing protein of the expected molecular weight were pooled and dialyzed against PBS using dialysis tubes. Dialyzed protein was sterilized by filtration and protein concentration was determined by measuring absorbance at 280 nm using the Nanodrop UV-spectrophotometer.

2.2.4. Molecular biology

2.2.4.1. Cloning of truncated and soluble variants of human TRAIL receptors

The gene sequence encoding the truncated variants of human TRAIL receptors was obtained after amplification by polymerase chain reactions (PCR) using appropriate primers (see 2.1.14 for a list of oligonucleotides used) and plasmids (see 2.1.15) and sequencing of the PCR products.

For the generation of R1ΔC-3FLAG the nucleotide sequence coding for three FLAG-tags followed by a STOP codon was inserted into the multiple cloning site of pBluescript SK+ in a first step. Therefore, the oligonucleotides 3FLAG for and 3FLAG rev were annealed and elongated using a standard PCR reaction mix (Table 1) and PCR program 1 (Table 2). The obtained DNA fragment was purified by agarose gel electrophoresis and isolated from the gel using NucleoSpin Extract II kit. The purified fragment was ligated into pBluescript SK+ after restriction digest with *Hind*III-HF and *Xba*I-HF yielding the plasmid pBluescript SK+ 3FLAG. Nucleotide sequence was verified by DNA sequencing. Subsequently, the nucleotide sequence of human TRAILR1 (amino acids 1-278) was amplified from the plasmid pCR3 DR4 using primers R1ΔCF for and R1ΔCF rev and the PCR program 2 (Table 3). The obtained fragment was inserted into pBluescript SK+ 3FLAG using the restriction endonucleases *Bam*HI-HF and *Eco*RI-HF. The resulting plasmid, pBluescript SK+ R1ΔC-3FLAG, was sequentially digested using *Bam*HI-HF and *Not*I, and the R1ΔC-3FLAG fragment ligated into the vector pSecTag, which was merely used as a shuttle vector to obtain appropriate restriction endonuclease cleavage sites at the 5'- and 3'-ends of R1ΔC-3FLAG. Accordingly, R1ΔC-3FLAG was excised from pSecTag R1ΔC-3FLAG using *Bam*HI-HF and *Xba*I and inserted into pEF PGKpuropA (v18).

For the amplification of R2ΔC-FLAG the primer pair R2ΔCF for and R2ΔCF rev was used and the plasmid pCR3 DR5 served as template. A standard PCR reaction mix (Table 1) and PCR program 3 (Table 4) was used. Length of the obtained PCR product was verified by electrophoresis on 1% agarose gel using 1 kb DNA Ladder as marker and EtBr-staining for visualization of DNA fragments. The band with the

expected length was excised from the gel and extracted using NucleoSpin Extract II Kit. The R2ΔC-FLAG fragment was digested using the restriction endonucleases *Bam*HI-HF and *Xba*I-HF and ligated into pEF PGKpuropA (v18).

Plasmids encoding for the truncated variants of TRAILR1 and TRAILR2 fused to the fluorescent proteins eGFP or mCherry were generated as follows. Nucleotide sequences encoding for the desired domains were amplified by PCR using pCR3 DR4 as template for TRAILR1-fusion proteins and pCR3 DR5 for TRAILR2 fusions. The used PCR program is given in Table 3 and the primers used were pCR3 for and R1ΔCFP rev for TRAILR1 and pCR3 for and R2ΔCFP rev for TRAILR2. Length of the amplified fragments was examined by agarose gel electrophoresis and EtBr staining. DNA fragments of the expected length were excised and isolated from the gel using Nucleo Spin Extract II kit. They were digested using restriction endonucleases *Bam*HI-HF and *Hind*III-HF and ligated into the plasmids pEGFP-N1 and pmCherry-N1, which had been linearized by digestion using the same restriction endonucleases. Plasmid pEGFP-N1 R4ΔC and pmCherry-N1 R4ΔC were constructed after amplification using pEF PGKpuropA (v18) TRAILR4 as template and R4ΔCFP for and rev as primers. The obtained fragment was ligated into pEGFP-N1 or pmCherry-N1 after digestion with the restriction enzymes *Sac*I and *Age*I. For stable expression in mammalian cells, R2ΔC-GFP and R4ΔC-GFP were subcloned from pEGFP-N1 into pCDNA3.1+ using *Hind*III and *Not*I, resulting in the plasmids pCDNA3.1+ R2ΔC and pCDNA3.1+ R4ΔC.

The gene sequences of soluble TRAIL receptor variants sTRAILR1 and sTRAILR4 were synthesized with optimized codon usage for the expression in human cells and provided in the vector pMA-T with the restriction endonuclease sites *Eco*RV and *Bam*HI by GeneArt. Both constructs were excised and inserted into the bicistronic expression plasmid pIRESpuro3 using *Eco*RV-*HF* and *Bam*HI-HF.

All vector sequences were verified by DNA sequencing. See appendix for plasmid maps and amino acid sequences of constructs described here.

2.2.4.2. Polymerase chain reaction

Specific DNA fragments were amplified by polymerase chain reaction (PCR). All polymerase chain reactions were performed using the reaction mix given in Table 1.

Table 1: PCR reaction mix

Reagent	Volume
DNA template (10 ng/µl)	3.0 µl
forward primer (100 pmol/µl)	0.2 µl
reverse primer (100 pmol/µl)	0.2 µl
dNTPs (2 mM each)	5.0 µl
KOD HotStart DNA Polymerase (1 U/µl)	1.0 µl
MgSO$_4$ (25 mM)	2.5 µl
10× PCR buffer	5.0 µl
ddH$_2$O	*ad* 50 µl

Table 2: PCR program 1 for annealing and amplification of 3FLAG for and rev oligonucleotides

Step	Temperature	Time	Cycles
Initial denaturation	95 °C	5 min	1
Denaturation	95 °C	30 s	
Annealing	58 °C	15 s	35
Elongation	72 °C	10 s	
Final elongation	72 °C	5 min	1

Table 3: PCR program 2 (touch-down PCR) for the amplification of truncated fragments of human TRAILR1, TRAILR2 and TRAILR4 for further cloning

Step	Temperature	Time	Cycles
Initial denaturation	95 °C	10 min	1
Denaturation	95 °C	1 min	
Annealing	69 °C	30 s	
	Annealing temperature was decreased by 0.5 K per cycle		18
Elongation	72 °C	1 min	
Denaturation	95 °C	1 min	
Annealing	60 °C	30 s	12
Elongation	72 °C	1 min	
Final elongation	72 °C	5 min	1

Table 4: PCR program 3 for the amplification of R2ΔC-FLAG

Step	Temperature	Time	Cycles
Initial denaturation	95 °C	5 min	1
Denaturation	95 °C	1 min	
Annealing	60 °C	30 s	30
Elongation	72 °C	1 min	
Final elongation	72 °C	10 min	1

2.2.4.3. Agarose gel electrophoresis and DNA extraction from gels

For analysis and purification of nucleic acids horizontal agarose gel electrophoresis was performed. Samples were mixed with 6× DNA sample buffer and separated on agarose gels containing 0.7 - 2% agarose and 1 µg/ml ethidiumbromide in TAE buffer. Gels were run at 80 – 100 V for 60 – 90 min. DNA bands were visualized under UV light. For gel purification of DNA fragments, bands of correct size were excised and isolated from the gel slice using Nucleo Spin Extract II kit according to the manufacturer's protocol. DNA was eluted using 25 µl ddH$_2$O.

2.2.4.4. Restriction digestion and ligation

1 µg of DNA (plasmid or purified PCR product) was incubated with 10 U of restriction enzyme(s) in appropriate buffer (according to manufacturer's instructions) for 2 hours at 37 °C in a total volume of 50 µl. For sequential digests, DNA was precipitated using isopropanol after the first restriction nuclease treatment, resuspended in ddH$_2$O and the second restriction digestion was set up. To avoid vector religation, 5 U of CIP was added to the reaction mix and incubated for 30 min at 37 °C. Digested DNA was purified by agarose gel electrophoresis and isolated using NucleoSpin Extract II kit. For ligation the dephosphorylated vector and the insert were combined at a molar ratio between 1:3 and 1:6. Ligation was performed according to manufacturer's instructions for 2 hours at 20 – 25 °C using 5 U of T4 DNA ligase in a total volume of 20 µl.

2.2.4.5. Transformation and plasmid isolation from *E. coli*

Chemical competent *Escherichia coli* DH5α (50 µl) were transformed using 5 µl of ligation reaction or approximately 100 ng of super-coiled plasmid. *E. coli* were thawed on ice. DNA was added and *E. coli* were incubated for 30 min. The cells were heat shocked for 20 s at 42 °C and cooled down on ice for 2 min. 500 µl of prewarmed SOC^{++} medium was added and the cells were incubated for 1 h at 37 °C to allow for the expression of the selection marker. Cells were collected by centrifugation and spread on LB-agar plates containing appropriate selection antibiotic. Plates were incubated overnight at 37 °C. Single clones were isolated and used to inoculate 2 ml LB containing selection antibiotic which were then incubated at 37 °C and 180 rpm for 16 – 18 h. Bacterial cells were harvested by centrifugation and plasmid DNA was isolated using Nucleo Spin Plasmid kit according to manufacturer's instructions. DNA was eluted using 30 µl of ddH$_2$O and concentration and purity were determined by UV-absorption. Identity of the isolated plasmids was confirmed by control digestion and sequence integrity of the insert was confirmed by DNA sequencing using appropriate primers (GATC Biotech, Konstanz, Germany). For larger scale isolation of plasmid DNA a single bacterial colony was inoculated into 100 ml of LB medium containing the appropriate selection antibiotic and incubated for 16 – 18 h at 37 °C and 180 rpm. The following day the cells were harvested by centrifugation and plasmid DNA was isolated using NucleoBond Xtra Midi kit according to

manufacturer's protocol. DNA was eluted using ddH$_2$O and purity and concentration of the DNA were determined by UV-absorption.

2.2.5. Cytotoxicity assays

To compare the TRAIL sensitivity of various cell lines, 2×10^4 cells/well were seeded into 96-well flat bottom tissue culture plates and incubated overnight (i.e. 16 - 18 h). The following day they were treated with serial dilutions of antibody crosslinked FLAG-tagged human recombinant sTRAIL in presence of 0.5 µg/ml cycloheximide (CHX). Each treatment was performed in triplicates. Antibody-crosslinking of FLAG-tagged sTRAIL was achieved by incubation with murine anti-FLAG antibody (M2) for 1 h at 37 °C. The final concentrations of sTRAIL and M2 antibody were 300 ng/ml and 1 µg/ml, respectively. Where indicated, cells were treated for 1 h with the pan-caspase-inhibitor zVAD-fmk (20 µM) before addition of sTRAIL + M2. Cell viability was determined after 24 h by crystal violet staining. Therefore the supernatant was discarded and the cells were incubated with 50 µl crystal violet solution per well for 15 min at 20 – 25 °C. Plates were gently washed with water and air dried. Stained cells were dissolved in 50 µl methanol per well. The absorbance was measured at 550 nm using a plate reader. Values were normalized to the untreated control.

2.2.6. SDS-Page and western blot analysis

2.2.6.1. SDS-Page

For protein separation, discontinuous Tris-glycine SDS-Page was performed using a vertical gel electrophoresis chamber. Resolving gels contained 8 to 15% of acrylamide, depending on the proteins analyzed, stacking gels contained 4.5% acrylamide. SDS-loading buffer containing 5% (final concentration) of β-mercaptoethanol was added to the samples, and they were boiled at 96 °C for 5 min. Mini-gels were run at 35 mA (1.5 mm thickness) or 25 mA (1 mm thickness) for approximately 90 min, maxi-gels were run at 45 mA for 4 to 5 hours. Gels were then subjected to western blotting or silver staining according to the manufacturer's instructions.

2.2.6.2. Western blot analysis

Separated proteins were transferred onto nitrocellulose membranes using a semi-dry blotting chamber for 90 min at 1.5 mA/cm^2. When the unstained high-precision protein marker was used, the membranes were stained using Ponceau S solution to visualize the bands of the molecular weight standard. After removal of the Ponceau staining by washing in PBS, membranes were blocked by incubation in either 5% (w/v) non-fat milk powder dissolved in PBST (PBS + 0.05% Tween-20), 1× Roche Blocking Reagent or 5% BSA in TBST (TBS + 0.1% Tween-20), depending on the primary antibody for one hour at 20 – 25 °C. Subsequently membranes were washed three times for 5 min at 20 – 25 °C using PBST or TBST. The blots were then incubated with the primary antibody, diluted in PBA or TBA, for 12 to 20 hours at 4 °C on a horizontal shaker. The following day, blots were washed again (3×5 min) with PBST or TBST. Horseradish peroxidase (HRP) coupled secondary antibodies were diluted in PBST or TBST according to the manufacturer's instructions. IRDye-coupled secondary antibodies were diluted in PBA. After 1 h incubation at 20 – 25 °C on a horizontal shaker blots were washed three times for five minutes. Blots were either detected using X-ray films after incubation with enhanced chemiluminescent (ECL) substrate (HRP-coupled secondary antibodies) or scanned using the Li-Cor Odyssey (IRDye-coupled secondary antibodies). In general, loading controls were detected using IRDye-coupled secondary antibodies and the Li-Cor Odyssey system, while all other western blot analyses were performed using HRP-coupled antibodies and ECL. For reprobing, membranes were stripped by incubation for 5 min at 20 – 25 °C in ddH$_2$O, followed by 5 min incubation in 0.2 M NaOH and again 5 min in ddH$_2$O. Membranes were then blocked again and incubate with primary antibody.

2.2.7. Chemical crosslinking of proteins

$1×10^6$ cells were seeded in 6 cm cell culture dishes and incubated for 16 – 18 h. The following day, cell culture medium was removed by aspiration, and the cells were washed in ice-cold PBS. Subsequently, the cells were incubated for 30 minutes on ice with the freshly dissolved crosslinking reagent bis-(sulfosuccinimidyl)-suberate in PBS. The used crosslinker concentrations ranged from 0 to 1000 µM. The reaction was stopped by addition of 10 mM Tris-HCl (pH 7.0).

Crosslinking of soluble proteins was performed by combining soluble protein with the two-fold concentrated fresh made solution of bis-(sulfosuccinimidyl)-suberate in PBS. Samples were incubated on ice for 30 min and the reaction was stopped by addition of 10 mM Tris-HCl (pH 7.0).

2.2.8. Preparation of whole cell lysates

Cells were harvested and resuspended in an appropriate volume of lysis buffer freshly supplemented with 1× complete protease-inhibitor and 1× PhosSTOP phosphatase-inhibitor cocktails followed by incubation on ice for 5 min. Lysates were briefly sonicated and centrifuged at 16,000 g and 4 °C for 15 min. Supernatants were transferred to a new micro-reaction tube and the protein concentration was determined by Bradford assay according to the manufacturer's protocol. For western blot analysis, 50 µg of total protein was used.

2.2.9. Immunoprecipitation

$3×10^6$ cells were seeded in 10 cm tissue culture dishes and cultivated over-night. The following day cells were treated with chemical crosslinker or left untreated. Subsequently cells were washed with PBS and harvested using a cell scraper. Cells were collected by centrifugation (400 g, 5 min) and homogenized in 200 µl lysis buffer supplemented with 1× complete protease-inhibitor for 30 min on ice. Lysates were centrifuged (10 min, 16.000 g, 4 °C) and supernatants were transferred to new micro-reaction tubes. Protein concentration was determined by Bradford assay as described by the manufacturer. 1 mg of total protein was incubated with 5 µg anti-FLAG M2 antibody for 2 h at 4 °C. Immunocomplexes were precipitated with Protein G Sepharose (50 µl) for 16 h at 4 °C. Precipitates were washed four times with wash buffer. For the elution of bound proteins, the precipitates were resuspended in SDS sample buffer containing 5% of β-mercaptoethanol and boiled at 96 °C for 5 min. Eluted proteins were then subjected to SDS-Page and analyzed by western blot.

2.2.10.   Flow cytometry

2.2.10.1.   Flow cytometric analysis of cell surface protein expression

Cells were harvested and washed once in ice-cold PBA. 2×10^5 cells were resuspended in 100 µl of PBA containing 4 µg/ml of the appropriate primary antibody. For isotype control, cells were incubated with 4 µg/ml control antibody of the corresponding isotype. Negative control consisted of cells which were incubated in PBA alone. After 1 h incubation on ice cells were pelleted by centrifugation (400 g, 5 min) and washed once in PBA. Anti-mouse IgG-FITC secondary antibody was diluted to a final concentration of 7.5 µg/ml, anti-mouse IgG-PE antibody to 5 µg/ml in PBA. Cells were resuspended in PBA containing the appropriate secondary antibody and incubated on ice for 45 min. Subsequently cells were washed again with PBA, resuspended in 400 µl of PBA and transferred to FACS tubes. Cells were then analyzed using Beckman Coulter Cytomics FC500 and appropriate acquisition protocols. Data analysis was performed using FlowJo 7.6.1. Results are presented as biexponential (logicle) histogram plots. Mean fluorescence intensities (MFI) of antibody stained samples were background corrected by subtracting MFI of the respective IgG-isotype control.

2.2.10.2.   Cell sorting

For fluorescence activated cell sorting 3×10^6 cells were incubated for 1 h with 4 µg/ml TRAIL-receptor specific antibody. Cells were pelleted by centrifugation, washed once in ice-cold PBS and resuspended in 1 ml of PBA containing 7.5 µg/ml anti-mouse IgG-FITC or 5 µg/ml anti-mouse IgG-PE secondary antibody. After 45 min cells were washed again and resuspended in 3 ml of PBA. Cell sorting was performed using Becton Dickinson FACS Vantage SE with FACSDiVa. Parameters were chosen to obtain maximal purity. Cells were collected in 3 aliquots (3×10^4 cells each) in 5 ml medium containing penicillin/streptomycin.

2.2.11.   Confocal laser scanning microscopy

Confocal laser scanning microscopy was performed using a Zeiss LSM710 equipped with a Zeiss Plan-Apochromat 63x/1.40 DIC M27 oil immersion objective.

2.2.11.1.   Acceptor photobleaching FRET

Protein-protein interactions were investigated by fluorescence resonance energy transfer. Therefore, cells were seeded and transiently transfected as described in 2.2.2.5. Transfected cells were washed with PBS and fixed using 4% PFA in PBS for 15 min at 20 - 25 °C. Coverslips were then mounted onto microscopy slides using Fluoromount G.

GFP was excited with the 488 nm line of the argon laser and fluorescence was detected at 490 – 550 nm. mCherry was excited with the 561 nm line of a diode-pumped solid state laser and fluorescence was detected at 570 – 650 nm. The imaging sequence was as follows: First donor and acceptor-channels were sequentially scanned at low laser intensity. Subsequently, the acceptor was bleached with the 561 nm laser line at 75% intensity. Finally, donor and acceptor channels were again scanned at low laser intensity. Acquired images were exported to 8-bit TIFF format using Zeiss ZEN 2010 software. For analysis of FRET efficiency, images were imported into Fiji and FRET efficiency was calculated using the ImageJ plug-in FRETcalc version 4.0 (Stepensky, 2007). False-colored FRET images for illustration purposes were calculated using the MATLAB standalone application FRET_Plotter.

2.2.12.   Quartz crystal microbalance measurements

Affinities of sTRAILR1 and sTRAILR4 to each other and the ligand scTRAIL were determined by quartz crystal microbalance measurements using an Attana A-100 C-Fast system. sTRAILR1 or sTRAILR4 were chemically immobilized to a low non-specific-binding carboxyl sensor chip using an amine coupling kit according to the manufacturer's protocol. Proteins were immobilized to a density resulting in a signal increase of 60 - 85 Hz. Experiments were performed in PBS + 0.1% Tween-20, pH 7.4 at a flow rate of 25 µl/min. For regeneration of the chip two injections of 25 µl NaOH (50 mM) were performed. Before each measurement, the baseline oscillation of the chip was recorded and subtracted from the binding curve. Attester 3.0 (Attana

AB, Stockholm, Sweden) was used for data collection. Data analysis was performed using Attache Office Evaluation Software.

2.2.13. Intracellular Signaling Array

The PathScan Intracellular Signaling Array was performed as described by the manufacturer. Cells (5×10^5) were seeded in 6 cm cell culture dishes. After 24 hours cells were washed three times with PBS and the medium was replaced with RPMI1640 containing 2 mM L-glutamine supplemented with 0.5% (v/v) FCS. Cells were cultured under reduced serum conditions for 18 h. Subsequently, they were treated with 300 ng/ml sTRAIL (previously crosslinked by incubation with 1 µg/ml anti-FLAG M2 antibody for 1 h at 37 °C) for the indicated times or left untreated. Cells were harvested, lysates were prepared and the protein concentration was determined by Bradford assay. Protein concentration of all samples was adjusted to 0.5 mg/ml. Samples were incubated on the array slides for two hours at 20 - 25 °C. Fluorescent images of the slides were captured using the Li-Cor Biotechnology Odyssey system. TIFF files (8 bit) were exported and pixel intensities were quantified using Fiji and the ImageJ plug-in Protein Array Analyzer (Carpentier, 2010).

2.2.14. Quantitative and statistical analyses

2.2.14.1. Densitometry

For quantification of western blot results X-ray films were scanned at high resolution and integrated optical densities were calculated using Fiji. Integrated optical densities were corrected for background signals.

2.2.14.2. General statistics

GraphPad Prism 4.03 was used for statistical analysis of experimental data. Significance was tested by one-way or two-way analysis of variance (ANOVA) in combination with Bonferroni post-test; p-values < 0.05 were considered significant as denoted by asterisk (*). Further significance levels were $p < 0.01$ (**) and $p < 0.001$ (***).
Heatmap analysis of antibody array data was performed using R (R Development Core Team, 2012).

3. Results

3.1. Ligand-independent oligomerization of human TRAIL receptors

3.1.1. Fluorescence resonance energy transfer analysis of receptor-receptor interactions

The group of TNF-related apoptosis-inducing ligand (TRAIL) and its receptors has gained significant interest in the scientific community in the past decades. This is mainly due to the fact that the ligand TRAIL has been shown to be capable to specifically induce apoptosis in susceptible tumor-derived cell lines (or primary tumor cells), while most untransformed cells or cell lines are resistant to the apoptotic effects of TRAIL. The signaling events leading to apoptosis induction are relatively well understood. However, the early events in TRAIL-mediated signaling, e.g. the configuration of the diverse receptors on the cellular membrane, are only poorly elucidated and some aspects remain controversial.

In order to clarify the potential ligand-independent oligomerization of TRAIL receptors on the plasma membrane, which had previously been shown for other members of the TNF receptor superfamily, fluorescence resonance energy transfer (FRET) experiments were performed. Therefore, the extracellular and transmembrane domains of TRAILR1, TRAILR2 and TRAILR4 were cloned and expressed as fusion proteins either to the enhanced green fluorescent protein (eGFP) or to the monomeric red fluorescent protein mCherry (Figure 3).
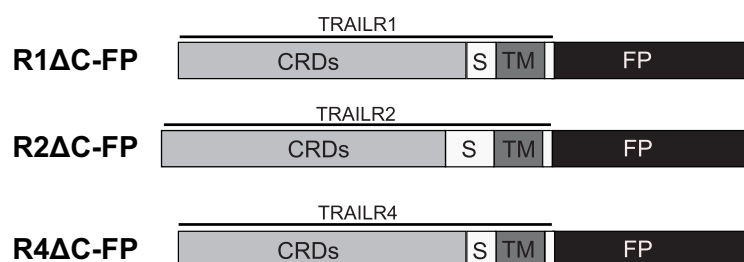

Figure 3: Schematic depiction of the TRAIL receptor fusion proteins used in the FRET experiments. The extracellular cysteine-rich domains (CRDs), the so-called stem (S) and the transmembrane domain (TM) as well the first 14 intracellular amino acids were fused to the amino-terminus of a fluorescent protein (FP). TRAIL receptor fusion proteins to eGFP served as FRET donors, while fusions to mCherry acted as FRET acceptors.

The eGFP fusion proteins served as FRET donors whereas the mCherry fusions acted as FRET acceptors. Plasmids encoding for donor/acceptor pairs of these fusion proteins were cotransfected into immortalized murine embryonic fibroblasts (MF). Expression and subcellular localization were verified microscopically. All receptor fusion proteins localized predominantly to the plasma membrane, with some fluorescence also being detected at intracellular membranes representing most likely the endoplasmic reticulum and the Golgi apparatus. The occasional detection of a fluorescent signal in the cytoplasm is most probably caused by the presence of free molecules of the fluorescent proteins. Ligand-independent interactions of the receptors were assessed by acceptor photobleaching FRET experiments, where an increase in donor fluorescence after selective bleaching of the acceptor fluorophore serves as a quantitative measure of energy transfer efficiency (Figure 4).
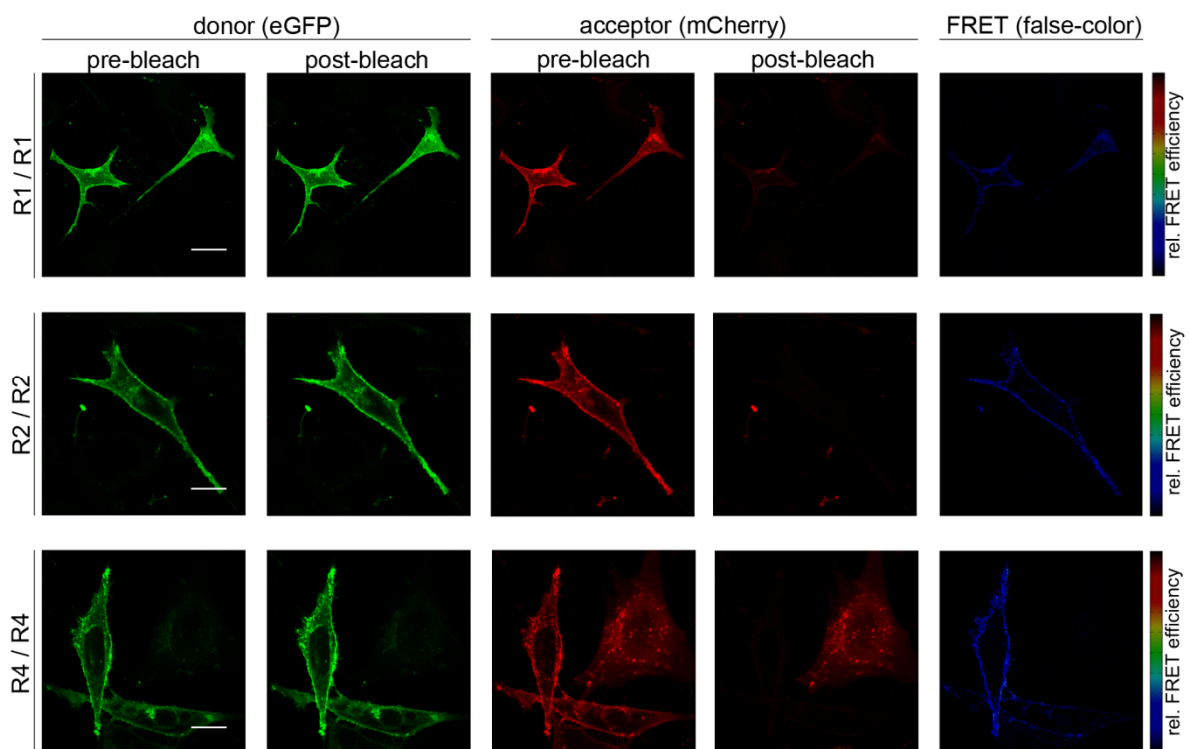

Figure 4: Acceptor photobleaching FRET reveals homophilic interactions of TRAIL receptors. Immortalized murine embryonic fibroblasts (MF) were transiently transfected with plasmids encoding the fusion proteins R1ΔC-GFP and R1ΔC-mCherry (R1/R1), R2ΔC-GFP and R2ΔC-mCherry (R2/R2) or R4ΔC-GFP and R4ΔC-mCherry (R4/R4). Transfected cells were cultivated for 24 h before being fixed with 4% PFA. Images shown are optical sections obtained by confocal laser scanning microscopy; scale bar = 20 μm. False-colored FRET images were calculated using FRET_Plotter and show relative FRET efficiencies.

In a first set of experiments homotypic interactions of the death receptors of the TRAIL family, receptors 1 and 2, were assessed. TNF receptor 1 (TNFR1), another member of the TNF receptor superfamily served as negative control. TNFR1 has been shown to undergo homotypic oligomerization via its pre-ligand binding assembly domain (PLAD). However it is not expected to interact specifically with TRAIL receptors. The extracellular and transmembrane domains of TNFR1 were fused to eGFP and coexpressed with either R1ΔC-mCherry or R2ΔC-mCherry. Neither of these control FRET pairs showed any specific FRET signals (FRET efficiency: 1.3 ± 1.3% for TNFR1-ΔCyt-GFP/R1ΔC-mCherry; 0.2 ± 2.5% for TNFR1-ΔCyt-GFP/R2ΔC-mCherry; mean ± SD, n = 6). In contrast, for the receptor combination R1ΔC-GFP/R1ΔC-mCherry a mean FRET efficiency of 8.0 ± 3.4% was obtained (Figure 6). In all imaged cells, the strongest FRET signal was observed at the cell membrane. However, in several cases a weak signal was also detected at intracellular structures. This can be explained by the interaction of receptors at intracellular membranes. Hereafter, homotypic oligomerization of the second death receptor in the TRAIL system, TRAILR2, was investigated. Therefore expression plasmids encoding the recombinant fusion proteins R2ΔC-GFP and R2ΔC-mCherry were cotransfected into MF cells. Acceptor photobleaching experiments yielded a mean FRET efficiency of 24.9 ± 5.0% (representative image is shown in Figure 4) for the interaction of these receptor fusion proteins. In subsequent experiments the ligand-independent homo-oligomerization of TRAILR4 was investigated (Figure 4). TRAILR3 was omitted from these studies as it is devoid of any intracellular and transmembrane domains. Thus the here conducted experimental approach was not feasible for this specific receptor. FRET by acceptor photobleaching yielded positive results also for the combination of the two fusion proteins R4ΔC-GFP and R4ΔC-mCherry. The mean FRET efficiency obtained in these experiments was 15.5 ± 2.8%, demonstrating that also TRAILR4 is capable to form oligomers in absence of its ligand.

Heterotypic interactions between death and decoy receptors could severely impact the outcome of TRAIL-mediated signaling through the pre-formation of mixed complexes of receptors comprising both functional death domains (TRAILR1 or TRAILR2) as well as non-functional or truncated death domains (TRAILR4). The potential occurrence of TRAIL receptor hetero-oligomers was elucidated through a

second set of FRET experiments. Initially, the interaction characteristics of the two TRAIL death receptors were assayed (Figure 5).
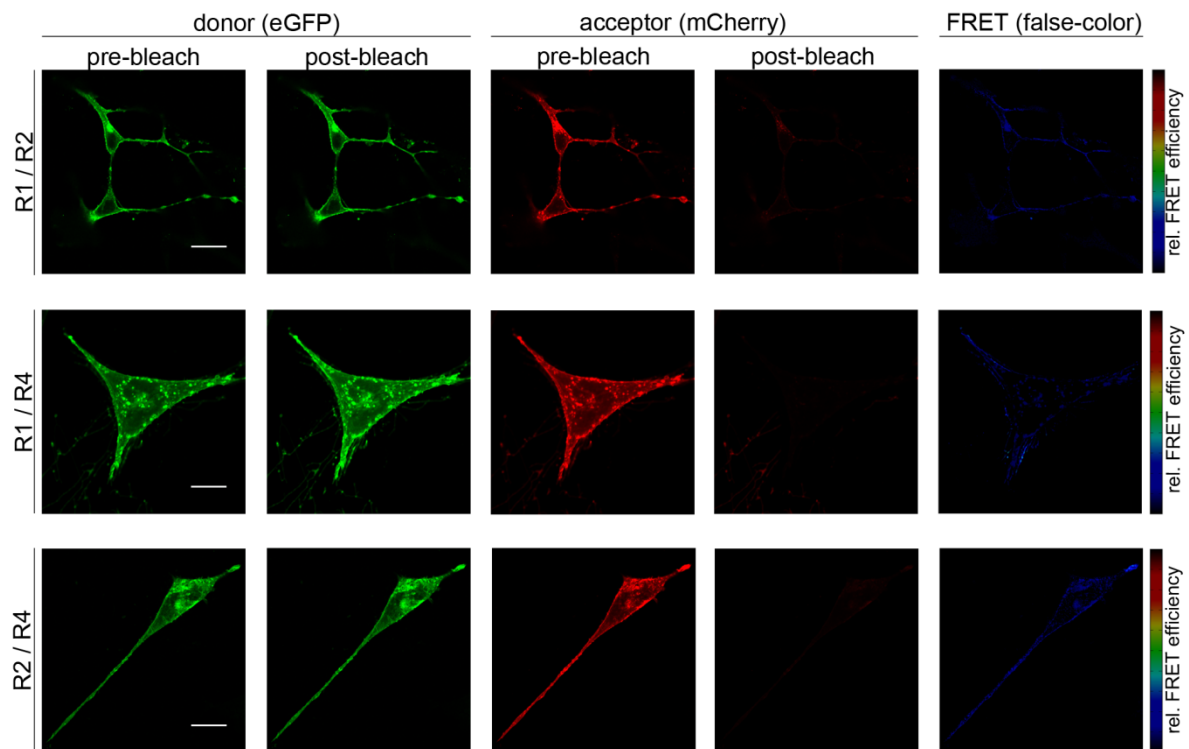

Figure 5: Heterotypic interactions of TRAIL receptors. Murine embryonic fibroblasts (MF) from TNFR1$^{-/-}$/TNFR2$^{-/-}$ mice were transiently transfected with plasmids encoding the fusion proteins R1ΔC-mCherry and R2ΔC-GFP (R1/R2), R1ΔC-mCherry and R4ΔC-GFP (R1/R4) or R2ΔC-mCherry and R4ΔC-GFP (R2/R4). Transfected cells were cultivated for 24 h before being fixed with 4% PFA. Images shown are optical sections obtained by confocal laser scanning microscopy; scale bar = 20 μm. False-colored FRET images were calculated using FRET_Plotter and show relative FRET efficiencies.

Coexpression of fusion proteins of the two death receptors TRAILR1 (fused to the amino-terminus of mCherry, thus serving as FRET acceptor) and TRAILR2 (fusion to eGFP) yielded a mean FRET efficiency of 9.4 ± 0.6% (mean ± SD). Inferring from this observation, TRAIL death receptors are not only capable of forming homomeric complexes, but also mixed complexes through heterotypic interactions. While the pre-aggregation of the two different TRAIL death receptors presumably still yields signaling competent complexes after ligand stimulation, heterotypic oligomerization of death and decoy receptors could have detrimental effects on apoptosis induction via TRAIL receptors. In fact, the performed FRET experiments confirmed ligand-independent interactions of both death receptors, TRAILR1 and TRAILR2 (Figure 5; middle and last row, respectively), with the so-called decoy receptor TRAILR4. The

FRET efficiencies obtained for both combinations of death and decoy receptor were overall similar. The heterotypic interaction of TRAILR1 (as fusion protein R1ΔC-mCherry) and TRAILR4 (R4ΔC-GFP) resulted in a FRET efficiency of 10.7 ± 5.0% (mean ± SD). For the hetero-oligomerization of TRAILR2 and TRAILR4 the measured FRET efficiency was 10.6 ± 2.7% (Figure 6).
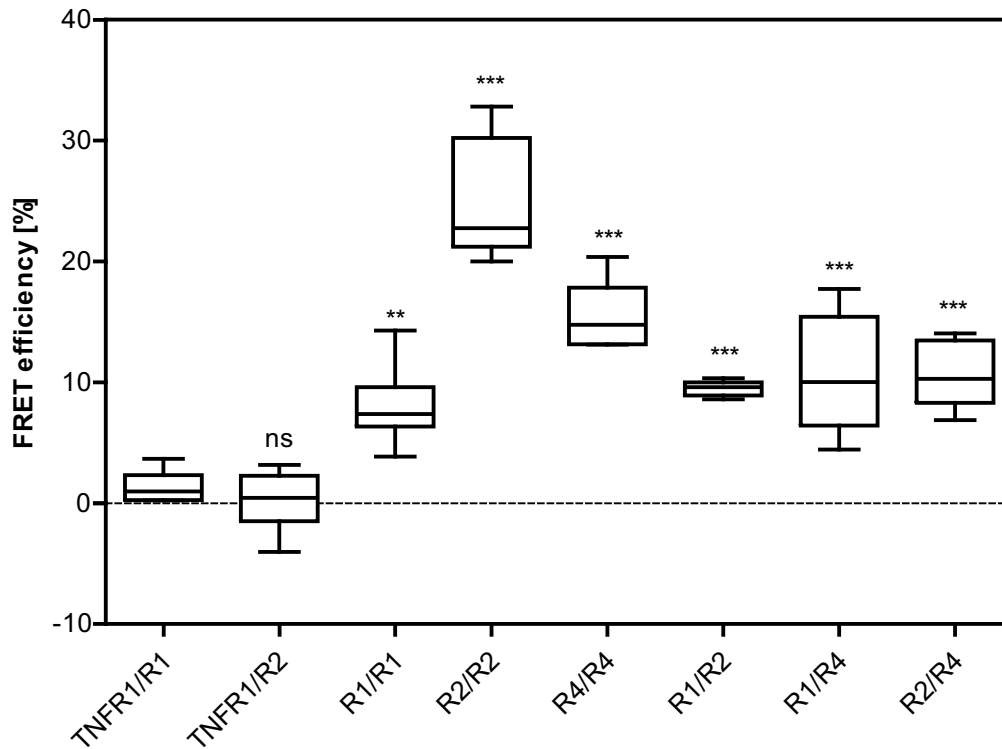
**Figure 6: Homo- and heterotypic interactions between TRAILR-FP fusion proteins.** Acceptor photobleaching FRET experiments were performed using MF expressing donor/acceptor pairs of TRAILR-FP fusion proteins and FRET efficiencies were calculated using the ImageJ plug-in FRETcalc. First two groups represent the negative controls (TNFR1-ΔCyt-GFP (TNFR1) in combination with R1ΔC-mCherry (R1) or R2ΔC-mCherry (R2)). Values shown are obtained from the analysis of 30 individual cells in 6 independent experiments for each receptor fusion protein combination. Box and whiskers plot: Box represents the 25th and 75th percentile, the median is depicted by a horizontal line; whiskers denote 5th and 95th percentile. Significance was tested by one-way ANOVA and comparison to the TNFR1/R1 negative control using Bonferroni multiple comparison test. **: $p < 0.01$, ***: $p < 0.001$, ns: not significant.

For all investigated combinations of the different TRAILR-FP fusion proteins FRET experiments revealed positive values that differed significantly from the two negative controls. While all heterotypic interactions yielded virtually the same FRET efficiencies, in the case of homotypic TRAIL receptor oligomerization the values obtained for the three TRAIL receptors differed significantly. The lowest energy transfer value was measured between donor/acceptor-fusion proteins of TRAILR1,

while investigation of homotypic interaction of the second TRAIL death receptor, receptor 2, yielded articulately higher FRET values (Figure 6).

3.1.2. The stoichiometry of pre-assembled TRAIL receptor 2

Interactions between unligated receptors has previously been shown for several members of the TNF receptor superfamily, e.g. for TNFR1 (Branschädel et al., 2010). However, conflicting reports exist concerning the exact stoichiometry of ligand-independent TNFR1 complexes. Both formation of homotrimers (Chan et al., 2000), yet more recently also homodimers (Branschädel et al., 2010) have been reported. Reports on the stoichiometry of TRAIL receptor oligomers are comparatively scarce. Molecular dynamics studies report the formation of an asymmetric receptor trimer (Wassenaar et al., 2008), and this stoichiometry is also reported from chemical crosslinking studies performed using full-length TRAILR2 (Valley et al., 2012).

Since in the previous experiments, interactions of TRAIL receptors could be demonstrated using recombinant receptor fusion proteins which lacked virtually the complete intracellular domain, chemical crosslinking experiments were performed using a FLAG-tagged TRAILR2 variant (Figure 7A) (again lacking all but the first 14 intracellular amino acids). The intention was to investigate complex formation mediated only by the extracellular and transmembrane domains of TRAILR2. The TRAILR2 deletion variant was stably expressed in murine embryonic fibroblasts yielding the cell line MF R2ΔC-FLAG. Cell surface expression was verified by flow cytometry (Figure 7B).

A

TRAILR2

| CRDs | S | TM | F |

B
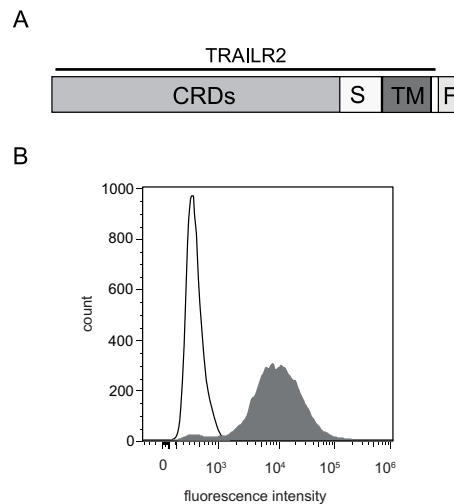
Figure 7: TRAILR2 variant used for chemical crosslinking experiments.
A: Schematic depiction of the TRAILR2 variant. The extracellular cysteine-rich domains (CRDs), the stem- (S) and transmembrane (TM) domain as well as the first 14 intracellular amino acids were fused to a carboxyl-terminal FLAG-tag (F). **B:** Cell surface expression of R2ΔC-FLAG. Cells were immunostained with anti-TRAILR2 antibody (grey histogram) or with murine IgG$_{2B}$ isotype control (white histogram) followed by incubation with anti-mouse IgG FITC-conjugated secondary antibody and analyzed by flow cytometry.

MF R2ΔC-FLAG cells were treated with dilutions of the amine-reactive and non-membrane permeable crosslinker bis(sulfosuccinimidyl)suberate (BS^3) at 4 °C. Western blot analysis using precise non-stained molecular weight markers revealed efficient homodimer formation of R2ΔC-FLAG (Figure 8). Depending on the crosslinker concentration used, a strong specific band with an apparent molecular weight of approximately 55 kDa could be detected in addition to the band representing the monomeric receptor variant which features a calculated molecular weight of 27 kDa. Higher oligomers (i.e. trimers or tetramers) could not be detected even at the highest BS^3 concentration used. The near to complete formation of homo-dimeric complexes at crosslinker concentrations ≥ 500 µM which was observed in these experiments indicates that dimerization of TRAILR2 in the plasma membrane is strongly favored.
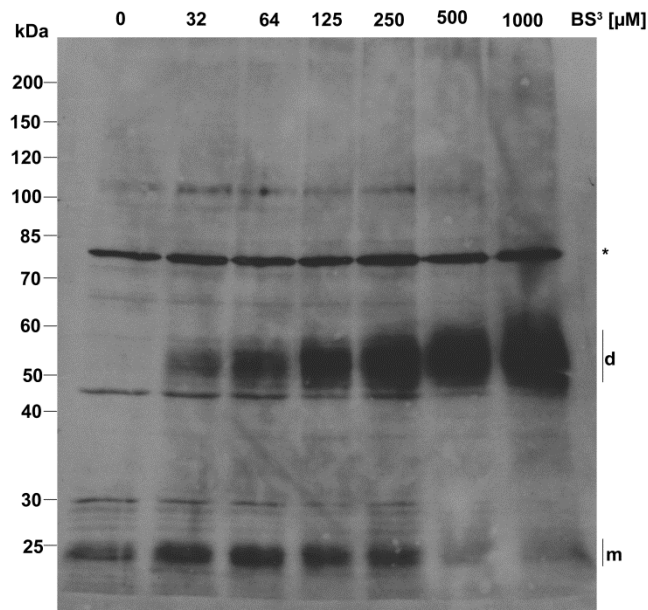
Figure 8: A truncated variant or TRAILR2 exists as preformed dimer on the plasma membrane. MF cells stably expressing a FLAG-tagged truncated version of human TRAILR2 were incubated with increasing concentrations of the chemical crosslinker BS^3. Whole cell lysates (50 µg per lane) were resolved by reducing SDS-Page and western blot analysis was performed using FLAG-tag specific antibody. Precise non-stained molecular weight marker is given on the left. m: monomer; d: dimer. The unspecific band indicated with an asterisk served as loading control. Blot shown is representative of at least three independent experiments.

As an additional approach to demonstrate and confirm ligand-independent dimerization of the death receptor TRAILR2, immunoprecipitation of BS^3 crosslinked cell surface proteins was performed. Therefore MF cells were engineered to stably coexpress R2ΔC-FLAG and R2ΔC-GFP (see Figure 3 for schematic depiction of this receptor fusion protein). Expression of the two different receptor fusion proteins was verified by flow cytometry (Figure 9A). Western blot analysis of the immunoprecipitated proteins and protein complexes revealed a BS^3-induced protein complex with an apparent molecular weight of approximately 80 kDa (rightmost lane in Figure 9B). The apparent molecular weight of this protein complex, which is absent in the untreated samples as well as in the BS^3 treated control sample, supports the notion that it constitutes a dimeric protein complex containing the two TRAILR2 fusion proteins R2ΔC-FLAG (27 kDa) and R2ΔC-GFP (53 kDa).

A

R2ΔC-FLAG

TRAILR2
CRDs | S | TM | F

R2ΔC-GFP

TRAILR2
CRDs | S | TM | GFP

B
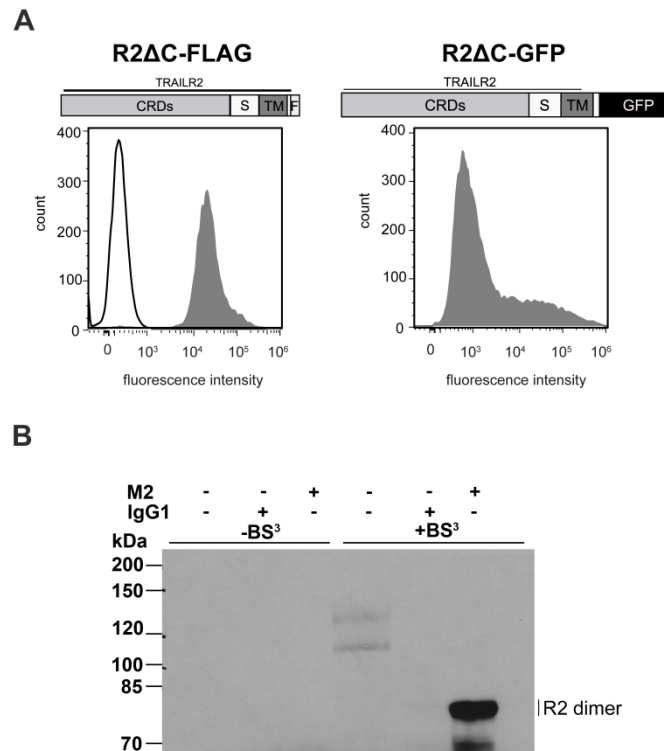
Figure 9: Immunoprecipitation of crosslinked cell surface proteins confirms predominant dimerization of TRAILR2. A: Schematic depiction of the TRAILR variants employed for the analysis of receptor-receptor interaction and flow cytometric analysis of cell surface expression of the receptor variants in the MF R2ΔC-FLAG/R2ΔC-GFP cell line. Cell surface proteins were immunostained with murine anti-TRAILR2 antibody (grey histogram) or the respective IgG_{2B} isotype control antibody (white histogram) followed by incubation with anti-murine IgG PE-conjugated secondary antibody (left panel, showing total expression of both TRAILR2 variants) or left unstained (right panel, showing fluorescence emission of R2ΔC-GFP). **B:** MF stably expressing R2ΔC-FLAG and R2ΔC-GFP were incubated with 500 µM BS^3 for 30 min at 4 °C or left untreated. 1 mg of whole cell lysate was subjected to immunoprecipitation using 5 µg anti-FLAG M2 antibody or 5 µg of IgG_1 isotype control antibody and protein G sepharose beads. Precipitated proteins were subjected to SDS-Page and western blot analysis using anti-GFP antibody. Precise non-stained molecular weight marker is given on the left. R2 dimer: R2ΔC-FLAG/R2ΔC-GFP dimer. Results shown are representative of three independent experiments.

3.1.3. Hetero-oligomerization of TRAIL receptors

In order to elucidate the stoichiometry of heteromeric receptor complexes, additional murine fibroblast cell lines stably expressing two different TRAIL receptor variants were generated. The three cell lines expressing each one FLAG-tagged receptor variant and one receptor-GFP fusion protein were termed MF R1ΔC-3FLAG/R2ΔC-GFP (Figure 10A), MF R1ΔC-3FLAG/R4ΔC-GFP (Figure 11A) and MF R2ΔC-FLAG/R4ΔC-GFP (Figure 12A). Stable expression of the receptor variants was achieved by fluorescent activated cell sorting and was confirmed by flow cytometry. Ligand-independent receptor complexes were then traced through chemical crosslinking experiments using the amine-reactive, non-membrane permeable crosslinker BS^3. FLAG-tagged receptor variants (or crosslinker-induced protein complexes containing this receptor) were subsequently immunoprecipitated and analyzed by western blot using GFP-specific antibody. Formation of a BS^3-induced protein complex showing an apparent molecular weight of 80 kDa could be demonstrated in the MF R1ΔC-3FLAG/R2ΔC-GFP cell line (Figure 10B). This protein complex, which is completely absent in the untreated samples as well as the BS^3-treated control samples most likely represents a heterodimeric complex of the two TRAIL death receptor variants used in this experiment.

Crosslinking of cell surface proteins of MF R1ΔC-3FLAG/R4ΔC-GFP resulted in the detection of a protein complex (rightmost lane in Figure 11B) whose apparent molecular weight (approximately 80 kDa) supports the hypothesis that TRAIL death and decoy receptors do dimerize through heterotypic interaction of their extracellular domains.
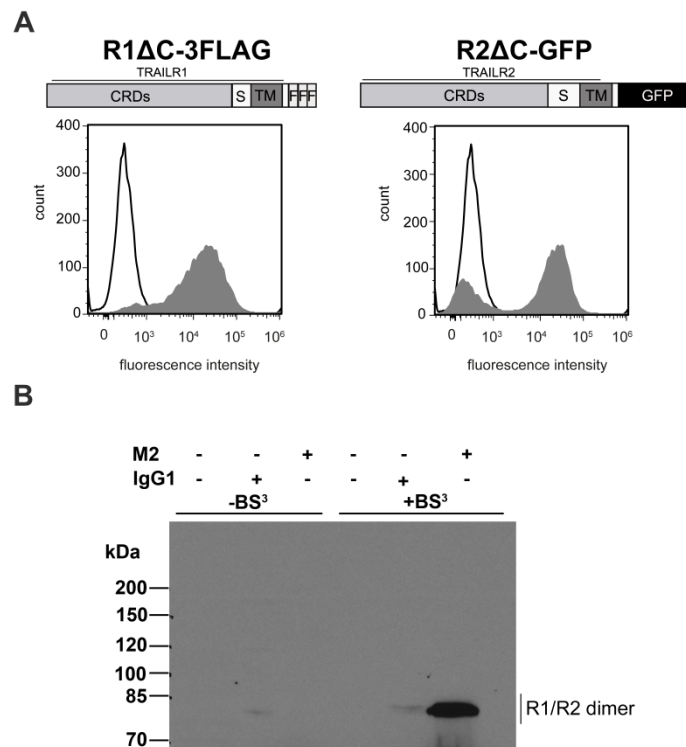
Figure 10: Analysis of BS³-induced TRAILR1/TRAILR2 complexes. A: Schematic depiction of the TRAILR variants employed for the analysis of receptor-receptor interaction and flow cytometric analysis of cell surface expression of the receptor variants in the MF R1ΔC-3FLAG/R2ΔC-GFP cell line. Cell surface proteins were immunostained with murine anti-TRAILR1 antibody (grey histogram) or the respective IgG$_1$ isotype control antibody (white histogram) followed by incubation with anti-murine IgG PE-conjugated secondary antibody (left panel). For detection of TRAILR2 surface expression, cells were stained with murine anti-TRAILR2 antibody (grey histogram) or IgG$_{2B}$ isotype control antibody (white histogram) followed by incubation with anti-murine IgG PE-conjugated secondary antibody (right panel). **B:** MF stably expressing R1ΔC-3FLAG and R2ΔC-GFP were incubated with 500 µM BS³ for 30 min at 4 °C or left untreated. 1 mg of whole cell lysate was subjected to immunoprecipitation using 5 µg anti-FLAG M2 antibody or 5 µg of IgG1 isotype control antibody and protein G sepharose beads. Precipitated proteins were subjected to SDS-PAGE and western blot analysis using anti-GFP antibody. Precise non-stained molecular weight marker is given on the left. R1/R2 dimer: R1ΔC-3FLAG/R2ΔC-GFP dimer. Results shown are representative of three independent experiments.

A

R1ΔC-3FLAG

TRAILR1

| CRDs | S | TM | FFF |

R4ΔC-GFP

TRAILR4

| CRDs | S | TM | GFP |

B
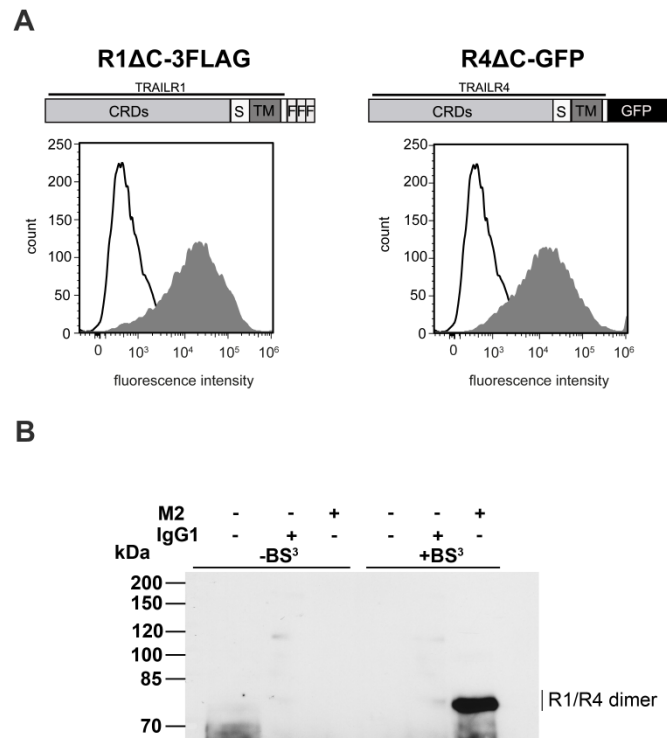
Figure 11: Heterodimer formation of death and decoy receptors. A: Schematic depiction of the TRAILR variants employed for the analysis of receptor-receptor interaction and flow cytometry analysis of cell surface expression of the receptor variants in the MF R1ΔC-3FLAG/R4ΔC-GFP cell line. Cell surface proteins were immunostained with murine anti-TRAILR1 antibody (grey histogram) or the respective IgG$_1$ isotype control antibody (white histogram) followed by incubation with anti-murine IgG PE-conjugated secondary antibody (left panel). For detection of TRAILR4 surface expression, cells were stained with murine anti-TRAILR4 antibody (grey histogram) or IgG$_1$ isotype control antibody (white histogram) followed by incubation with anti-murine IgG PE-conjugated secondary antibody (right panel). **B:** MF stably expressing R1ΔC-3FLAG and R4ΔC-GFP were incubated with 500 µM BS^3 for 30 min at 4 °C or left untreated. 1 mg of whole cell lysate was subjected to immunoprecipitation using 5 µg anti-FLAG M2 antibody or 5 µg of IgG1 isotype control antibody and protein G sepharose beads. Precipitated proteins were subjected to SDS-PAGE and western blot analysis using anti-GFP antibody. Precise non-stained molecular weight marker is given on the left. R1/R4 dimer: R1ΔC-3FLAG/R4ΔC-GFP dimer. Results shown are representative of three independent experiments.

Comparable crosslinking characteristics as for TRAILR1/TRAILR2 and TRAILR1/TRAILR4 variants could also be demonstrated for the combination of death receptor TRAILR2 and decoy receptor TRAILR4 in the cell line MF R2ΔC-FLAG/R4ΔC-GFP (Figure 12B). Again, a FLAG-tag and eGFP containing protein complex whose apparent molecular weight coincided with the combined molecular weights of the TRAILR2 (27 kDa) and the TRAILR4 variant (55 kDa) could be detected in the crosslinker treated sample (Figure 12B).

Treatment of cell surface proteins with the chemical crosslinker BS^3 gave rise to protein complexes which could be precipitated using FLAG-tag specific antibody. Western blot analysis using GFP-specific antibody allowed the identification of these complexes as heterodimers of the different TRAIL receptor variants coexpressed in the MF cell lines. The detection of these complexes using recombinant receptors devoid of intracellular domains points towards PLAD-mediated oligomerization.
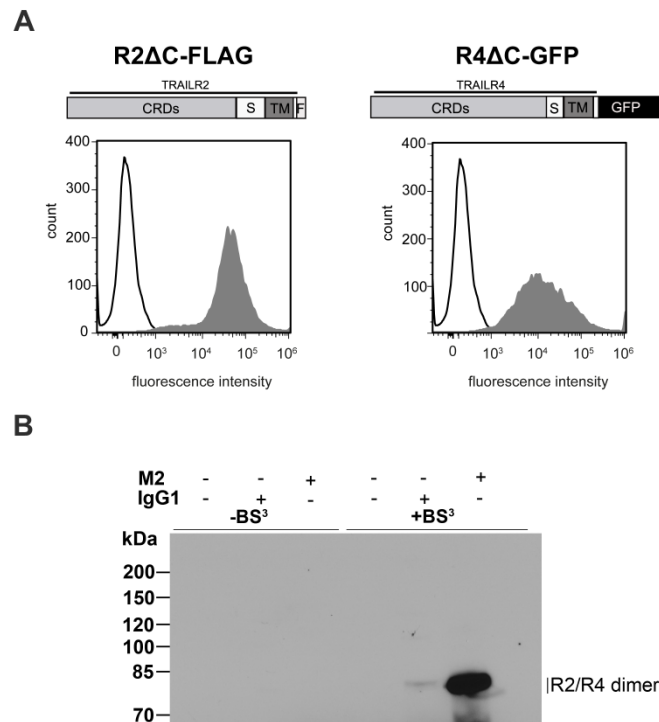

Figure 12: Heterodimer formation of death and decoy receptors. A: Schematic depiction of the TRAILR variants employed for the analysis of receptor-receptor interaction (top) and flow cytometry analysis of cell surface expression of the receptor variants in the MF R2ΔC-FLAG/R4ΔC-GFP cell line. Cell surface proteins were immunostained with murine anti-TRAILR1 antibody (grey histogram) or the respective IgG_1 isotype control antibody (white histogram) followed by incubation with anti-murine IgG PE-conjugated secondary antibody (left panel). For detection of TRAILR4 surface expression, cells were stained with murine anti-TRAILR4 antibody (grey histogram) or IgG_1 isotype control antibody (white histogram) followed by incubation with anti-murine IgG PE-conjugated secondary antibody (right panel). **B:** MF stably expressing R2ΔC-FLAG and R4ΔC-GFP were incubated with 500 µM BS^3 for 30 min at 4 °C or left untreated. 1 mg of whole cell lysate was subjected to immunoprecipitation using 5 µg anti-FLAG M2 antibody or 5 µg of IgG1 isotype control antibody and protein G sepharose beads. Precipitated proteins were subjected to SDS-PAGE and western blot analysis using anti-GFP antibody. Precise non-stained molecular weight marker is given on the left. R2/R4 dimer: R2ΔC-FLAG/R4ΔC-GFP dimer. Results shown are representative of three independent experiments.

3.2. Interactions of the extracellular domains of TRAILR1 and TRAILR4

To analyze interactions of the isolated extracellular domains of TRAIL receptors alone, soluble variants of the death receptor TRAILR1 (sTRAILR1) and the decoy receptor TRAILR4 (sTRAILR4) were recombinantly expressed in HEK293T cells. The recombinant proteins consisted of the three cysteine-rich domains and the first 12 amino acids of the stem-region and were expressed as fusion to a carboxyl-terminal 6× His-tag to allow purification by immobilized metal affinity chromatography (IMAC). In addition, soluble TRAILR1 featured a myc-tag and soluble TRAILR4 a FLAG-tag amino-terminal to the 6× His-tag (Figure 13A). Both proteins were purified by IMAC to an approximate purity of 80% and showed an apparent molecular weight of about 25 kDa in SDS-Page (Figure 13B). The apparent molecular weight of sTRAILR1 is in concordance with its calculated molecular weight of 27.7 kDa. In the case of sTRAILR4, calculations revealed a considerably lower molecular weight of 20 kDa. Homotypic interactions of the soluble receptors were investigated by incubation with serial dilutions of BS^3 and western blot analysis using receptor-specific antibodies. Oligomerization of the soluble ECDs of TRAILR1 could already be detected at BS^3 concentrations as low as 63 µM. The molecular weight of the observed complexes was two-fold higher compared to monomeric sTRAILR1. With rising crosslinker concentrations higher-order complexes (molecular weight > 100 kDa) increased in abundance. BS^3 concentrations of 500 µM and more resulted in a reduction of the dimeric complexes, but also the higher-order oligomers, most likely resulting in the formation of multimeric protein aggregates which were excluded from SDS-Page analysis (Figure 13C). Incubation of sTRAILR4 with increasing amounts of BS^3 resulted in formation of protein complexes showing twice the molecular weight of the monomeric protein. Oligomers of higher order could be detected with relatively low abundance when crosslinker concentrations of 250 µM or more were used (Figure 13D).
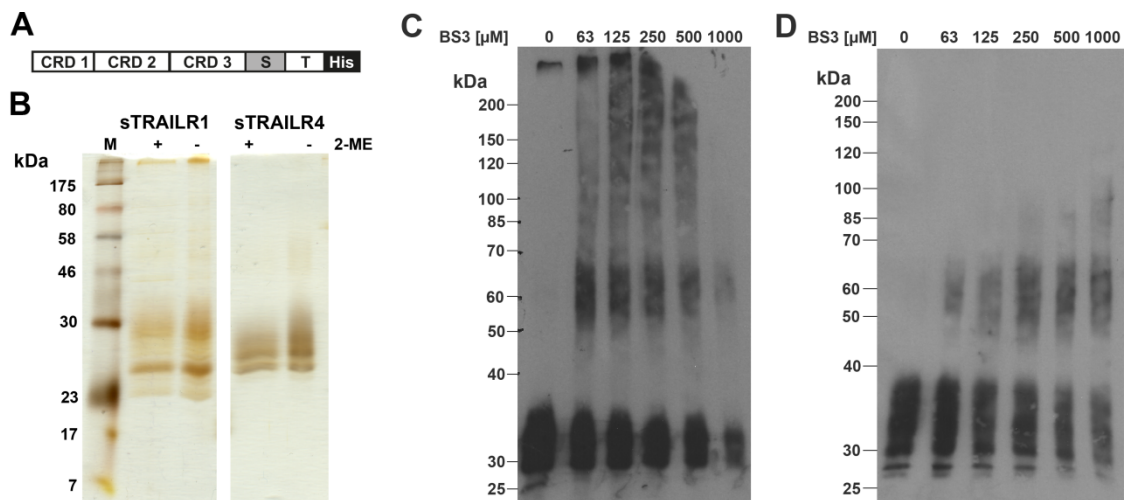
Figure 13: Construction and purification of soluble ECDs of TRAILR1 and TRAILR4. A: Extracellular cysteine-rich domains (CRD) 1 to 3 and the stem-domain (S) of TRAILR1 and TRAILR4, respectively, were expressed as fusion to myc-tag or FLAG-tag (T) and a 6× Histidin-tag (His). **B:** SDS-Page analysis of purified sTRAILR1 and sTRAILR4 under reducing (+ 2-ME) and non-reducing (- 2-ME) conditions. 500 ng of protein were analyzed per lane and the gel was stained by silver staining. **C:** Soluble ECDs of TRAILR1 (sTRAILR1; 2.5 µg per sample) were incubated with increasing concentrations of BS^3 for 30 min on ice. Samples were subjected to reducing SDS-Page and analyzed by western blot using anti-TRAILR1 antibody. Precise non-stained molecular weight marker is given on the left. **D:** Soluble ECDs of TRAILR4 (sTRAILR4; 2.5 µg per sample) were incubated with increasing concentrations of BS^3 for 30 min on ice. Samples were subjected to reducing SDS-Page and analyzed by western blot using anti-TRAILR4 antibody. Precise non-stained molecular weight marker is given on the left. Blots shown are representative of three independent experiments.

These results show that the soluble ECDs of TRAILR1 and TRAILR4 retain the capability to undergo homotypic interactions, resulting in the predominant formation of receptor dimers. Heterotypic interactions were subsequently addressed. Affinity measurements using a quartz crystal microbalance system were performed to assess the dissociation constant of the interaction between sTRAILR1 and sTRAILR4. Initially binding of the ligand single-chain TRAIL (scTRAIL; three TRAIL protomers expressed as a single polypeptide chain) to the soluble receptors was investigated. Therefore sTRAILR1 was immobilized on a low non-specific-binding (LNB) carboxyl-sensor chip at a density resulting in a signal increase of 85 Hz. Subsequently, binding of increasing concentrations of scTRAIL was monitored (Figure 14A) and the on- and off-rate as well as the dissociation constant were calculated from the binding curves (Table 5).
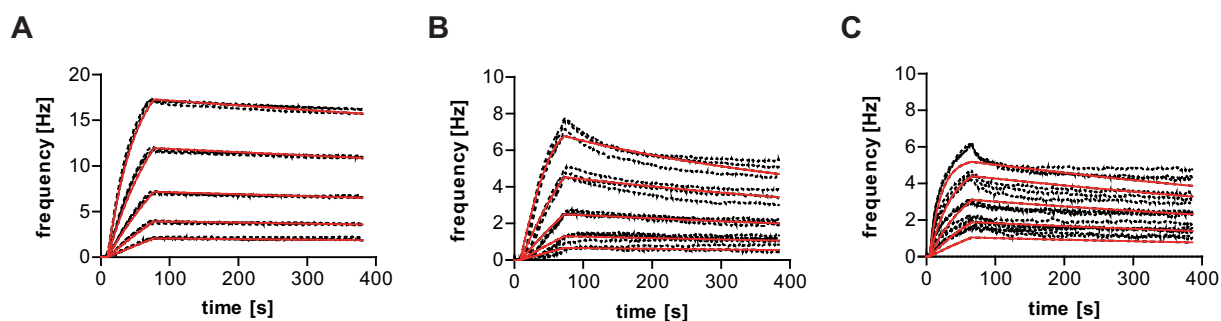
Figure 14: Affinity measurements of soluble ECDs of TRAILR1 and TRAILR4.
A: Affinity of sTRAILR1 to the ligand scTRAIL was determined by quartz crystal microbalance measurements using immobilized ECDs of receptor 1 and increasing concentrations of scTRAIL (62.5 nM – 1 µM). **B:** Binding of scTRAIL to immobilized sTRAILR4 was monitored using immobilized soluble ECDs of TRAILR4 and increasing concentrations of scTRAIL (62.5 nM – 1 µM). **C:** Binding of sTRAILR4 to immobilized sTRAILR1 was measured using increasing concentrations of the soluble ECDs (250 nM – 4 µM). Dotted lines: results from three single measurements per concentration; solid red line: fitted curves. Representative measurements from three independent experiments are shown for A and C.

The obtained results show a strong and specific binding of the ligand to the soluble receptor, hence confirming that sTRAILR1 has retained its ligand binding capabilities. Thereafter sTRAILR4 was immobilized to a LNB carboxyl-sensorchip resulting in a signal increase of 60 Hz. As for sTRAILR1, measurements showed specific binding of scTRAIL (Figure 14B), albeit with a lower overall affinity (Table 5). Nonetheless, it could be shown that also sTRAILR4 retained the capacity to bind its ligand. The question whether the extracellular domains are sufficient to induce the formation of heteromeric TRAIL receptor complexes was then addressed by monitoring the binding of sTRAILR4 to immobilized sTRAILR1 (Figure 14C). Again, the binding curves show a specific interaction between the two TRAIL receptor ECDs. The calculated association (k_{on}) and dissociation rates (k_{off}) confirm a fast and stable complex formation and a reasonable affinity (Table 5). However, the fitted curves do not ideally reproduce the measurements. Accordingly the obtained values should be considered as an approximation.

Table 5: Binding characteristics of soluble TRAILR1 and TRAILR4

immobilized protein	analyte	k_{on} [M^{-1} s^{-1}]	k_{off} [s^{-1}]	K_d [M]
sTRAILR1	scTRAIL	$6.23 \times 10^4 \pm 1.6 \times 10^4$	$4.14 \times 10^{-4} \pm 1.28 \times 10^{-4}$	$6.59 \times 10^{-9} \pm 3.83 \times 10^{-10}$
sTRAILR4	scTRAIL	1.41×10^5	1.77×10^{-3}	1.26×10^{-8}
sTRAILR1	sTRAILR4	$2.06 \times 10^4 \pm 0.4 \times 10^4$	$1.0 \times 10^{-3} \pm 0.17 \times 10^{-3}$	$4.92 \times 10^{-8} \pm 2.25 \times 10^{-9}$

3.3. Implications of receptor-receptor interactions on apoptotic signaling

3.3.1. TRAIL treatment induces apoptosis in HeLa cells

To investigate the impact of heteromeric receptor-receptor interactions on TRAIL signaling, the moderately TRAIL-sensitive human cervix carcinoma cell line HeLa was chosen as a model cell line. Treatment of HeLa cells in combination with the protein synthesis inhibitor cycloheximide (CHX) induced cell death in a concentration-dependent manner (Figure 15A). To determine the type of cell death which is induced in HeLa cells in response to TRAIL treatment, cytotoxicity assays in presence of the pan-caspase inhibitor N-Benzyloxycarbonyl-valyl-alanyl-aspartyl-[O-methyl]-fluoromethylketone (zVAD-fmk) were performed. The obtained results clearly show that HeLa cells undergo cell death after TRAIL treatment in a caspase-dependent manner (Figure 15B).
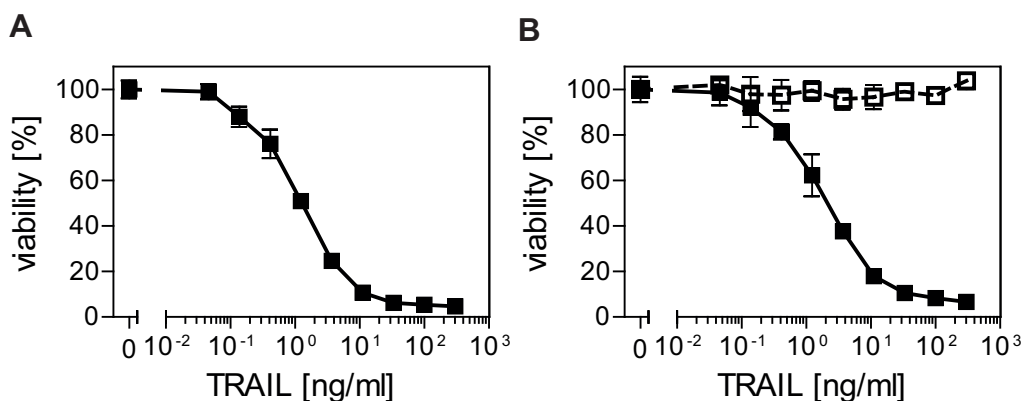

Figure 15: Crosslinked soluble TRAIL induces cell death in HeLa cells in a concentration-dependent manner. A: HeLa cells were treated with serial dilutions of FLAG-tagged soluble TRAIL (previously crosslinked by incubation with 1 µg/ml anti-FLAG M2 antibody (1 h at 37 °C)) in combination with 0.5 µg/ml CHX. After 24 h cell viability was determined by crystal violet staining. Values shown are mean ± SD calculated from triplicates. One representative experiment out of nine is shown. **B:** HeLa were pre-incubated with the pan-caspase inhibitor zVAD-fmk (20 µM) (open squares, dashed line) or treated with the vehicle (DMSO) only (filled squares, solid line) for one hour before being treated with serial-dilutions of antibody-crosslinked sTRAIL (TRAIL) in combination with 0.5 µg/ml CHX. After 24 h cell viability was determined by crystal violet staining. Values shown are mean ± SD calculated from triplicates. One representative experiment out of three is shown.

Flow cytometric analysis of the cell surface expression of the four human TRAIL receptors revealed that both so-called decoy receptors TRAILR3 and TRAILR4 are not expressed in HeLa cells (Figure 16). In addition, the death receptor TRAILR1 is expressed at considerably higher levels (MFI 1994 ± 233; mean ± SD; n = 7) than TRAILR2 (MFI 167 ± 67). Accordingly, apoptosis induction in HeLa cells is most likely mediated through signaling by TRAILR1 rather than TRAILR2.
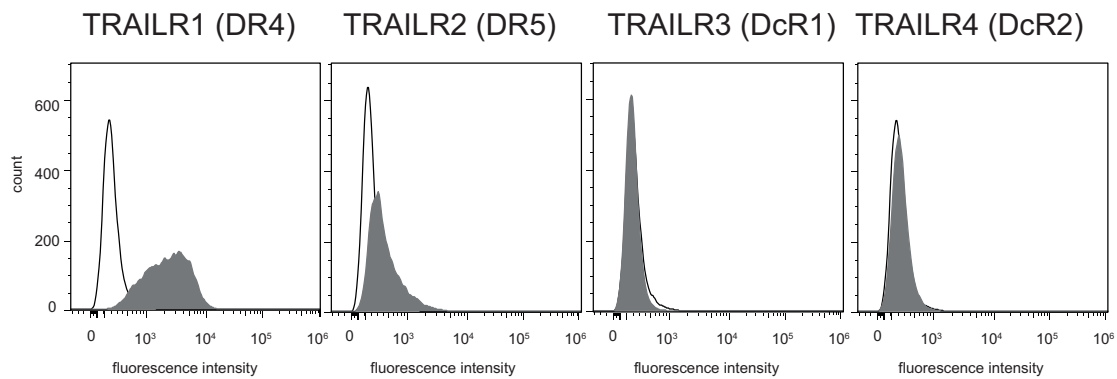
Figure 16: HeLa cells express predominantly TRAILR1 (DR4). Expression of the four human cell surface TRAIL receptors in HeLa cells was analyzed by flow cytometry. Cells were immunostained with murine monoclonal antibodies directed against human TRAILR1, TRAILR2, TRAILR3 or TRAILR4 (grey histograms) followed by incubation with anti-murine PE-conjugated antibody. Respective IgG$_1$ (for TRAILR1-, R3- and R4-specific antibodies) or IgG$_{2B}$ isotype (for TRAILR2-specific antibody) controls are shown as white histograms.

3.3.2. Expression of TRAILR4 impairs apoptosis induction

To approach the question to which extent TRAILR4 can influence signaling by the death receptor TRAILR1, TRAILR4 (DcR2) was stably expressed in HeLa cells, yielding the cell line HeLa R4. Expression of the four human cell surface TRAIL receptors was assessed by flow cytometry and showed a stable and considerable overexpression of TRAILR4 (Figure 17). The expression levels of the death receptor TRAILR1 (MFI 2163 ± 389) and of TRAILR4 (MFI 1767 ± 196) were overall comparable.
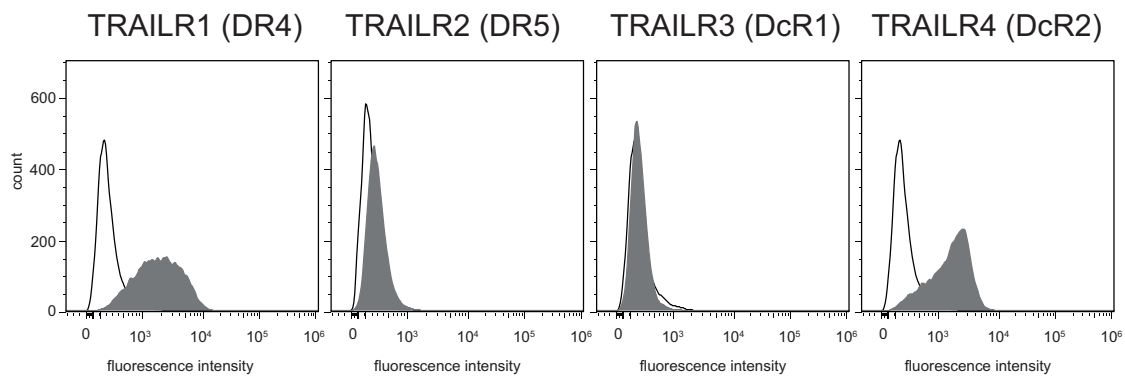
Figure 17: TRAIL receptor expression in HeLa R4 cells. HeLa cells were transfected with eukaryotic expression plasmid encoding for human wild type TRAILR4 and sorted for high expression of TRAILR4. Surface expression of the four human cell surface TRAIL receptors in HeLa R4 cells was analyzed by flow cytometry. Cells were immunostained with murine monoclonal antibodies directed against human TRAILR1, TRAILR2, TRAILR3 or TRAILR4 (grey histograms) followed by incubation with anti-murine PE-conjugated antibody. Respective IgG$_1$ (for TRAILR1-, R3- and R4-specific antibodies) or IgG$_{2B}$ (for TRAILR2-specific antibody) isotype controls are shown as white histograms.

In addition to the cell line HeLa R4, in which the expression levels of the death receptor TRAILR1 and the decoy receptor TRAILR4 were comparable, a second cell line, HeLa R4+ was generated through an additional round of fluorescence activated cell sorting. Parameters for cell sorting were chosen to obtain a several-fold higher expression of TRAILR4 as compared to HeLa R4 cells. Frequent analysis of the cell surface expression of the relevant receptors by flow cytometry confirmed a stable and very high expression of TRAILR4 (MFI 6949 ± 490), while the expression levels of TRAILR1 (MFI 1837 ± 214) and the two remaining receptors remained unchanged (Figure 18).
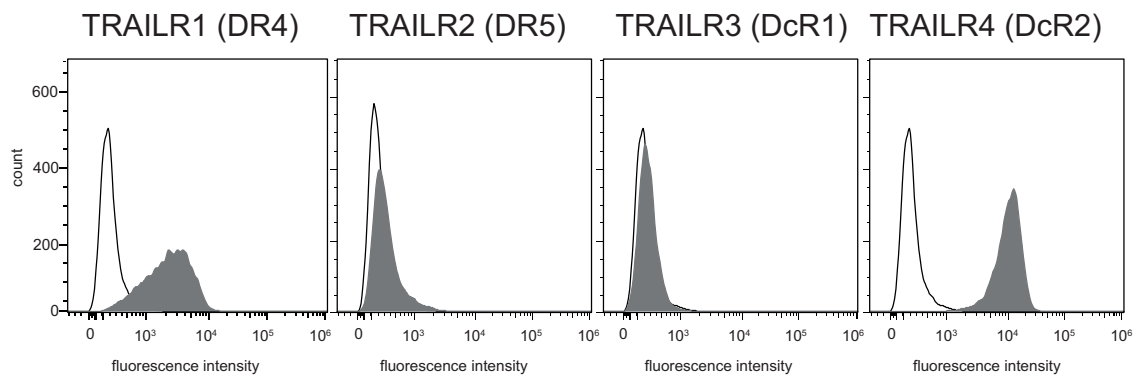
Figure 18: HeLa R4+ cells show a several-fold higher cells surface expression of TRAILR4. HeLa R4 cells were subjected to an additional round of cell sorting to obtain cells stably overexpressing high level of human TRAILR4. Surface expression of the four human cell surface TRAIL receptors in HeLa R4+ cells was analyzed by flow cytometry. Cells were immunostained with murine monoclonal antibodies directed against human TRAILR1, TRAILR2, TRAILR3 or TRAILR4, respectively (grey histograms) followed by incubation with anti-murine PE-conjugated antibody. Respective IgG_1 (for TRAILR1-, R3- and R4-specific antibodies) or IgG_{2B} (for TRAILR2-specific antibody) isotype controls are shown as white histograms.

Cytotoxicity assays using antibody-crosslinked soluble TRAIL in combination with cycloheximide showed that cells overexpressing TRAILR4 were significantly less susceptible to TRAIL-induced apoptosis than the parental HeLa cells (Figure 19A). Treatment with 300 ng/ml antibody crosslinked sTRAIL (the highest concentration used) resulted in significantly less cell death in HeLa R4 and HeLa R4+ (75.7 ± 5.7 and 16 ± 15.6% cell death, respectively) cells compared to the parental HeLa cells (92.9 ± 3.4% cell death; mean ± SD; n = 9). The experiments also revealed a clear dependency of TRAIL susceptibility to the TRAILR4 expression level in this cellular model. At TRAIL concentrations > 2 ng/ml HeLa R4+ cells showed considerably higher viability than HeLa R4 cells. This characteristic persisted for all sTRAIL concentrations tested in these experiments.

Co-treatment with the pan-caspase inhibitor zVAD-fmk completely inhibited TRAIL-induced cell death in these two cell lines (Figure 19B), hence confirming that both TRAILR4 overexpressing cell lines undergo apoptotic cell death upon TRAIL treatment.

A

B
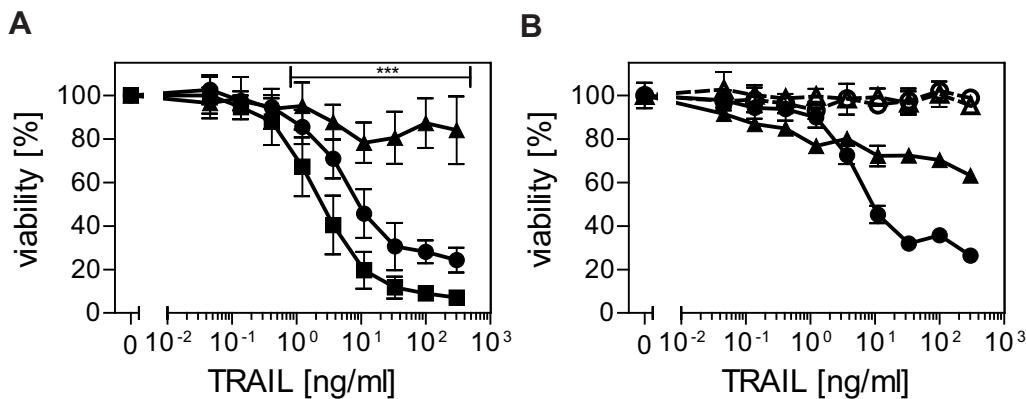
Figure 19: Cells overexpressing TRAILR4 are less susceptible to TRAIL-induced cell death compared to the parental HeLa cell line. A: HeLa (squares), HeLa R4 (circles) and HeLa R4+ (triangles) cells were treated with serial dilutions of antibody-crosslinked sTRAIL (TRAIL) in combination with 0.5 µg/ml CHX. After 24 h cell viability was determined by crystal violet staining. Values shown are mean viability ± SD calculated from nine independent experiments. Significance was tested using two-way ANOVA in combination with Bonferroni post-test. ***: $p < 0.001$. **B:** HeLa R4 (circles) and HeLa R4+ (triangles) cells were pre-incubated with the pan-caspase inhibitor zVAD-fmk (20 µM) (open symbols, dashed line) or treated with the vehicle (DMSO) only (filled symbols, solid line) for one hour before being treated with serial-dilutions of antibody-crosslinked sTRAIL (TRAIL) in combination with 0.5 µg/ml CHX. After 24 h cell viability was determined by crystal violet staining. Values shown are mean ± SD calculated from triplicates. One representative experiment out of three is shown

3.3.3. Apoptosis inhibition is mediated by TRAILR4 mutant lacking any signaling competence

Having shown that overexpression of TRAILR4 confers protection from TRAIL-induced apoptosis in HeLa cells, the molecular mechanism was subsequently addressed. TRAILR4 has originally been described as a decoy receptor (Marsters et al., 1997) and its signaling capabilities remain only vaguely defined (Degli-Esposti et al., 1997a; Marsters et al., 1997; Harper et al., 2001; Lalaoui et al., 2011). However, evidence suggests that TRAILR4 is rather an inhibitory or regulatory than a decoy receptor (Clancy et al., 2005). To investigate the contribution of signaling to the protective effect conferred by TRAILR4, HeLa cells overexpressing a truncated, hence signaling-incapable variant of TRAILR4 were generated. This truncated receptor variant (termed R4ΔC, see Figure 3 for a schematic representation) consisted of the complete extracellular and transmembrane domains of the wild type receptor, thus retaining the capability to bind both its ligand via the ligand binding site, as well as TRAIL receptors via the pre-ligand binding assembly domain (PLAD). All but the first 14 intracellular amino acids had been deleted and replaced by the

enhanced green fluorescent protein (eGFP) to ensure this receptor was incapable of transducing intracellular signals. Parental HeLa cells were transfected with a eukaryotic expression plasmid encoding for the receptor variant R4ΔC. Stable transfectants were selected using appropriate antibiotics. In order to obtain high expression of the receptor variant in the HeLa R4ΔC cells, two rounds of cell sorting were performed. Flow cytometry confirmed a high and stable expression of the receptor 4 variant (MFI 4155 ± 660, mean ± SD, n = 7) while the expression levels of the other TRAIL receptors (Figure 20) remained unchanged compared to the parental cell line.
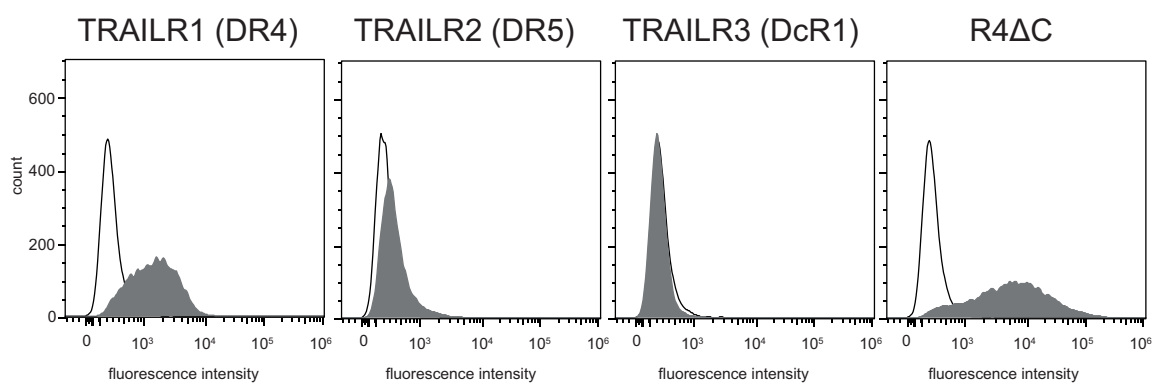
Figure 20: Expression of wild type TRAIL receptors and the truncated TRAILR4 variant R4ΔC in HeLa R4ΔC cells. Surface expression of the human wild type TRAIL receptors TRAILR1, TRAILR2 and TRAILR3 and the recombinant variant R4ΔC in HeLa R4ΔC cells was analyzed by flow cytometry. Cells were immunostained with murine monoclonal antibodies directed against human TRAILR1, TRAILR2, TRAILR3 or TRAILR4 respectively (grey histograms) followed by incubation with anti-murine PE-conjugated antibody. Respective IgG$_1$ (for TRAILR1-, R3- and R4-specific antibodies) or IgG$_{2B}$ (for TRAILR2-specific antibody) isotype controls are shown as white histograms.

Cytotoxicity assays using antibody-crosslinked soluble TRAIL in combination with the protein synthesis inhibitor cycloheximide showed significantly less cell death in HeLa R4ΔC compared to HeLa cells (43 ± 18.6 *versus* 92.9 ± 3.4% cell death) at the highest TRAIL concentration used (Figure 21A). Pretreatment of HeLa R4ΔC cells with the pan-caspase inhibitor zVAD-fmk to block the apoptotic pathway confirmed the caspase-dependency of the cell death observed after TRAIL stimulation (Figure 21B).
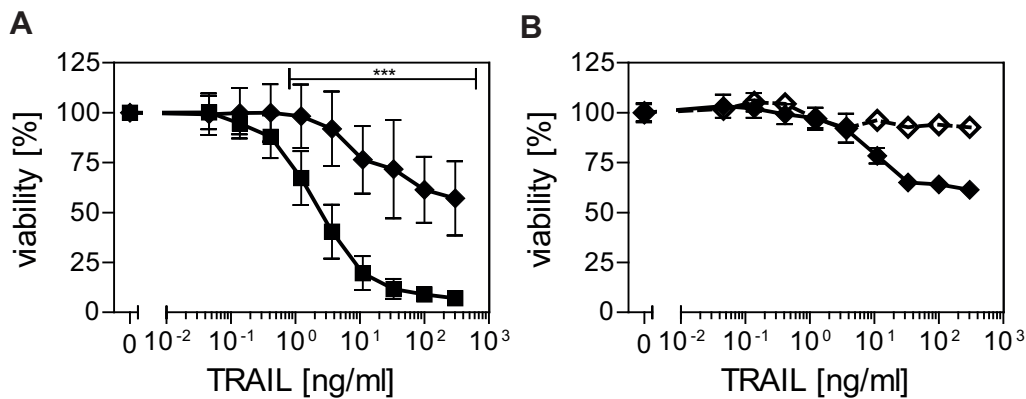
Figure 21: A truncated, signaling-incapable TRAILR4 variant confers protection from TRAIL-induced apoptosis. A: HeLa R4ΔC (diamonds) and HeLa (squares) cells were treated with serial dilutions of antibody-crosslinked sTRAIL (TRAIL) in combination with 0.5 µg/ml CHX. After 24 h cell viability was determined by crystal violet staining. Values shown are mean viability ± SD calculated from nine independent experiments. Significance was tested using two-way ANOVA in combination with Bonferroni post-test. ***: $p < 0.001$. **B:** HeLa R4ΔC cells were pre-incubated with the pan-caspase inhibitor zVAD-fmk (20 µM) (open diamonds, dashed line) or treated with the vehicle (DMSO) only (filled diamonds, solid line) for one hour before being treated with serial-dilutions of antibody-crosslinked sTRAIL in combination with 0.5 µg/ml CHX. After 24 h cell viability was determined by crystal violet staining. Values shown are mean ± SD calculated from triplicates. One representative experiment out of three is shown.

3.4. Reduced caspase activation in HeLa cells overexpressing TRAILR4

3.4.1. Impaired activation of caspase-8 and caspase-3

As HeLa cells show higher levels of caspase-dependent cell death upon TRAIL treatment, kinetics of initiator caspase-8 and effector caspase-3 activation were investigated. TRAIL treatment induced cleavage of caspase-8 in all four investigated cell lines. The intermediate caspase-8 fragment p43/41 could be detected in all cell lines after 2 h of stimulation, albeit in reduced amounts in cells expressing wild type or the truncated variant of TRAILR4. Cleavage of caspase-8 to the p43/41 fragment continued in all cell lines for the duration of the experiment, reaching its maximum at the time-point of 6 h. For all investigated time-points, HeLa cells showed the highest levels of caspase-8 p43/41. The fragment representing fully activated caspase-8, p18, was detected in HeLa at the time-points 4 and 6 h. In HeLa R4 and HeLa R4ΔC cells caspase-8 cleavage to the p18 fragment was considerably reduced in comparison to HeLa cells. Even after 6 h of TRAIL treatment, fully active caspase-8

could not be detected in HeLa R4+ cells. As a consequence of the reduced initiator caspase activation, cleavage of the effector caspase-3 was strongly reduced in the TRAILR4 overexpressing HeLa cells. Complete activation of caspase-3, i.e. cleavage into the p19 and p17 fragments, in HeLa cells became apparent after 4 and 6 h of TRAIL treatment. HeLa R4+ cells showed no cleavage of caspase-3 under these experimental conditions. HeLa R4 and HeLa R4ΔC show lower expression of wild type or truncated TRAILR4, respectively, as HeLa R4+ cells. Accordingly, low amounts of the p19, but not the p17, fragment of cleaved caspase-3 were detected at time-points 4 and 6 h (Figure 22). Overall, activation of both caspase-8 and caspase-3 could be shown to be significantly reduced in response to TRAIL treatment in HeLa cells engineered to express either full-length or a truncated variant of TRAILR4.
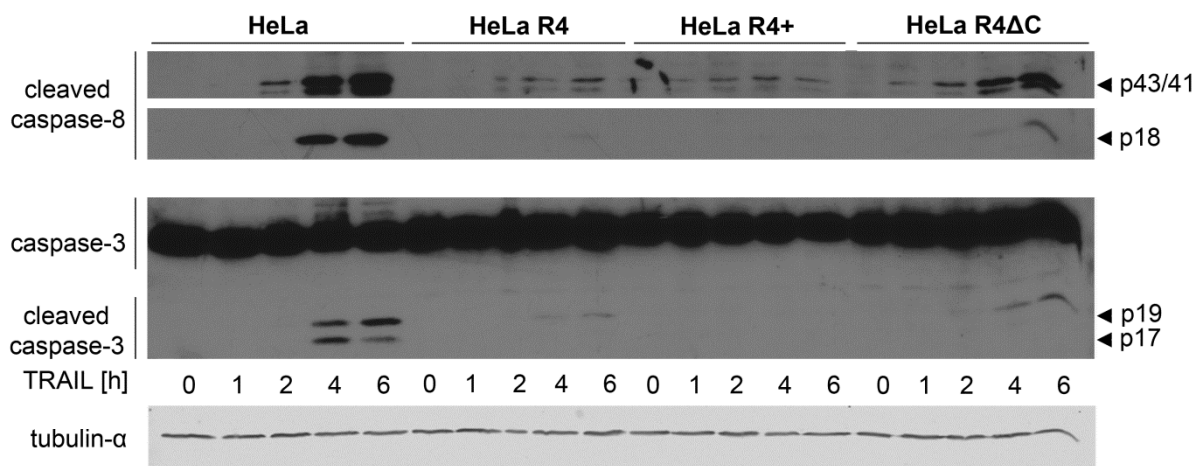
Figure 22: Distinct patterns of caspase cleavage in HeLa wild type cells and cells overexpressing TRAILR4. Cells were treated with 300 ng/ml M2-crosslinked sTRAIL for the indicated times or left untreated. Total cell extracts (50 µg of protein per sample) were subjected to SDS-Page and western blot analysis using antibodies directed against cleaved caspase-8 or caspase-3. Tubulin-α was used as loading control. Blots shown are representative of three independent experiments.

3.4.2. TRAILR4 expressing cells show reduced caspase-9 activation

Stimulation of death receptors initially leads to induction of the extrinsic apoptosis pathway by activation of the initiator caspase-8 at the DISC. In many cells, called type II cells, the attained levels of active caspase-8 are not sufficient to induce apoptosis (Scaffidi et al., 1998). Therefore type II cells rely on induction of the intrinsic pathway to amplify apoptotic signaling via activation of caspase-9. As HeLa cells are generally classified as type II cells, the extent and kinetics of caspase-9 activation as result of TRAIL stimulation were investigated. The inactive procaspase-

9 could be detected in all four cell lines (HeLa, HeLa R4, HeLa R4+ and HeLa R4ΔC) at comparable levels. In HeLa cells low levels of active caspase-9, i.e. a caspase-9 fragment with a molecular weight of 37 kDa, could be detected after 2 hours of TRAIL treatment. The levels of active caspase-9 increased only slightly with longer incubation times. However, co-treatment of HeLa cells with CHX for 6 h (see lane 5 in Figure 23) in addition to the TRAIL treatment led to the detection of considerably higher levels of caspase-9 p37. HeLa R4 and HeLa R4+ cells showed similar kinetics, but generally lower levels, of caspase-9 cleavage. Interestingly, in TRAIL treated HeLa R4ΔC virtually no activation of caspase-9 could be detected (see lanes 15 to 18 in Figure 23).
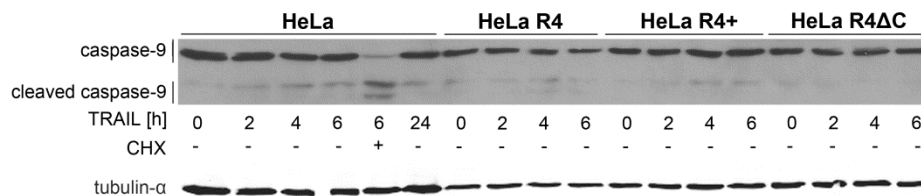
Figure 23: Activation of caspase-9 in response to TRAIL treatment. Cells were treated with 300 ng/ml M2-crosslinked sTRAIL alone or in combination with 2.5 µg/ml CHX or for the indicated times, or left untreated. Activation of caspase-9 was analyzed by western blotting using anti-caspase-9 antibody. Tubulin-α was used as loading control. Blots shown are representative of three independent experiments.

3.5. Activation of the transcription factor NFκB

Although a truncated variant of TRAILR4 could confer protection from TRAIL-induced apoptosis in the HeLa cell model used in this study, additional signaling-mediated protective effects could not be excluded. The transcription factor NFκB has been shown to become activated in response to TRAIL stimulation and is capable to induce the transcription of antiapoptotic genes. Direct activation of NFκB through TRAILR4 has been demonstrated in various cell lines, however this effect is very likely cell type-dependent. Activation of NFκB in HeLa and HeLa-derived cell lines was investigated by analyzing the phosphorylation of its inhibitor IκBα (Figure 24).
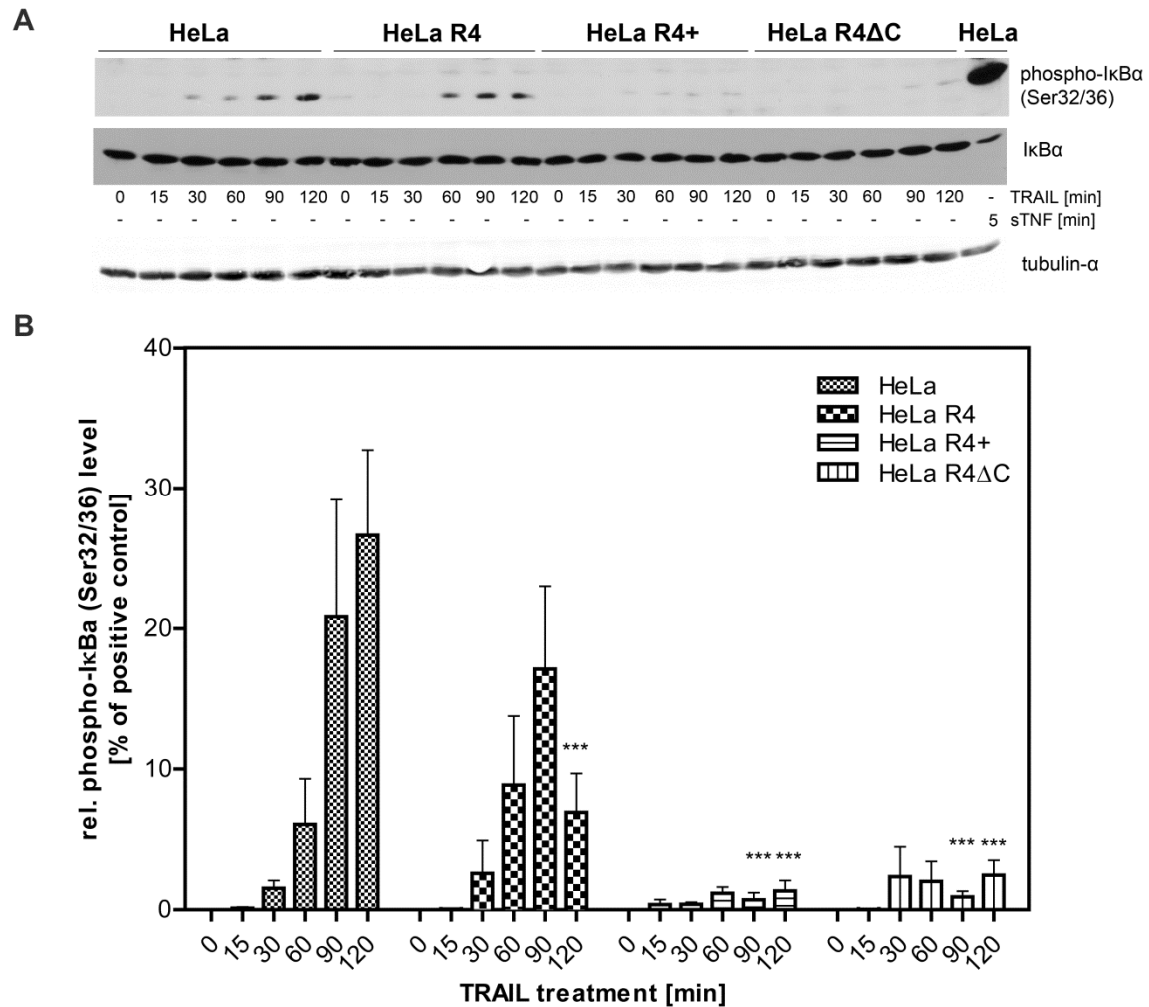
Figure 24: Receptor 4 inhibits TRAIL-induced phosphorylation of IκBα.
A: Cells were treated with 300 ng/ml sTRAIL (previously crosslinked by incubation with 1 µg/ml anti-FLAG M2 antibody) for the indicated time. As positive control, HeLa cells were treated with 10 ng/ml sTNF for 5 min (very right lane). Cell lysates (50 µg per sample) were subjected to western blot analysis using phospho-IκBα (Ser32/36) specific antibody. Blots were then re-probed for expression of total IκBα. Tubulin-α was used as loading control. **B:** Relative phospho-IκBα band intensities were quantified and normalized to the tubulin-α loading control. The normalized phospho-IκBα level of sTNF treated HeLa cells (i.e. the positive control) was set to 100% and all other values were normalized to this control. Values shown are mean ± SEM (n = 5). ***: $p < 0.001$ was considered to be significant as determined by two-way ANOVA and Bonferroni post-test in comparison to the respective time-point of TRAIL treated HeLa cells.

In HeLa cells phosphorylation of IκBα could be detected after 30 min of treatment with 300 ng/ml of antibody-crosslinked sTRAIL. The level of phospho-IκBα increased until it reached its maximum after 120 min of TRAIL treatment. Kinetics of IκBα phosphorylation in the HeLa-derived, TRAILR4-expressing cell line HeLa R4 were similar. Although the highest phospho-IκBα level was reached already 90 min after addition of TRAIL, activation of NFκB was reduced in comparison to the parental cell

line. In HeLa R4+ cells, which overexpress TRAIL receptor 4 at a considerably higher level than HeLa R4, phosphorylation of IκBα could barely be detected even at late time-points. Similar, significantly reduced, kinetics of NFκB activation were observed in HeLa R4ΔC cells expressing high levels of a truncated TRAILR4 variant (Figure 24).

3.6. Intracellular signaling in HeLa and TRAILR4 expressing HeLa cells

TRAILR4-mediated activation of survival pathways could potentially counteract TRAIL-induced apoptosis, hence contributing to the inhibitory effect of TRAILR4. The PKB/Akt pathway had recently been shown to be constitutively activated in TRAILR4 overexpressing HeLa cells (Lalaoui et al., 2011). In order to investigate a potential involvement of the PKB/Akt pathway in the observed inhibitory effect, the abundance of phosphorylated Akt (at serine residue 473) in HeLa wild type, HeLa R4, HeLa R4+ and HeLa R4ΔC was determined by western blotting (Figure 25). Basal levels of phosphorylated Akt were comparably low in all four cells lines. In addition, TRAIL treatment for up to 120 min did not result in any detectable alteration of phospho-Akt levels.
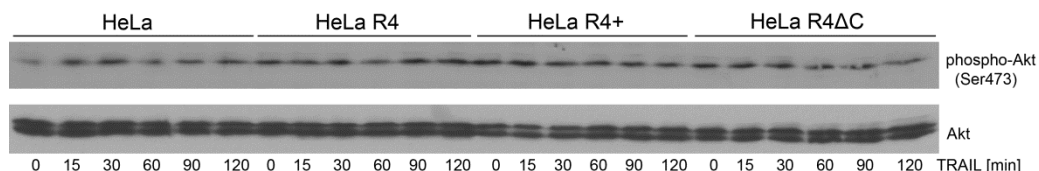
Figure 25: Akt phosphorylation is unaffected by TRAILR4 and TRAIL treatment. HeLa, HeLa R4, HeLa R4+ and HeLa R4ΔC were grown under reduced serum conditions (0.5% FCS) for 18 h. Following TRAIL treatment (300 ng/ml sTRAIL, previously crosslinked by incubation with 1 µg/ml anti-FLAG M2 antibody) for the indicated times, levels of Akt phosphorylated at serine residue 473 were determined by western blot analysis using phospho-Akt (Ser473) specific antibody. Akt was used as loading control. Blots shown are representative of three independent experiments.

Potential differences in intracellular signaling between HeLa and HeLa R4 cells were assessed using an antibody array. The PathScan Intracellular Signaling Array Kit allows for the parallel detection of 18 signaling molecules when becoming cleaved or phosphorylated. Heatmap analysis of the array results showed that basal phosphorylation levels were similar for most targets in the two cell lines. The most notable difference in untreated cells was the higher phospho-Bad level in HeLa cells

(Figure 26). In response to TRAIL treatment, phosphorylation of Bad increased slightly in both cell lines, with HeLa showing the highest level after 240 min TRAIL treatment. In HeLa R4 cells the level of phosphorylated Bad started to decrease at time-point 60 min. interestingly, the highest phospho-Bad signal in HeLa cells was detected after a long time of TRAIL treatment, while TRAIL rather induced a reduction of the phospho-Bad level in HeLa R4. PARP cleavage at aspartate 214 in HeLa cells increased with the time of TRAIL treatment, HeLa R4 cells showed only minor changes. High levels of phosphorylated PRAS40 were detected in untreated HeLa and HeLa R4 cells. TRAIL treatment (for 30 to 60 min) reduced phospho-PRAS40 levels in both cell lines. In response to longer stimulation PRAS40 phosphorylation increased again. In HeLa cells, PRAS40 phosphorylation evened out at levels comparable to unstimulated cells after 120 min of TRAIL treatment. Despite the increasing phospho-PRAS40 levels after continuous TRAIL treatment in HeLa R4 cells, the values remained lower than in untreated cells.

Cluster analysis (see dendrogram in Figure 26) showed that HeLa cells treated for 4 h with TRAIL were most distinct from all other experimental groups. The remaining experimental groups subdivided into two clusters. The first one contained both the untreated and the experimental groups of both cell lines which had been subjected to 120 min of TRAIL stimulation. The remaining groups, i.e. HeLa and HeLa R4 treated for 30 and 60 min as well as HeLa R4 which had been stimulated for 4 h, formed a more distant cluster.
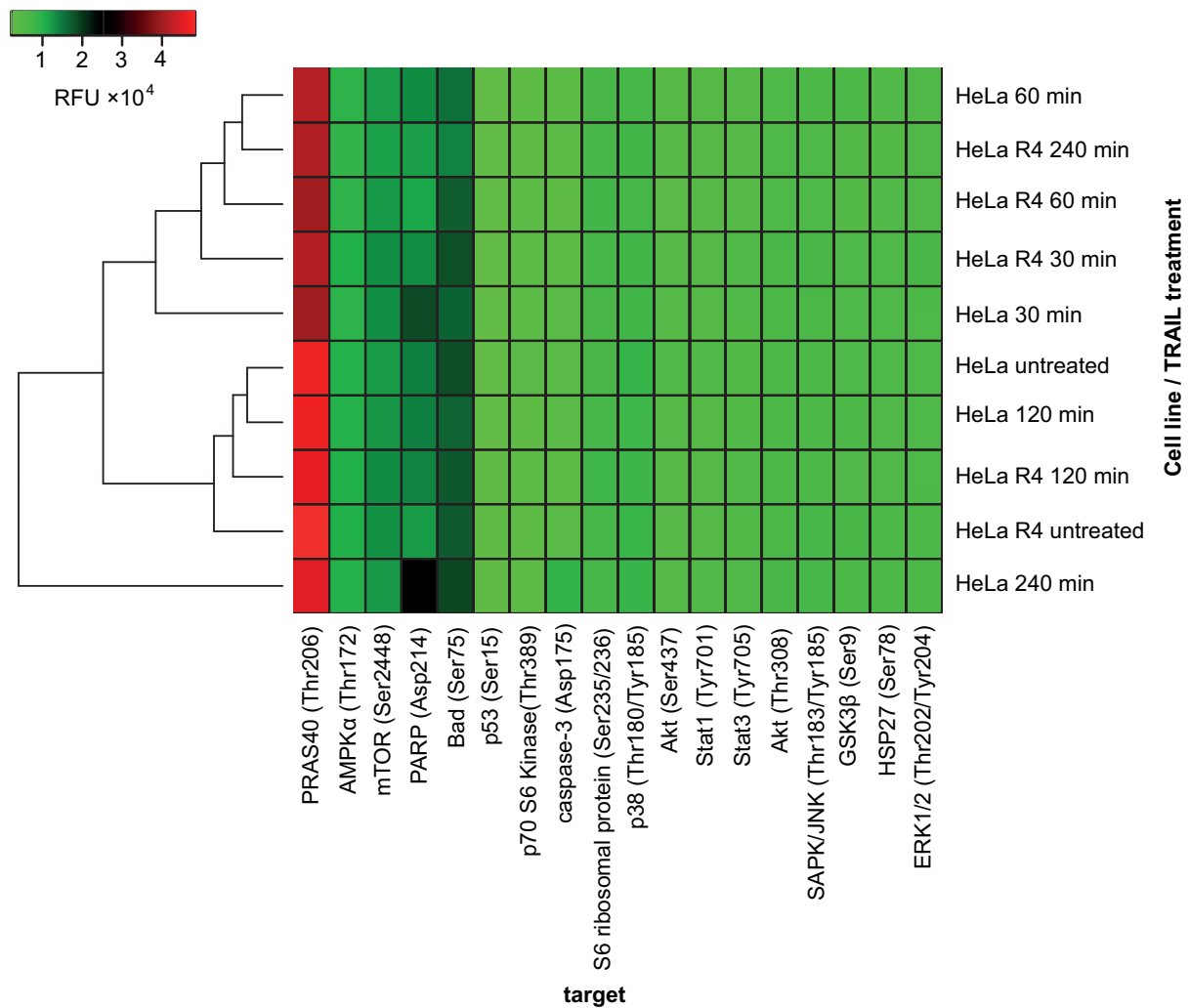
Figure 26: Intracellular signaling antibody array. HeLa and HeLa R4 cells were grown under reduced serum conditions (0.5% FCS) for 18 h and subsequently treated with 300 ng/ml M2-crosslinked sTRAIL for the indicated times or left untreated. Cell extracts were prepared and analyzed using the PathScan Intracellular Signaling Array Kit. Images were acquired using the Li-Cor Odyssey Bio-Imaging system and pixel intensities were quantified using Fiji. RFU: relative fluorescence units. Heatmap was generated using R. Results shown are mean values from two independent experiments calculated from duplicates.

4. Discussion

4.1. Receptor-receptor interactions in the human TRAIL system

The crystal structures of complexes between several members of the TNF receptor superfamily and their cognate ligands (TNFR1/LTα and TRAILR2/TRAIL) reveal interactions of the trimeric ligands with three monomeric receptors (Banner et al., 1993; Hymowitz et al., 1999; Mongkolsapaya et al., 1999). But not all complexes show this stoichiometry. For example, the crystal structure of CD40 in complex with its ligand CD154 (CD40L) reveals that only two of the three receptor binding sites of the ligand are occupied (An et al., 2011). In addition, a highly intricate structure for the TNFR2/TNF complex has been reported, showing a large aggregate containing two subunits of three receptor monomers and one ligand trimer each, undergoing interactions mediated by cysteine-rich domains of the receptors (Mukai et al., 2010). Based on the trimeric structures, the ligand-induced trimerization model was postulated to describe signal initiation in the TNFR superfamily. According to this hypothesis, three monomeric receptors are engaged by the trimeric ligand resulting in the formation of a small complex showing a 3:3-stoichiometry of receptor monomers and ligand protomers. This complex formation brings the intracellular domains of the receptors in close proximity thus enabling them to recruit downstream intracellular adapter proteins through homotypic interactions, hence triggering intracellular signals. This paradigm was challenged when CD95/Fas and TNFR1 were shown to exist on the cell membrane as pre-assembled oligomers even in absence of their ligands (Chan et al., 2000; Siegel et al., 2000). Receptor oligomerization is mediated by the pre-ligand binding assembly domain (PLAD) and was proposed to either represent a mechanism to achieve sufficient binding of cytokines, which are in a physiological context present only at low concentrations, by increasing the avidity or to prevent signal interference by promiscuous ligands (Chan, 2007). Furthermore, formation of large ligand-receptor clusters has been shown to be necessary for signal-initiation in the TNF and Fas systems. These high molecular weight complexes are presumably formed by ligand-receptor as well as receptor-receptor interactions through the PLAD (Krippner-Heidenreich et al., 2002; Henkler et al., 2005; Branschädel et al., 2010; Lewis et al., 2012). More recently, an important role for large ligand-receptor clusters was implicated in the TRAIL system, too (Wagner et al.,

2007; Adams et al., 2008; Valley et al., 2012). Although the importance of receptor clustering for successful signal initiation has been acclaimed, TRAIL receptor-receptor interactions mediated by the PLAD have only been partially elucidated to date. For TNFR1 and TNFR2, ligand-independent oligomerization has been established in several studies, however the stoichiometry of the oligomers (i.e. whether they form dimeric or trimeric complexes) is still a subject of discussion (Chan et al., 2000; Branschädel et al., 2010).

Clancy and colleagues showed co-immunoprecipitation of recombinant TRAIL receptors fused to different protein tags and implicated a role of PLAD-mediated receptor pre-assembly between TRAILR2 and TRAILR4 in the antiapoptotic effects of TRAILR4 (Clancy et al., 2005). However, these findings were refuted to a certain extent by a study of Mérino and colleagues. These authors demonstrated ligand-dependent oligomerization of TRAILR2 and TRAILR4 indicating that the spontaneous interaction between the death and decoy receptor observed by Clancy and colleagues might be mediated by membrane-bound TRAIL on the surface of the Jurkat T lymphocyte line used in these experiments (Mérino et al., 2006).

On account of these contradictory data, the first part of the here presented work focused on the elucidation and re-evaluation of ligand-independent receptor interactions in the human TRAIL system. The GPI anchored TRAILR3 is generally assumed to be located predominantly in particular membrane microdomains, also called lipid-rafts. Thus, it was proposed that this localization renders the receptor incapable to interact with the other human TRAIL receptors (Mérino et al., 2006). Therefore, TRAILR3 was not included in this study. Ectopic expression of the receptor fusion proteins in murine fibroblasts allowed the investigation of receptor pre-assembly without implicit interference from endogenous human TRAIL receptors. Ligand-independent interactions between TRAILR1, TRAILR2 and TRAILR4 could be demonstrated for all six permutations by fluorescence resonance energy transfer experiments. All FRET efficiencies measured for both homophilic and heterophilic interactions were significantly different from those values obtained from control experiments where TNFR1 was coexpressed as FRET donor together with TRAILR1 or TRAILR2 as FRET acceptor (Figure 6). Homophilic interaction of TRAIL receptors resulted in an articulate increase of donor fluorescence after acceptor photobleaching for all three FRET pairs (Figure 4). Efficient fluorescence resonance energy transfer depends on several factors, especially on the correct alignment of the dipoles and

the distance between donor and acceptor. For the eGFP/mCherry FRET pair used in this study, the Förster distance (i.e. the distance between the two fluorophores where the energy transfer efficiency is 50%) was reported to be 5.1 nm (Albertazzi et al., 2009). The highest energy transfer efficiency was measured for oligomerization of TRAILR2, being almost twice as high as the values measured for homo-oligomerization of TRAILR1 or TRAILR4. This could simply be caused by more favorable positioning of the two fluorophores at the intracellular part of these fusion proteins, resulting in better arrangement of the dipoles and hence more efficient energy transfer. Yet it could also point towards a stronger homophilic interaction of TRAILR2 fusion proteins or a different, presumably tighter, conformation of this receptor oligomer. In line with this argumentation, chemical crosslinking of TRAILR2 yielded homodimers in a highly efficient, near to quantitative manner (Figure 8 and see below). In fact, TRAILR2 carries in its transmembrane domain a GXXXG motif (amino acids 212 – 216, Gly-Ile-Ile-Ile-Gly) that is absent in the other TRAIL receptors. GXXXG motifs are known to represent dimerization motifs in helical transmembrane domains (Senes et al., 2004). This motif could contribute to the high FRET efficiency measured for TRAILR2 homo-oligomerization by inducing dimerization of the transmembrane domains, which would also bring the intracellular fluorescent proteins into closer proximity and/or simply by enhancing the overall affinity of receptor interaction, hence enabling more efficient energy transfer. The GXXXG motif has been shown to cooperate with a specific adjacent cysteine residue (Cys209) in the transmembrane domain of TRAILR2 to form a dimeric interaction interface involved in ligand-mediated formation of high molecular weight clusters (Valley et al., 2012). Hence, inferring from this report and the results obtained from acceptor photobleaching experiments, a contribution of this motif to the potent ligand-independent receptor dimerization could well be causative for the highly efficient fluorescence resonance energy transfer between TRAILR2 fusion proteins.

In agreement with this reasoning, the affinity of the mere PLAD-PLAD interaction of TRAILR2 appears not to be higher compared to that of TRAILR1 or TRAILR4, as determined by surface plasmon resonance studies (SPR) using the respective extracellular parts of these receptors (Lee et al., 2005). Interestingly, in these experiments the authors concluded that interactions between all receptors are possible, with the exception of TRAILR2 with the so-called decoy receptors (TRAILR3 and TRAILR4). However, interaction of receptor 4 with receptor 2 is

exactly the mechanism to which Clancy and coworkers ascribed the regulatory effect they observed in their experiments (Clancy et al., 2005). Consequently, heteromeric receptor-receptor interactions in the TRAIL system remain for the most part elusive.

As the exact impact of decoy receptor expression on TRAIL-mediated signaling is largely unclear and a definite correlation between TRAIL susceptibility and a cell's receptor endowment has so far not been satisfactorily demonstrated, this matter clearly requires clarification. Further, recent studies demonstrate that expression of TRAILR4 correlates with higher tumor grade, e.g. in breast cancer (Ganten et al., 2009), underlining the importance to deepen the general understanding of the characteristics and capabilities of the different TRAIL receptors. Accordingly, the acceptor photobleaching FRET experiments were repeated with different combinations of the TRAIL receptor fusion proteins to investigate possible heterophilic interactions (Figure 5). Energy transfer efficiencies obtained for the three different permutations of TRAILR-FP fusion proteins were overall similar and significantly different from the values measured in the experiments serving as negative controls (Figure 6).

The results concerning TRAIL receptor-receptor interactions presented in this work are in accordance with the findings reported by Clancy and colleagues (Clancy et al., 2005) and strongly substantiate the hypothesis of ligand-independent homo- and heterophilic interactions of TRAIL receptors. Furthermore, the here reported findings eliminate the ambiguity subsisting in the matter of heterotypic TRAIL receptor pre-assembly and they constitute the most comprehensive report of homo- and heteromeric pre-oligomerization of human TRAIL receptors 1, 2 and 4 in the plasma membrane of intact cells to date, thereby increasing the complexity of the already elaborate TRAIL system. Thus, in the case of TRAIL receptors, PLAD interactions appear not to prevent signal interference by promiscuous ligands, as proposed for TNF receptors (Chan, 2007), but could rather promote it. The implications of heterotypic receptor-receptor interactions on TRAIL signal transduction will be discussed later.

4.2. The stoichiometry of pre-assembled TRAIL receptor oligomers in the plasma membrane

Ligand-independent receptor pre-assembly of members of the TNF receptor superfamily has emerged as eminent foundation for signal induction in the TNF/TNFR superfamily. Albeit the capability of various receptors to interact in absence of their ligand has been the subject of several studies, the stoichiometry of these complexes is still a matter of discussion. In the first report on TNF receptor pre-assembly, Chan and colleagues presented data from crosslinking studies of cell surface proteins. They concluded that PLAD-mediated interactions result in trimerization of TNFR1 (Chan et al., 2000). In the case of CD95/Fas trimer formation was reported, too (Siegel et al., 2000). However, already several years earlier, the crystal structure of the soluble extracellular domains of TNFR1 in absence of ligand had been solved, demonstrating, among other structural arrangements, the formation of parallel homodimers (Naismith et al., 1995). Besides, more recently, PLAD-mediated trimerization was questioned as crosslinking data using a different chemical crosslinker and analysis under reducing conditions clearly showed that chimeric TNFR1- as well as TNFR2-Fas receptors interact in absence of their ligand to form dimeric complexes (Boschert et al., 2010; Branschädel et al., 2010). For TNFR1, this model is supported by data from FRET measurements as well as molecular dynamics simulation studies (Lewis et al., 2012).

Reports concerning the stoichiometry of pre-assembled TRAIL receptors are comparatively scarce. A molecular dynamics study performed by Wassenaar and colleagues revealed formation of an asymmetric TRAILR2 trimer (Wassenaar et al., 2008). This included a specific interaction between two receptor molecules, while the third one was only loosely bound. In addition, these authors stated that due to the limited simulation time and the fact that the simulation cell contained only three receptor molecules, trimer formation might be disproportionally favored. Of note, the observed self-association between the receptors was stabilized by interactions between the second cysteine-rich domains (CRD2). This domain is distinct from the proposed localization of the PLAD (Clancy et al., 2005) and is involved in ligand binding (Hymowitz et al., 1999).

In order to elucidate the composition of unligated TRAIL receptor complexes on the plasma membrane, chemical crosslinking experiments using the amine-reactive,

membrane impermeable and non-cleavable chemical crosslinking agent BS[3] were performed. As homo-oligomerization of TRAILR2 yielded the most efficient energy transfer in the FRET experiments (Figure 6) this receptor was chosen as paradigm. Considering that the death domains of TNFR1 and CD95/Fas are prone to self-association (Boldin et al., 1995), a truncated variant of TRAILR2, lacking the intracellular death domain, was used (see Figure 7A). Application of a non-thiol-cleavable chemical crosslinker allowed the analysis of crosslinked cell surface proteins under reducing conditions, eliminating a potential influence of the structure of the receptor complex on molecular weight determination. The monomeric receptor migrated closely to the calculated molecular weight of 27 kDa. Addition of the crosslinker (even at low concentrations) induced the formation of a covalently linked receptor dimer showing an apparent molecular weight of 55 kDa. The near to quantitative crosslinking efficiency, as indicated by the disappearance of the receptor monomer band, substantiates the hypothesis that pre-assembly of TRAILR2 on the plasma membrane is strongly favored and results in formation of dimeric complexes (Figure 8). Complexes of higher order could not be detected in any of the performed crosslinking experiments, even at the highest crosslinker concentration used. BS[3] features two amine-reactive groups at each end of an eight carbon atom spacer arm (length of the spacer is 1.14 nm). In order to accurately capture the stoichiometry of pre-assembled receptor complexes on the cell surface, the investigated receptors need to feature a sufficient number of accessible amine-groups. These are present at the amino-termini of proteins and the side chains of lysine residues. The extracellular domain of TRAILR2 contains eight lysine residues, which should provide enough possible reaction sites for BS[3] to link all the subunits of the oligomeric complexes. Hence, an underestimation of the numbers of receptors in the pre-assembled complex due to incomplete crosslinking is very unlikely.

The observed prevalence of pre-assembled receptor dimers is presumably the combined result of PLAD interactions and interactions mediated by the GXXXG motif in the transmembrane domain of TRAILR2. A cysteine residue (Cys209) in close proximity to the GXXXG motif has recently been implicated in the ligand-dependent formation of TRAILR2 dimers (Valley et al., 2012). Valley and colleagues reasoned that TRAILR2 exists pre-assembled in trimeric complexes, which undergo a conformational change after ligand binding resulting in the formation of highly ordered receptor networks composed of receptor dimers. The dimeric interaction

motif could be localized to the transmembrane domain, comprising the previously mentioned GXXXG motif and a disulfide-bond formed between the cysteine residues at position 209 (Cys209 is merely present in the long splice variant of TRAILR2 (TRICK2B), also termed DR5-L, which was also used in the presented work) of adjacent receptors. Yet, they concede the possibility that the complex is further stabilized by interactions of the ECDs, presumably mediated by the PLAD. The results presented by Valley and colleagues concerning the formation of organized TRAILR2 networks are indisputably intriguing, however their findings concerning the stoichiometry of unligated TRAILR2 invoke alternative interpretations. First of all, samples were analyzed by non-reducing SDS-polyacrylamide gel-electrophoresis. Under these conditions the elongated structure of the receptor may be retained, possibly influencing its migration and hence the reliable determination of the molecular weight of the complexes. Secondly, the proposed agonist-induced dimeric complex is absent in all crosslinker-treated samples. The authors state that this structure, as well as the ligand-bound trimer, could exists only transiently and be rapidly incorporated into multimeric complexes (molecular weight > 200 kDa) of TRAILR2. In contrast, earlier experiments in the TNF system performed in our group showed the specific description of the stoichiometry of a chemically crosslinked TNF ligand-receptor complex (Branschädel, 2007).

Furthermore, the variance in the reported stoichiometries could be caused by different temperatures during the crosslinking reaction. Crosslinking at room temperature could allow for the formation of larger complexes as a result of diffusion of the receptor oligomers in the plasma membrane, potentially allowing for crosslinking of non-interacting receptors. The fluidity of the plasma membrane, and hence also diffusion of transmembrane proteins, is strongly reduced at lower temperatures. Since the here presented elucidation of the stoichiometry of pre-assembled TRAILR2 oligomers was conducted using samples from chemical crosslinking experiments performed at low temperatures (i.e. on ice), the oligomerization status of this receptor is captured more precisely than in experiments performed at higher temperatures.

The demonstration of ligand-independent trimer formation by Valley and colleagues could also be a result of interactions of the receptors' death domains, as they show that transient overexpression of TRAILR2 (DR5-L) in HEK293 cells leads to the formation of high molecular weight clusters. Consequently, western blot analyses of

crosslinked cell surface proteins revealed dimeric, trimeric and oligomeric complexes of TRAILR2 (Valley et al., 2012). The detection of receptor dimers, which were previously described to be ligand-induced, is ascribed to receptor crowding in the membrane. Crosslinking of truncated TRAILR2 (which is devoid of the intracellular death domain) as performed in the here presented work, resulted in the exclusive detection of dimeric receptor oligomers. No higher oligomers could be detected, so that artifacts through overexpression-induced protein crowding are unlikely (see Figure 8). Inferring from these findings, pre-assembly of TRAILR2, as mediated by the ECD and possibly the TM domain, results in the formation of dimeric complexes. As the proposed pre-ligand binding assembly domain of TRAIL receptors is highly conserved, it can be hypothesized that this holds true for all homotypic interactions of TRAIL receptors.

A potential influence on TRAIL signaling has been attributed to the pre-assembly of TRAIL receptors into heteromeric complexes (Kimberley and Screaton, 2004; Clancy et al., 2005). However, no reports concerning the stoichiometry of heteromeric receptor oligomers have been published to date. Given that truncated TRAILR2 undergoes dimerization with high efficiency, this receptor was chosen to set up and optimize an experimental approach for the sensitive and specific detection and characterization of heteromeric TRAIL receptor oligomers. Truncated, FLAG-tagged TRAILR2 was coexpressed with a GFP-tagged version of the same receptor in murine fibroblast cells. After crosslinker treatment, the FLAG-tagged TRAILR2 variant was immunoprecipitated and western blot analysis using GFP-specific antibody confirmed efficient dimer formation (Figure 9). By means of this experimental approach the ligand-independent heterotypic pre-assembly of TRAIL receptors, already reported in this work based on FRET experiments, could be confirmed. In addition, the stoichiometry of these oligomers was reported. Crosslinked, immunoprecipitated hetero-oligomers of the two death receptors (TRAILR1 and TRAILR2), and also of either of these death receptors and one of the decoy receptors (TRAILR1/TRAILR2 and TRAILR4) clearly showed a dimeric stoichiometry (see Figure 10 to Figure 12). Consequently, the three human TRAIL receptors included in the presented work undergo homo- and heterotypic interactions on the plasma membrane, resulting in formation of dimeric complexes.

Although all experimental findings gathered in this work support the hypothesis of predominant ligand-independent dimerization of TRAIL receptors, the existence of

higher order oligomers cannot be completely excluded. Yet, several other members of the TNF receptor superfamily, including not only TNFR1 but also the herpes virus entry mediator (HVEM), the p75-nerve growth factor receptor, decoy receptor 3 (DcR3) and CD40 have been shown to assemble in dimeric complexes in absence of their respective ligand (Connolly et al., 2002; He and Garcia, 2004; Zhan et al., 2011; Smulski et al., 2013). Thus, ligand-independent dimerization might well be a mutual characteristic of many, if not all, TNF receptor superfamily members.

4.3. Role of the ECD in receptor-receptor interaction

The only solved crystal structure of a TRAIL receptors is that of TRAILR2 in complex with its ligand (Hymowitz et al., 1999; Mongkolsapaya et al., 1999; Cha et al., 2000). Similar to the structure of TNFR1 in complex with LTα (Banner et al., 1993), three receptor monomers are shown in tight interaction with one ligand trimer, while no receptor-receptor interactions are apparent. Yet, for TNFR1 additional crystal structures of the unligated receptor could be solved, delivering insight into domains potentially involved in receptor-receptor interactions (Naismith et al., 1995; Naismith et al., 1996). The parallel structure of unligated TNFR1 shows extensive contacts between the membrane-distal cysteine-rich domains (CRD1) of the two receptor monomers, indicating the likely localization of the pre-ligand binding assembly domain. As no structures of unligated TRAIL receptors have been reported to date, information about the localization of the PLAD in TRAIL receptors is only available from the study of deletion mutants. Deletion of the partial CRD1 of TRALR2 and TRAILR4 was shown to abolish receptor-receptor interactions (Clancy et al., 2005). However, CRD1 deletion also negatively influenced the ligand binding capacity, raising the question whether this resulted in misfolding of adjacent domains, as was the case for TNFR1 (Branschädel et al., 2010). The partial CRD1, which is conserved in all TRAIL receptors, features merely one disulfide bond, opposed to three in the complete CRD1 of CD95/Fas and the two TNF receptors. Accordingly, the feasibility of receptor-receptor interactions mediated by this partial CRD was doubted (Lee et al., 2005). Clearly, the crystal structure of the TRAILR2/TRAIL complex reveals extensive contacts of the ligand with CRD2 and CRD3 of the receptor (Hymowitz et al., 1999), questioning whether these domains could additionally mediate receptor-receptor interactions. Consequently, CRD1 would be the only part of the extracellular domain capable of forming these interactions in ligand-receptor complexes. However,

the possibility of one CRD harboring two distinctive binding sites, one for the receptor's cognate ligand and the second one for receptor-receptor interactions, cannot be excluded. Notably, the extracellular domain of the receptor for the cytokine TNF-like weak inducer of apoptosis (TWEAK), Fn14 (TNFRSF12A), forms merely one single CRD (He et al., 2009). Pre-assembly of this receptor has however not been investigated. Under the premise that receptor-receptor interactions are common features of receptors of the TNF superfamily, the single CRD would have to account for both interactions with the ligand and a second receptor molecule.

Lee and colleagues showed that bacterially expressed, recombinant soluble extracellular domains of TRAIL receptors interact specifically and retain ligand binding capacity (Lee et al., 2005). However, the absence of post-translational modifications in bacterially expressed proteins could potentially alter their behavior and interaction characteristics. Particularly O-linked glycosylation has been shown to determine the aggregation state of glycosylated membrane-bound proteins and could hence affect signaling or binding properties of proteins (Hermiston et al., 2003; Hang and Bertozzi, 2005). The extracellular domains of TRAILR1 and TRAILR2 contain several conserved O-glycosylation sites and O-linked glycosylation of death receptors was shown to modulate the induction of intracellular signals by promoting ligand-dependent receptor clustering (Wagner et al., 2007). Hypothetically, post-translational modifications could also influence ligand-independent pre-assembly of receptors. In order to investigate this, the soluble ECDs of TRAILR1 and TRAILR4 were recombinantly expressed in HEK293T cells. Production was hampered by low yield and the precise determination of the molecular weights was complicated by post-translational modifications. However, crosslinking of the soluble proteins demonstrated that the ECDs of TRAILR1 and TRAILR4 are sufficient to mediate homo-oligomerization. As demonstrated for homotypic pre-assembly of TRAILR2, the predominant oligomeric species was the dimer. However, at higher crosslinker concentrations multimerization of the soluble receptors was observed. Importantly, this was more pronounced for TRAILR1, where both monomeric and dimeric complexes decreased in abundance, presumably being incorporated into high molecular weight complexes, which were excluded from analysis by SDS-polyacrylamide gel-electrophoresis (Figure 13C). Soluble TRAILR4 showed an overall lower propensity to oligomerize. Dimer formation became apparent already at low crosslinker concentrations and only treatment with high BS^3 concentrations

induced low abundant formation of higher order oligomers, intriguingly of apparently trimeric complexes (Figure 13D). Supposedly, TRAIL receptors are in a dynamic equilibrium between monomers, dimers and oligomers with the plasma membrane limiting the allowed conformations to dimers. Howbeit, the results obtained from crosslinking of soluble recombinant TRAIL receptors 1 and 4 show that predominant dimerization is an intrinsic capacity of the ECDs of these receptors.

Quartz crystal microbalance measurements confirmed that soluble TRAILR1 and TRAILR4 retained their ligand binding capacity (Figure 14). The determined values for the dissociation constants (K_d) for the receptor-ligand interactions are well within the range of affinities reported in literature, confirming again that TRAILR4 has a lower affinity to its ligand than for example the death receptor TRAILR1 (Truneh et al., 2000; Clancy et al., 2005; Lee et al., 2005). Measuring the association and dissociation of sTRAILR4 to immobilized sTRAILR1 yielded a dissociation constant of approximately 50 nM. This is considerably higher than the value reported by Lee et al. for heterophilic interactions of bacterially expressed soluble receptors. Interestingly, the dissociation rate constant values were virtually equal (1×10^{-3} *versus* 1.13×10^{-3} s^{-1}), confirming that the sTRAILR1/sTRAILR4 complex remains relatively stable once formed. Accordingly, the observed affinity difference can be completely attributed to different association rate constants. Compared to the SPR measurements performed by Lee and colleagues, the QCM experiments reported in this work yielded an approximately 30-fold higher association rate constant. This discrepancy can be explained in two different ways. First, inaccurate determination of the molecular weight of the recombinant proteins due to post-translational modifications could influence the calculated rates and constants to a certain degree. Second, using a 1:1 binding model, the here obtained curve fit could only approximate the actual measurements indicating a more complex binding pattern. For example, glycosylation of the ECDs could hypothetically favor ligand-independent pre-assembly while causing some heterogeneity in affinities, which would explain the overall higher association rate constant.

4.4. Possible implications of receptor pre-assembly on DISC formation

Heteromeric pre-assembly of TRAIL receptors has the potential to negatively affect productive DISC formation. Due to their comparably lower affinity for their ligand TRAIL (Truneh et al., 2000; Clancy et al., 2005; Lee et al., 2005), both decoy receptors would be less likely incorporated into high molecular weight ligand-receptor complexes if TRAIL receptors were either only capable to undergo homophilic interactions or unable to interact at all. However, the demonstrated heterophilic interactions of death and decoy receptors indicate a dynamic equilibrium between death receptor-only, decoy receptor-only and mixed death/decoy receptor complexes, with the equilibrium distribution of these three complexes driven by the different affinities of the respective PLAD-mediated interactions. Hence, in a DISC composed of death receptor-only, decoy receptor-only and mixed receptor dimers, the functional death domains of TRAILR1 and/or TRAILR2 would incur interference from the truncated, non-functional death domain of TRAILR4. This could constrain the recruitment of the adapter protein FADD, hence inhibiting downstream signaling. As the structure of the TRAIL-induced DISC is not known in its exact molecular composition, no conclusive statements can be made as to which extent decoy receptors might hamper effective DISC formation. Various studies from the CD95/Fas system, however, give insight into the structure and stoichiometry of the FasL-induced DISC. The first hints regarding the DISC stoichiometry were obtained when it was reported that a hexameric FasL construct (i.e. a dimer of three ligand protomers) is the minimal oligomer of FasL capable to induce apoptosis (Holler et al., 2003). The demonstration of FADD self-association in complexes of activated death receptors and FADD, resulting in FADD-bridges, gave rise to the concept of the 'honeycomb' DISC (Carrington et al., 2006; Sandu et al., 2006). Alternative to FADD-bridges, formation of the hexagonal 'honeycomb' structure has also been attributed to interactions of the death domains of CD95/Fas in a tetrameric complex with the death domain of FADD (Scott et al., 2008). However, an alternative crystal structure of the Fas-FADD death domain complex was solved, showing asymmetric oligomerization of five to seven Fas and five FADD death domains (Wang et al., 2010). This structure illustrates the need for hexameric or membrane-bound FasL for efficient signal initiation and shows high resemblance to the PIDD-RAIDD death domain complex

(forming the core of the PIDDosome, the caspase-2 activation complex (Park et al., 2007b)), hence demonstrating conserved interactions in the DD superfamily. Crucially, it also provides a basis for the structural mechanisms underlying the autoimmune lymphoproliferative syndrome (ALPS), which is often caused by mutations in the intracellular death domain of Fas.

The prevailing model describing formation of the DISC states that binding of the ligand to death receptors triggers recruitment of the intracellular adapter protein FADD, which then associates to the DD of the receptor via homotypic interactions. FADD then recruits DED-only proteins (procaspase-8, -10, cFLIP) to its DED, hence forming the active DISC (Krammer et al., 2007). Activation of procaspase-8 (or -10) then occurs through dimerization and proteolytic cleavage (Hughes et al., 2009; Oberst et al., 2010). For effective caspase-8 activation, close proximity between two procaspase-8 dimers (i.e. four procaspase-8 molecules) appears to be required, as cleavage and activation can follow an intermolecular/interdimer processing model (Chang et al., 2003; Hughes et al., 2009; Dickens et al., 2012a). Both crystal structures of the Fas-FADD death domain complex could provide a dimerization interface for procaspase-8 activation. The structure solved by Scott and coworkers in addition demonstrates a need for the formation of ligand-receptor clusters in order to stabilize the DISC (Scott et al., 2008). Though, none of the mentioned studies reports the structure resulting from the interaction of full-length Fas and FADD. Hence, the molecular structure and exact composition of the native DISC remains unknown.

A recent study focusing on the composition of the native TRAIL DISC reports that the amount of FADD molecules in the active DISC is considerably lower than the numbers of TRAIL receptors and DED-only proteins. Accordingly, the death domains of several receptors (two to five) could be necessary to recruit one molecule of FADD, while FADD presumably recruits several molecules of procaspase-8 (or other DED-only proteins), resulting in the formation of DED-chains which form the scaffold for effective procaspase dimerization and activation (Dickens et al., 2012a). Hypothetically, pre-assembled TRAIL (death) receptors could, subsequent to ligand binding, cooperate to conjointly recruit one molecule of FADD. Pursuant to this model, mixed death-receptor only complexes would retain the capability to recruit FADD to their death domain(s). However, heteromeric complexes composed of death and decoy receptor would be severely incapacitated in this respect.

Notwithstanding these recent findings, also according to the original model (one molecule of FADD recruited to each death domain, with the two FADD molecules forming a dimeric interface for the recruitment and activation of procaspase-8) the ability of heterodimeric (death/decoy) receptor complexes to contribute to productive DISC formation would be greatly reduced. Decoy receptors could thereby, via formation of heteromeric complexes with DD-containing receptors, have a strong inhibitory effect, possibly even in a dominant negative manner.

4.5. Signal interference through receptor pre-assembly

The impact of receptor pre-assembly on TRAIL signaling was studied using HeLa cells, which show almost exclusive expression of TRAILR1 (Figure 16), as cellular model. TRAIL treatment in combination with protein synthesis inhibition induced cell death in a concentration-dependent manner. Pretreatment with a pan-caspase inhibitor confirmed that the observed cell death was apoptotic. HeLa cells engineered to stably express wild type TRAILR4 were significantly less susceptible to the apoptotic effects of TRAIL and the extent of the inhibitory effect of TRAILR4 was clearly correlated to the cell surface expression of this receptor (Figure 19). Interestingly, resistance to apoptosis was not mediated by intracellular signal transduction emanating from TRAILR4, as a truncated variant lacking virtually the complete intracellular domain was capable to confer protection to a similar extent as the wild type receptor (Figure 21). The antagonistic effect of TRAILR4 on apoptosis induction had been reported already shortly after its molecular cloning. Similar to TRAILR3, TRAILR4 was originally proposed to act as a decoy receptor, i.e. to antagonize TRAIL signaling by competing for the ligand with the two death receptors (Degli-Esposti et al., 1997a; Pan et al., 1998). Yet, affinity measurements have shown that TRAILR4 does not bind TRAIL with higher affinity than the other TRAIL receptors (Degli-Esposti et al., 1997a; Truneh et al., 2000; Clancy et al., 2005; Lee et al., 2005), hence questioning the decoy hypothesis.

The exact number of TRAIL receptors on the surface of the HeLa-derived cell lines used in this work is not known. However, estimation of the receptor numbers on the basis of cytofluorometric data show that the number of ligand molecules in the cytotoxicity experiments is at least 1000-fold higher than the total number of receptors. Hence, it can be assumed that during the whole experiment the ligand concentrations remain constant at least at the highest TRAIL concentration.

Accordingly, the decoy hypothesis, in terms of wastage of ligand, does not suffice to describe the observed inhibitory effect of TRAILR4 on TRAIL-induced apoptosis.

Formation of mixed receptor complexes is an additional mechanism through which TRAILR4 could antagonize TRAIL signaling. Initially, complex formation was proposed to be ligand-dependent (Ashkenazi and Dixit, 1999) and this had later been confirmed experimentally (Mérino et al., 2006). However, at least for the combination of TRAILR2 and TRAILR4, compelling evidence for a regulatory effect through ligand-independent receptor pre-assembly had also been reported (Clancy et al., 2005), but this interpretation of the presented results was later questioned by other authors (Mérino et al., 2006). Furthermore, alike the decoy hypothesis, mixed complex formation through a ligand-driven mechanism should be rendered rather inefficient due to the comparably low affinity of the antagonistic receptors for the ligand (Truneh et al., 2000; Lee et al., 2005). Taking these considerations into account, the exclusion of TRAILR1 from ligand-receptor complexes in a cellular system expressing both TRAIL death receptors as well as TRAILR4, as reported by Mérino and coworkers (Mérino et al., 2006), raises questions. The distribution of bound ligand to the different receptors should be governed mainly by the receptors' respective ligand binding affinity and possibly in a particular manner by the association rate constant. Thus, under the premise of comparable receptor expression levels, the majority of the death receptors should be ligated at certain ligand concentrations, whereas the decoy receptors are not, resulting in efficient activation of the apoptotic pathway. Essentially, this assumption might hold true also for pre-assembled heterodimeric receptor complexes although the situation is much more complex.

Assuming dimerized receptors in a conformation similar to that of the crystallized parallel form of TNFR1 (Naismith et al., 1995), the first low affinity binding step would be the interaction of one TRAIL homotrimer with one of the dimerized receptors without interfering with the PLAD-PLAD interaction. According to theoretical studies the next likely step is a conformational change of this primary complex resulting in release of the PLAD-PLAD interaction but leading to a complex where both receptors are bound to two of the trimeric ligand's receptor binding sites (Winkel et al., 2012). Most likely, formation of this secondary complex defines the affinity values obtained under conditions suitable for equilibrium binding studies, i.e. performed on ice, as

described in literature (Boschert et al., 2010). These affinity values, accordingly, already include avidity effects, as the ligand is bound by two receptor molecules.

In any case, all forms of receptor dimers will interact with ligand and form the mentioned secondary complex presumed the concentration of the ligand is high enough. Assuming that the death receptor in a heterodimeric complex binds the ligand with the same affinity as in a homodimeric complex, the likelihood of ligand binding by the decoy receptor in the complex would be augmented by the mechanism proposed by Winkel and coworkers (Winkel et al., 2012). Hence, both subunits of a heteromeric complex could be incorporated into a ligand-receptor cluster with similar efficiency as the receptors in a death receptor-only dimer.

Generally, whether ligand-independent receptor-receptor interactions play a role in signaling interference in the TRAIL system remained unanswered to date. Although the presented work cannot offer full proof for this hypothesis, it does convincingly support it. Pre-assembly of TRAILR4 with both death receptors could be demonstrated and was confirmed by a second, fundamentally different method (see Figure 5, Figure 11 and Figure 12). Interaction of receptors 1 and 4 was even reconfirmed in a third set of experiments (Figure 14). Hence, in cells coexpressing TRAILR1 and TRAILR4, a certain fraction of TRAILR1 molecules will be existent in heterodimeric complexes with TRAILR4. Thus, it can be proposed that TRAILR4 exhibits the observed effects in the HeLa-derived cell lines through ligand-independent pre-assembly with TRAILR1. Interestingly, Clancy and colleagues proposed the heterophilic interaction between receptor 1 and 4 to be rather weak compared to the respective homophilic interactions (Clancy et al., 2005), while SPR measurements show that the heterophilic interaction occurs with similar or even higher affinity than the homophilic ones (Lee et al., 2005). These findings were not reproduced by the energy transfer efficiency values in the FRET experiments (Figure 6), as comparable values for both homophilic and heterophilic interactions of TRAILR1 and TRAILR4 could be demonstrated. However, as stated earlier, other factors in addition to the mere affinity of the two interaction partners could strongly influence the measured FRET efficiencies

Differences with respect to apoptosis induction in HeLa cells expressing full-length or truncated receptor 4 became apparent already at the level of initiator caspase activation. Cleavage, and consequently full activation, of procaspase-8 after TRAIL treatment was considerably impaired in TRAILR4 expressing cells (Figure 22). This

effect could also be observed in cells expressing a truncated variant of TRAILR4 that lacked any signaling competence. Hence it appears likely that TRAILR4 interferes with productive DISC assembly and impedes efficient recruitment of FADD and as a result also initiator caspase recruitment and activation, merely by its lack of a functional death domain. Additional signaling-mediated effects that could impair induction or transduction of the apoptotic signal do not seem to play a prominent role, at least in the cellular system investigated here. This can be inferred from the observation that the signaling-incapable truncated receptor 4 variant (R4ΔC) was also capable to confer protection and in addition, an intracellular signaling array did not yield any articulate differences between the parental HeLa cell line and HeLa R4 cells (Figure 26, further discussed in 4.7). The differences in initiator caspase activation are mirrored in the kinetics of effector caspase-3 cleavage. Strikingly, HeLa R4ΔC cells are protected from TRAIL-induced apoptosis to a higher extent than HeLa R4 cells, despite showing slightly higher levels of activated caspase-8 and of the caspase-3 fragment p19, albeit the p17 fragment is undetectable in both cell lines indicating incomplete activation of caspase-3 (Nicholson et al., 1995). Whether this observation is connected to the not detectable activation of caspase-9 in HeLa R4ΔC (Figure 23) remains to be elucidated. Nonetheless, the protective or inhibitory effect of full-length and truncated TRAILR4 could be shown to be by and large equally effective in blocking apoptotic signaling.

In several studies, the transcription factor NFκB has been implicated in conferring protection from TRAIL-induced apoptosis (Plantivaux et al., 2009). Actually, activation of a NFκB-mediated survival pathway emanating from TRAILR4 has been proposed as a model for apoptosis inhibition (Degli-Esposti et al., 1997a), although a later study showed that activation of NFκB, while protecting cells from the deleterious effects of TNF, was not sufficient to counteract TRAIL-induced apoptosis (Hu et al., 1999). In addition, as previously mentioned, several studies were unable to confirm TRAIL-induced activation of NFκB by TRAILR4 (Marsters et al., 1997; Harper et al., 2001). Despite these discrepancies and the already proposed hypothesis that TRAILR4 mainly exerts its protective effects in the cellular models used in this work through the ligand-independent pre-assembly with TRAILR1, kinetics of IκBα phosphorylation were investigated (Figure 24). TNF treatment, which induces rapid phosphorylation and degradation of IκBα in HeLa cells (Miyamoto et al., 1994), was included in the experiments as positive control. Previous reports showed that TRAIL

does not activate NFκB in HeLa cells unless apical caspases are inhibited (Harper et al., 2001) or protein synthesis is blocked by cycloheximide (Wajant et al., 2000). Nonetheless, a weak but significant TRAIL-induced phosphorylation of IκBα, albeit no degradation of this inhibitory protein, could be observed in the parental HeLa cell line. Interestingly, coexpression of TRAILR4 considerably inhibited TRAIL-induced phosphorylation of IκBα mediated by TRAILR1. This effect was most apparent in cells expressing high levels of full-length or truncated TRAILR4. But also in HeLa R4 cells, expressing TRAILR1 and TRAILR4 in an approximate ratio of 1:1, a significant reduction of IκBα phosphorylation compared to wild type HeLa cells was observed. This observation indicates that TRAILR4 could exert a general regulatory or inhibitory effect on signaling by TRAILR1. NFκB activation by TRAIL receptors has been described to be RIP1-dependent (Lin et al., 2000) and to emanate from a secondary signaling complex which is assembled subsequent to formation of the DISC. This intracellular complex II retains several DISC components and its association requires caspase-8 activity (Varfolomeev et al., 2005).

Recently, an additional model for the TRAIL-mediated activation of NFκB describing a RIP1-independent, yet FADD- and caspase-8-dependent mechanism, was proposed (Grunert et al., 2012). Both models show a crucial requirement for caspase-8 in the TRAIL-induced activation of NFκB. Hence, the attenuated IκBα phosphorylation in TRAILR4 expressing cells was likely caused by reduced recruitment of procaspase-8 into the DISC, and/or the resulting less efficient activation of caspase-8 at the DISC, leading to less efficient formation of the cytoplasmic complex II.

Caspase-8 is not only necessary for apoptosis induction and activation of NFκB by TRAIL, yet also additional non-apoptotic signaling pathways, like JNK and p38, can be blocked by caspase-8 knockdown (Kavuri et al., 2011). While the active site of caspase-8 was shown to be necessary for NFκB activation (Grunert et al., 2012), caspase-8 activity appears non-essential as TRAIL-induced NFκB activation is not blocked by pan-caspase inhibitors (Kavuri et al., 2011). Accordingly, the formation of mixed receptor complexes between TRAIL death and decoy receptors could have a general inhibitory effect on both apoptotic and non-apoptotic signaling induced by TRAIL. Whether this effect can be solely ascribed to reduced procaspase-8 recruitment into or activation at the DISC remains to be clarified. Further possible mechanisms include interference of TRAILR4 with cluster formation by TRAILR1,

altered kinetics of ligand-receptor complex internalization or inhibition of the formation of functional complex II.

4.6. The mechanism underlying the inhibitory effect of TRAILR4: Reduction of signaling competent units?

In the studied cellular system, TRAILR4 can efficiently antagonize signals emanating from TRAILR1. As a decoy mechanism can be excluded, the principle underlying this antagonism is likely to be based on the formation of mixed receptor complexes through ligand-independent interactions mediated by the extracellular domains. Analysis of cell surface expression of both receptors on HeLa R4 cells by flow cytometry using saturating antibody concentrations revealed a death to decoy receptor ratio of about 1:1. At this receptor concentration, TRAILR4 does render the cells overall less susceptible to TRAIL-induced apoptosis, reducing cell death at the highest TRAIL concentration by 18%. But also the absolute EC_{50} value (i.e. the TRAIL concentration that induces 50% cell death) is increased 3.3-fold compared to parental HeLa cells. This reduced sensitivity is caused by less productive DISC formation due to the interference of the non-death domain containing TRAILR4.

Accumulating evidence, both experimental and based on molecular modeling, indicates that receptor dimers represent the actual signaling competent unit in the TNF superfamily. For TNF, ligands with individually mutated receptor binding sites, resulting in molecules with only two receptor binding sites, were shown to be similarly effective as the wild type ligand (Boschert et al., 2010). Furthermore, the structure of the ligand-receptor complex, which was reported for several TNF superfamily members based on X-ray diffraction crystallography (Banner et al., 1993; Hymowitz et al., 1999), has been indicated to be energetically unfavorable based on molecular dynamics studies. In contrast, association of either one or two receptor molecules with one ligand trimer is favored (Mascarenhas and Kästner, 2012). Inferring from these reports, ligation of death receptors by their trimeric ligand could primarily result in the formation of hexameric ligand-receptor complexes containing six receptor dimers complexed by the same number of ligand trimers. These hypothetical structures closely resemble the proposed 'honeycomb' DISC (Carrington et al., 2006; Sandu et al., 2006) and their basic composition is in accordance with both resolved crystal structures of the Fas-FADD death domain complex (Scott et al., 2008; Wang et al., 2010).

Experimental corroboration for the hypothesis of signal transduction emanating from receptor dimers within multimeric ligand-receptor networks is gained from a recent study demonstrating that TNFR1 dimers are in principle signaling competent and that ligand binding in combination with the formation of ligand-receptor clusters urges receptor dimers to assume their functional conformation and is thus sufficient and necessary for signal induction (Lewis et al., 2012).

Lastly, also data from the TRAIL system support the necessity of dimeric receptor-receptor interactions for efficient signal transduction. Albeit Valley et al. reported a stoichiometry of unligated TRAIL receptor complexes deviating from the one demonstrated in the here presented work (discussed in 4.2), they present conclusive evidence for ligand-induced receptor clusters composed of receptor dimers (Valley et al., 2012). Inferring from these studies, the pre-assembled TRAIL receptor dimers are likely the units that mediate signal initiation and transduction subsequent to binding of ligand molecules and integration into larger clusters. Hence, the reduced sensitivity of HeLa R4 cells, expressing death and decoy receptors in approximately equal amounts, can be readily explained by an apparent reduction of signaling competent units. This reduction can be verified and explained through quantitative considerations. Assuming comparable affinities for homophilic and heterophilic interactions of TRAILR1 and TRAILR4, as well as for both receptors towards the ligand, and disregarding any potential restraints exerted from e.g. limited diffusion in the plasma membrane or compartmentalization into membrane microdomains, the equilibrium distribution would show one-third each of death receptor-only, decoy receptor-only and mixed complexes. Thus the amount of signaling competent TRAILR1 homodimers is reduced by one-third. As already mentioned, in HeLa R4 cells a 3.3-fold higher TRAIL concentration is necessary to induce 50% cell death. A simplified description of the kinetics of TRAIL binding to the receptor dimers can be given according to Equation 1, deduced from the Langmuir adsorption isotherm (Langmuir, 1916).

$$\theta_i = \frac{c_i}{c_i \times K_d}$$

Equation 1: θ_i: fraction of receptor bound to ligand, c_i: relative ligand concentration and K_d: dissociation constant. For c_i we assume relative concentrations, that is $c_1 = 1$ and $c_2 = 3.3$. For K_d we assume an arbitrary value between c_1 and c_2, hence $K_d = 1.65$.

Solving this equation for c_1 results in $\theta_1 = 0.38$ and for c_2 in $\theta_2 = 0.67$. Accordingly, increasing the ligand concentration by a factor of 3.3 results in a 1.76-fold increase of the fraction of receptors that are complexed by their ligand. As in HeLa R4 cells the number of signaling competent receptor dimers is reduced by 33%, the fraction of signaling homomeric TRAILR1 complexes at concentration c_2 is 44%. At the same concentration, in HeLa cells, the amount of homodimeric TRAILR1 complexes bound by the ligand would be 1.5-fold higher, which would result in a considerably stronger apoptotic signal. Thus this estimation supports the hypothesis that TRAILR4 can exert its inhibitory effect solely through heteromeric pre-assembly with TRAILR1, provided this heteromer is signaling incompetent after incorporation into a ligand-receptor cluster.

However, published values for the dissociation constants of homophilic and heterophilic PLAD-mediated interactions of TRAILR1 and TRAILR4 are not entirely equal. While the K_d values for homophilic interactions of TRAILR4 and for heterophilic interactions of TRAILR1 and TRAILR4 are essentially the same, the K_d value reported for homotypic association of TRAILR1 is 5.5-fold higher (Lee et al., 2005). Consequently the formation of heterodimeric complexes should be favored over homodimerization of TRAILR1, leading to a further reduction of signaling units. Hence an even stronger inhibitory effect of TRAILR4 expression could be expected. Yet, one must take into account that several additional factors are likely to influence the equilibrium distribution of ligand-independent receptor complexes. TRAILR1 has been shown to undergo post-translational modification through palmitoylation (Rossin et al., 2009) and glycosylation (Wagner et al., 2007). Both modifications are likely to promote homotypic oligomerization by increasing the local concentration of TRAILR1 in membrane microdomains or by altering aggregation characteristics. Hence, the comparably low dissociation constant for homophilic PLAD-mediated association of TRAILR1 could be canceled out. Accordingly, albeit representing merely a simplification, the estimation given for the inhibitory effect of TRAILR4 is reasonable and provides insight into the mechanism through which it can interfere with apoptotic signaling.

4.7. Intracellular signals emanating from TRAILR4

The capability of TRAILR4 to induce intracellular signals has only been partially elucidated. Particularly its proficiency to activate the transcription factor NFκB appears to be strongly contextual and cell type-dependent (Degli-Esposti et al., 1997a; Marsters et al., 1997; Harper et al., 2001). This observation also applies, at least to a certain degree, to the induction of non-apoptotic signals by TRAILR1 and TRAILR2 (Wajant et al., 2000; Secchiero et al., 2003; Di Pietro and Zauli, 2004; Zauli et al., 2005; Song et al., 2007).

In addition to the demonstrated formation of heteromeric receptor complexes, activation of antiapoptotic and/or survival pathways are mechanisms that could potentially counteract TRAIL death receptor-induced apoptosis. Overexpression of TRAILR4 has been shown to induce constitutive phosphorylation of PKB/Akt in retrovirally transfected HeLa cells (Lalaoui et al., 2011). In contrast, in the here performed studies no alteration of constitutive or TRAIL-induced Akt phosphorylation could be detected in any of the three cell lines engineered to express full-length or truncated TRAILR4 (Figure 25). Accordingly, the PKB/Akt survival pathway has no influence on the TRAILR4-mediated reduced cellular sensitivity demonstrated here. Concerning this aspect, the results reported in the presented work are at variance with those published by Lalaoui and coworkers. The reasons for these discrepancies are unclear. Hypothetically, the different techniques used to generate the TRAILR4 expressing cell lines (retroviral *versus* lipid-based transfection), or rather distinct integration of the TRAILR4 gene into the genome, might somehow differentially influence the PKB/Akt pathway.

A more comprehensive comparison of TRAIL-induced intracellular signaling in HeLa and HeLa R4 cells was achieved using a commercially available antibody array. Analysis of the array data revealed no significant differences in the activation of PKB/Akt. This strongly suggests the degree of susceptibility of wild type and TRAILR4 expressing cells to TRAIL-induced apoptosis to be unaffected by the PKB/Akt pathway. Over the course of the experiment, i.e. TRAIL stimulation, Akt phosphorylation, at both threonine residue 308 and serine residue 473 changed only slightly, but to a similar extent in both cell lines.

Apart from cleavage of caspase-3 and the caspase-3 substrate PARP, which was as expected considerably stronger in TRAIL-treated HeLa cells compared to both

untreated HeLa and TRAIL-treated HeLa R4 cells, only two additional targets could be shown to be slightly differentially regulated in HeLa and HeLa R4 cells (Figure 26). Both cell lines showed high basal levels of phosphorylated PRAS40. TRAIL treatment for up to 60 min resulted in a slight decrease of phospho-PRAS40 levels. After longer stimulation, the level of phospho-PRAS40 returned to approximately the basal level in the parental cell line, while it remained lower in TRAILR4 expressing cells. PRAS40 has been shown to inhibit the kinase activity of the mammalian target of rapamycin complex 1 (mTORC1) and it additionally exerts a proapoptotic effect, presumably through a mechanism that is independent from inhibition of mTORC1 (Thedieck et al., 2007). Phosphorylation of PRAS40 at threonine residue 246 is mediated by Akt and high levels of phospho-PRAS40 are linked to tumor progression in malignant melanoma (Madhunapantula et al., 2007). Given that the changes of PRAS40 phosphorylation were similar in both cells lines investigated and the fact that PRAS40 (the non-phosphorylated, hence rather proapoptotic molecule) was more abundant in HeLa R4, it is likely to assume that this molecule exerts no articulate influence on the different TRAIL sensitivities of wild type and TRAILR4 expressing HeLa cells. In addition, the comparable pattern of PRAS40 phosphorylation/dephosphorylation in both cell lines underscores similar, i.e. unaffected by TRAILR4, Akt activities.

The second target showing differential responses to TRAIL stimulation in HeLa compared to HeLa R4 cells was the proapoptotic BH3-only protein Bad (Bcl-2-associated death promoter). Bad can form heterodimers with the antiapoptotic proteins Bcl-2 and Bcl-x$_L$. Dimerization of Bad with Bcl-x$_L$ displaces Bax, hence facilitating activation of the intrinsic apoptosis pathway (Yang et al., 1995; Adachi and Imai, 2002). Phosphorylation of Bad at specific serine residues is enhanced in response to certain survival factors and induces the association of Bad with regulatory 14-3-3 proteins, hence inhibiting binding to Bcl-2 and Bcl-x$_L$ and abolishing its proapoptotic effects (Zha et al., 1996). Two different kinases have been shown to mediate phosphorylation of Bad at the key serine residues. Serine residue 75 (corresponding to serine 112 in the murine Bad sequence) is phosphorylated by p90 ribosomal R6 kinase via a protein kinase C-dependent pathway (Tan et al., 1999), while phosphorylation at serine residue 99 (serine 136 in the murine Bad sequence) is mediated by PKB/Akt (Datta et al., 1997). Distinct phosphatases, calcineurin and protein phosphatase 2A, can dephosphorylate Bad, thereby enabling it to bind to Bcl-x$_L$ and to regain its proapoptotic function (Springer et al., 2000; Chiang et al., 2003).

The phospho-Bad levels in untreated HeLa and HeLa R4 cells were virtually identical. TRAIL treatment resulted in the detection of a lower signal for phospho-Bad in the antibody array. This is consistent with the notion that dephosphorylation of Bad reduces inhibition on this proapoptotic protein. However, the decrease was more prominent in HeLa R4 compared to parental HeLa cells. For unknown reasons, Bad phosphorylation in HeLa cells increased again at later time-points reaching the level of untreated cells after 240 min of TRAIL stimulation.

Generally speaking, the antibody array did not reveal any fundamental differences in intracellular signaling between HeLa (i.e. intracellular signals emanating from TRAILR1) and HeLa R4 (i.e. signals emanating from TRAILR1 and/or TRAILR4). The most prominent variance between these two cell lines could be shown for targets constituting key apoptotic markers, namely caspase-3 activation and, as a result, cleavage of PARP. Two additional targets, which are both implicated to some extent in activation or the process of the apoptotic program, could be shown to be regulated slightly different in the two cell lines. Notably, in response to TRAIL treatment abundance of the non-phosphorylated forms of both PRAS40 and Bad increased slightly more in cells expressing TRAILR4 than in the parental cell line. Dephosphorylation of these proteins constitutes a shift towards their proapoptotic functions. Hence this could potentially constitute a compensatory mechanism used by the cell to partially counterbalance the antiapoptotic effects of TRAILR4 expression. In summary, expression of TRAILR4 in HeLa cells did not induce any changes in TRAIL-induced non-apoptotic or antiapoptotic signaling which could be directly attributed to TRAILR4 signal transduction.

4.8. Conclusions

Human TRAIL and its four cognate cell surface receptors constitute an elaborate signaling system involved in various physiological and pathophysiological processes. Signaling by the two death receptors, TRAILR1 and TRAILR2, is comparably well understood, while the capabilities of TRAILR3 and TRAILR4 are not. But these two receptors might represent important modulators of TRAIL signaling acting at several levels. Besides the apparent function to act as ligand-depleting decoy receptors, TRAILR4, and this might hold true also for TRAILR3, can act as powerful down regulator of TRAILR1 (and likely also TRAILR2) signaling via ligand-independent formation of mixed complexes with severely inhibited signaling capacity.

In addition, TRAILR4 can induce antiapoptotic signaling in an apparently contextual and cell type specific manner. Especially with respect to TRAIL-based therapeutic approaches for tumor treatment, implications of signal inhibition by TRAILR4, yet also TRAILR3, could be disastrous. In fact, expression of decoy receptors has been shown to be of prognostic relevance in certain tumors (Granci et al., 2008; Ganten et al., 2009), thus a detailed understanding of the mechanisms underlying the inhibitory effect(s) of decoy receptors on signaling by death receptors is inevitable.

A next important step in understanding TRAIL signal initiation at the cell membrane would aim at a quantitative description. Several questions have to be answered in order to achieve this: Is the PLAD-mediated formation of homo- and heteromers indeed driven simply by their affinities? What is the role of additional factors like the GXXXG motif of TRAILR2 or of membrane microdomains (especially for TRAILR3)? To what extent do post-translational modifications influence receptor pre-assembly? Are death domain-containing TRAIL receptors paired with "decoy" receptors indeed fully nonfunctional? Are TRAILR1/TRAILR2 heterodimers equally signaling competent as the respective homodimers? Many additional questions can be formulated and each answer will finally help to obtain a deeper understanding of the functions fulfilled by TRAIL "decoy" receptors in physiology and pathophysiology.

5. Bibliography

Adachi, M. and Imai, K. (2002). The proapoptotic BH3-only protein BAD transduces cell death signals independently of its interaction with Bcl-2. *Cell Death and Differentiation* 9(11): 1240-1247.

Adams, C., Totpal, K., Lawrence, D., Marsters, S., Pitti, R., Yee, S., Ross, S., Deforge, L., Koeppen, H., Sagolla, M., Compaan, D., Lowman, H., Hymowitz, S. and Ashkenazi, A. (2008). Structural and functional analysis of the interaction between the agonistic monoclonal antibody Apomab and the proapoptotic receptor DR5. *Cell Death and Differentiation* 15(4): 751-761.

Adams, J. M. and Cory, S. (2002). Apoptosomes: engines for caspase activation. *Current Opinion in Cell Biology* 14(6): 715-720.

Aggarwal, B. B. (2003). Signalling pathways of the TNF superfamily: A double-edged sword. *Nature Reviews Immunology* 3(9): 745-756.

Aggarwal, B. B., Gupta, S. C. and Kim, J. H. (2012). Historical perspectives on tumor necrosis factor and its superfamily: 25 years later, a golden journey. *Blood* 119(3): 651-665.

Albertazzi, L., Arosio, D., Marchetti, L., Ricci, F. and Beltram, F. (2009). Quantitative FRET Analysis With the E(0)GFP-mCherry Fluorescent Protein Pair. *Photochemistry and Photobiology* 85(1): 287-297.

An, H.-J., Kim, Y. J., Song, D. H., Park, B. S., Kim, H. M., Lee, J. D., Paik, S.-G., Lee, J.-O. and Lee, H. (2011). Crystallographic and Mutational Analysis of the CD40-CD154 Complex and Its Implications for Receptor Activation. *Journal of Biological Chemistry* 286(13): 11226-11235.

Ashkenazi, A. and Dixit, V. M. (1999). Apoptosis control by death and decoy receptors. *Current Opinion in Cell Biology* 11(2): 255-260.

Ashkenazi, A., Pai, R. C., Fong, S., Leung, S., Lawrence, D. A., Marsters, S. A., Blackie, C., Chang, L., McMurtrey, A. E., Hebert, A., DeForge, L., Koumenis, I. L., Lewis, D., Harris, L., Bussiere, J., Koeppen, H., Shahrokh, Z. and Schwall, R. H. (1999). Safety and antitumor activity of recombinant soluble Apo2 ligand. *The Journal of Clinical Investigation* 104(2): 155-162.

Bader, M. and Steller, H. (2009). Regulation of cell death by the ubiquitin-proteasome system. *Current Opinion in Cell Biology* 21(6): 878-884.

Banner, D. W., D'Arcy, A., Janes, W., Gentz, R., Schoenfeld, H.-J., Broger, C., Loetscher, H. and Lesslauer, W. (1993). Crystal structure of the soluble human 55 kd TNF receptor-human TNF[beta] complex: Implications for TNF receptor activation. *Cell* 73(3): 431-445.

Boatright, K. M. and Salvesen, G. S. (2003). Mechanisms of caspase activation. *Current Opinion in Cell Biology* 15(6): 725-731.

Boatright, K. M., Deis, C., Denault, J. B., Sutherlin, D. P. and Salvesen, G. S. (2004). Activation of caspases-8 and-10 by FLIP$_L$. *Biochemical Journal* 382: 651-657.

Bodmer, J.-L., Schneider, P. and Tschopp, J. (2002). The molecular architecture of the TNF superfamily. *Trends in Biochemical Sciences* 27(1): 19-26.

Boldin, M. P., Mett, I. L., Varfolomeev, E. E., Chumakov, I., Shemer-Avni, Y., Camonis, J. H. and Wallach, D. (1995). Self-association of the ``Death Domains'' of the p55 Tumor Necrosis Factor (TNF) Receptor and Fas/APO1 Prompts Signaling for TNF and Fas/APO1 Effects. *Journal of Biological Chemistry* 270(1): 387-391.

Boschert, V., Krippner-Heidenreich, A., Branschädel, M., Tepperink, J., Aird, A. and Scheurich, P. (2010). Single chain TNF derivatives with individually mutated receptor binding sites reveal differential stoichiometry of ligand receptor complex formation for TNFR1 and TNFR2. *Cellular Signalling* 22(7): 1088-1096.

Branschädel, M. (2007). Analysis of molecular components essential for the formation of signalling-competent TNF-TNFR complexes. PhD thesis. *Institute of Cell Biology and Immunology* University of Stuttgart.

Branschädel, M., Aird, A., Zappe, A., Tietz, C., Krippner-Heidenreich, A. and Scheurich, P. (2010). Dual function of cysteine rich domain (CRD) 1 of TNF receptor type 1: Conformational stabilization of CRD2 and control of receptor responsiveness. *Cellular Signalling* 22(3): 404-414.

Budd, R. C., Yeh, W. C. and Tschopp, J. (2006). cFLIP regulation of lymphocyte activation and development. *Nature Reviews Immunology* 6(3): 196-204.

Carpentier, G. (2010). Protein Array Analyzer for ImageJ. Retrieved 2012-09-01, from http://rsbweb.nih.gov/ij/macros/toolsets/Protein%20Array%20Analyzer.txt.

Carrington, P. E., Sandu, C., Wei, Y. F., Hill, J. M., Morisawa, G., Huang, T., Gavathiotis, E., Wei, Y. and Werner, M. H. (2006). The structure of FADD and its mode of interaction with procaspase-8. *Molecular Cell* 22(5): 599-610.

Carswell, E. A., Old, L. J., Kassel, R. L., Green, S., Fiore, N. and Williamson, B. (1975). An endotoxin-induced serum factor that causes necrosis of tumors. *Proceedings of the National Academy of Sciences of the United States of America* 72(9): 3666-3670.

Cha, S.-S., Sung, B.-J., Kim, Y.-A., Song, Y.-L., Kim, H.-J., Kim, S., Lee, M.-S. and Oh, B.-H. (2000). Crystal Structure of TRAIL-DR5 Complex Identifies a Critical Role of the Unique Frame Insertion in Conferring Recognition Specificity. *Journal of Biological Chemistry* 275(40): 31171-31177.

Chan, F. K.-M., Chun, H. J., Zheng, L., Siegel, R. M., Bui, K. L. and Lenardo, M. J. (2000). A Domain in TNF Receptors That Mediates Ligand-Independent Receptor Assembly and Signaling. *Science* 288(5475): 2351-2354.

Chan, F. K. M. (2007). Three is better than one: Pre-ligand receptor assembly in the regulation of TNF receptor signaling. *Cytokine* 37(2): 101-107.

Chang, D. W., Xing, Z., Capacio, V. L., Peter, M. E. and Yang, X. L. (2003). Interdimer processing mechanism of procaspase-8 activation. *The EMBO Journal* 22(16): 4132-4142.

Chen, X. F., Kandasamy, K. and Srivastava, R. K. (2003). Differential roles of RelA (p65) and c-Rel subunits of nuclear factor kappa B in tumor necrosis factor-related apoptosis-inducing ligand signaling. *Cancer Research* 63(5): 1059-1066.

Chiang, C.-W., Kanies, C., Kim, K. W., Fang, W. B., Parkhurst, C., Xie, M., Henry, T. and Yang, E. (2003). Protein Phosphatase 2A Dephosphorylation of Phosphoserine 112 Plays the Gatekeeper Role for BAD-Mediated Apoptosis. *Molecular and Cellular Biology* 23(18): 6350-6362.

Chipuk, J. E., Moldoveanu, T., Llambi, F., Parsons, M. J. and Green, D. R. (2010). The BCL-2 Family Reunion. *Molecular Cell* 37(3): 299-310.

Cho, Y., Challa, S., Moquin, D., Genga, R., Ray, T. D., Guildford, M. and Chan, F. K. M. (2009). Phosphorylation-Driven Assembly of the RIP1-RIP3 Complex Regulates Programmed Necrosis and Virus-Induced Inflammation. *Cell* 137(6): 1112-1123.

Clancy, L., Mruk, K., Archer, K., Woelfel, M., Mongkolsapaya, J., Screaton, G., Lenardo, M. J. and Chan, F. K.-M. (2005). Preligand assembly domain-mediated ligand-independent association between TRAIL receptor 4 (TR4) and TR2 regulates TRAIL-induced apoptosis. *Proceedings of the National Academy of Sciences of the United States of America* 102(50): 18099-18104.

Connolly, S. A., Landsburg, D. J., Carfi, A., Wiley, D. C., Eisenberg, R. J. and Cohen, G. H. (2002). Structure-based analysis of the herpes simplex virus glycoprotein D binding site present on herpesvirus entry mediator HveA (HVEM). *Journal of Virology* 76(21): 10894-10904.

Czabotar, P. E., Westphal, D., Dewson, G., Ma, S., Hockings, C., Fairlie, W. D., Lee, E. F., Yao, S., Robin, A. Y., Smith, B. J., Huang, D. C. S., Kluck, R. M., Adams, J. M. and Colman, P. M. (2013). Bax Crystal Structures Reveal How BH3 Domains Activate Bax and Nucleate Its Oligomerization to Induce Apoptosis. *Cell* 152(3): 519-531.

Datta, S. R., Dudek, H., Tao, X., Masters, S., Fu, H., Gotoh, Y. and Greenberg, M. E. (1997). Akt Phosphorylation of BAD Couples Survival Signals to the Cell-Intrinsic Death Machinery. *Cell* 91(2): 231-241.

De Toni, E. N., Thieme, S. E., Herbst, A., Behrens, A., Stieber, P., Jung, A., Blum, H., Göke, B. and Kolligs, F. T. (2008). OPG Is Regulated by β-Catenin and Mediates Resistance to TRAIL-Induced Apoptosis in Colon Cancer. *Clinical Cancer Research* 14(15): 4713-4718.

Declercq, W., Vanden Berghe, T. and Vandenabeele, P. (2009). RIP Kinases at the Crossroads of Cell Death and Survival. *Cell* 138(2): 229-232.

Degli-Esposti, M., Dougall, M., Smolak, P. J., Waugh, J., Smith, C. and Goodwin, R. G. (1997a). The novel receptor TRAIL-R4 induces NF-kappaB and protects against TRAIL-mediated apoptosis, yet retains an incomplete death domain. *Immunity* 7(6): 813-820.

Degli-Esposti, M. A., Smolak, P. J., Walczak, H., Waugh, J., Huang, C. P., DuBose, R. F., Goodwin, R. G. and Smith, C. A. (1997b). Cloning and characterization of TRAIL-R3, a novel member of the emerging TRAIL receptor family. *Journal of Experimental Medicine* 186(7): 1165-1170.

Degterev, A., Boyce, M. and Yuan, J. (2003). A decade of caspases. *Oncogene* 22(53): 8543-8567.

Degterev, A., Huang, Z. H., Boyce, M., Li, Y. Q., Jagtap, P., Mizushima, N., Cuny, G. D., Mitchison, T. J., Moskowitz, M. A. and Yuan, J. Y. (2005). Chemical inhibitor of nonapoptotic cell death with therapeutic potential for ischemic brain injury. *Nature Chemical Biology* 1(2): 112-119.

Degterev, A. and Yuan, J. (2008). Expansion and evolution of cell death programmes. *Nature Reviews Molecular Cell Biology* 9(5): 378-390.

Delavallee, L., Cabon, L., Galan-Malo, P., Lorenzo, H. K. and Susin, S. A. (2011). AIF-mediated Caspase-independent Necroptosis: A New Chance for Targeted Therapeutics. *Iubmb Life* 63(4): 221-232.

Deveraux, Q. L., Leo, E., Stennicke, H. R., Welsh, K., Salvesen, G. S. and Reed, J. C. (1999). Cleavage of human inhibitor of apoptosis protein XIAP results in fragments with distinct specificities for caspases. *The EMBO Journal* 18(19): 5242-5251.

Di Pietro, R. and Zauli, G. (2004). Emerging non-apoptotic functions of tumor necrosis factor-related apoptosis-inducing ligand (TRAIL)/Apo2L. *Journal of Cellular Physiology* 201(3): 40.

Dickens, L. S., Boyd, R. S., Jukes-Jones, R., Hughes, M. A., Robinson, G. L., Fairall, L., Schwabe, J. W. R., Cain, K. and MacFarlane, M. (2012a). A Death Effector Domain Chain DISC Model Reveals a Crucial Role for Caspase-8 Chain Assembly in Mediating Apoptotic Cell Death. *Molecular Cell* 47(2): 291-305.

Dickens, L. S., Powley, I. R., Hughes, M. A. and MacFarlane, M. (2012b). The 'complexities' of life and death: Death receptor signalling platforms. *Experimental Cell Research* 318(11): 1269-1277.

Du, C. Y., Fang, M., Li, Y. C., Li, L. and Wang, X. D. (2000). Smac, a mitochondrial protein that promotes cytochrome c-dependent caspase activation by eliminating IAP inhibition. *Cell* 102(1): 33-42.

Dutta, J., Fan, Y., Gupta, N., Fan, G. and Gelinas, C. (2006). Current insights into the regulation of programmed cell death by NF-kappaB. *Oncogene* 25(51): 6800-6816.

Eckelman, B. P. and Salvesen, G. S. (2006). The human anti-apoptotic proteins cIAP1 and cIAP2 bind but do not inhibit caspases. *Journal of Biological Chemistry* 281(6): 3254-3260.

Eckelman, B. P., Salvesen, G. S. and Scott, F. L. (2006). Human inhibitor of apoptosis proteins: why XIAP is the black sheep of the family. *EMBO Reports* 7(10): 988-994.

Ehrlich, S., Infante-Duarte, C., Seeger, B. and Zipp, F. (2003). Regulation of soluble and surface-bound TRAIL in human T cells, B cells, and monocytes. *Cytokine* 24(6): 244-253.

Emery, J. G., McDonnell, P., Burke, M. B., Deen, K. C., Lyn, S., Silverman, C., Dul, E., Appelbaum, E. R., Eichman, C., DiPrinzio, R., Dodds, R. A., James, I. E., Rosenberg, M., Lee, J. C. and Young, P. R. (1998). Osteoprotegerin Is a Receptor for the Cytotoxic Ligand TRAIL. *Journal of Biological Chemistry* 273(23): 14363-14367.

Falschlehner, C., Emmerich, C., Gerlach, B. and Walczak, H. (2007). TRAIL signalling: Decisions between life and death. *The International Journal of Biochemistry & Cell Biology* 39(7-8): 1462–1475.

Falschlehner, C., Schaefer, U. and Walczak, H. (2009). Following TRAIL's path in the immune system. *Immunology* 127(2): 145-154.

Fanger, N. A., Maliszewski, C. R., Schooley, K. and Griffith, T. S. (1999). Human dendritic cells mediate cellular apoptosis via tumor necrosis factor-related apoptosis-inducing ligand (TRAIL). *Journal of Experimental Medicine* 190(8): 1155-1164.

Fiers, W., Beyaert, R., Boone, E., Cornelis, S., Declercq, W., Decoster, E., Denecker, G., Depuydt, B., De Valck, D., De Wilde, G., Goossens, V., Grooten, J., Haegeman, G., Heyninck, K., Penning, L., Plaisance, S., Vancompernolle, K., Van Criekinge, W., Vandenabeele, P., Vanden Berghe, W., Van de Craen, M., Vandevoorde, V. and Vercammen, D. (1996). TNF-induced intracellular signaling leading to gene induction or to cytotoxicity by necrosis or by apoptosis. *Journal of Inflammation* 47(1-2): 67-75.

Fischer, U., Janicke, R. U. and Schulze-Osthoff, K. (2003). Many cuts to ruin: a comprehensive update of caspase substrates. *Cell Death and Differentiation* 10(1): 76-100.

Fuchs, Y. and Steller, H. (2011). Programmed Cell Death in Animal Development and Disease. *Cell* 147(4): 742-758.

Fulda, S., Meyer, E. and Debatin, K. M. (2002). Inhibition of TRAIL-induced apoptosis by Bcl-2 overexpression. *Oncogene* 21(15): 2283-2294.

Galban, S. and Duckett, C. S. (2010). XIAP as a ubiquitin ligase in cellular signaling. *Cell Death and Differentiation* 17(1): 54-60.

Ganten, T., Sykora, J., Koschny, R., Batke, E., Aulmann, S., Mansmann, U., Stremmel, W., Sinn, H.-P. and Walczak, H. (2009). Prognostic significance of tumour necrosis factor-related apoptosis-inducing ligand (TRAIL) receptor expression in patients with breast cancer. *Journal of Molecular Medicine* 87(10): 995-1007.

Gerken, M., Krippner-Heidenreich, A., Steinert, S., Willi, S., Neugart, F., Zappe, A., Wrachtrup, J., Tietz, C. and Scheurich, P. (2010). Fluorescence correlation spectroscopy reveals topological segregation of the two tumor necrosis factor membrane receptors. *Biochimica et Biophysica Acta* 1798(6): 1081-1089.

Gerspach, J., Schneider, B., Müller, N., Otz, T., Wajant, H. and Pfizenmaier, K. (2011). Genetic Engineering of Death Ligands for Improvement of Therapeutic Activity. Advances in TNF Family Research. D. Wallach, A. Kovalenko and M. Feldmann. New York, Springer. 691: 507-519.

Geserick, P., Drewniok, C., Hupe, M., Haas, T. L., Diessenbacher, P., Sprick, M. R., Schon, M. P., Henkler, F., Gollnick, H., Walczak, H. and Leverkus, M. (2007). Suppression of cFLIP is sufficient to sensitize human melanoma cells to TRAIL- and CD95L-mediated apoptosis. *Oncogene* 27(22): 3211-3220.

Gilmore, T. D. (2006). Introduction to NF-kappa B: players, pathways, perspectives. *Oncogene* 25(51): 6680-6684.

Golks, A., Brenner, D., Fritsch, C., Krammer, P. H. and Lavrik, I. N. (2005). c-FLIP$_R$, a New Regulator of Death Receptor-induced Apoptosis. *Journal of Biological Chemistry* 280(15): 14507-14513.

Granci, V., Bibeau, F., Kramar, A., Boissiere-Michot, F., Thezenas, S., Thirion, A., Gongora, C., Martineau, P., Del Rio, M. and Ychou, M. (2008). Prognostic significance of TRAIL-R1 and TRAIL-R3 expression in metastatic colorectal carcinomas. *European Journal of Cancer* 44(15): 2312-2318.

Gross, A., Yin, X.-M., Wang, K., Wei, M. C., Jockel, J., Milliman, C., Erdjument-Bromage, H., Tempst, P. and Korsmeyer, S. J. (1999). Caspase Cleaved BID Targets Mitochondria and Is Required for Cytochrome c Release, while BCL-XL Prevents This Release but Not Tumor Necrosis Factor-R1/Fas Death. *Journal of Biological Chemistry* 274(2): 1156-1163.

Grunert, M., Gottschalk, K., Kapahnke, J., Gundisch, S., Kieser, A. and Jeremias, I. (2012). The adaptor protein FADD and the initiator caspase-8 mediate activation of NF-kappa B by TRAIL. *Cell Death & Disease* 3(e414).

Guicciardi, M. E., Mott, J. L., Bronk, S. F., Kurita, S., Fingas, C. D. and Gores, G. J. (2011). Cellular inhibitor of apoptosis 1 (cIAP-1) degradation by caspase 8 during TNF-related apoptosis-inducing ligand (TRAIL)-induced apoptosis. *Experimental Cell Research* 317(1): 107-116.

Hang, H. C. and Bertozzi, C. R. (2005). The chemistry and biology of mucin-type O-linked glycosylation. *Bioorganic & Medicinal Chemistry* 13(17): 5021-5034.

Hardy, K., Handyside, A. H. and Winston, R. M. L. (1989). The human blastocyst - cell number, death and allocation during late preimplantation development *in vitro*. *Development* 107(3): 597-604.

Harper, N., Farrow, S. N., Kaptein, A., Cohen, G. M. and MacFarlane, M. (2001). Modulation of Tumor Necrosis Factor Apoptosis-inducing Ligand- induced NF-κB Activation by Inhibition of Apical Caspases. *Journal of Biological Chemistry* 276(37): 34743-34752.

Hayden, M. S., West, A. P. and Ghosh, S. (2006). NF-kappa B and the immune response. *Oncogene* 25(51): 6758-6780.

Hayden, M. S. and Ghosh, S. (2008). Shared principles in NF-kappa B signaling. *Cell* 132(3): 344-362.

He, F., Dang, W. R., Saito, K., Watanabe, S., Kobayashi, N., Guntert, P., Kigawa, T., Tanaka, A., Muto, Y. and Yokoyama, S. (2009). Solution structure of the cysteine-rich domain in Fn14, a member of the tumor necrosis factor receptor superfamily. *Protein Science* 18(3): 650-656.

He, X. L. and Garcia, K. C. (2004). Structure of nerve growth factor complexed with the shared neurotrophin receptor p75. *Science* 304(5672): 870-875.

Hellwig, C. T. and Rehm, M. (2012). TRAIL Signaling and Synergy Mechanisms Used in TRAIL-Based Combination Therapies. *Molecular Cancer Therapeutics* 11(1): 3-13.

Hengartner, M. O. (2000). The biochemistry of apoptosis. *Nature* 407(6805): 770-776.

Henkler, F., Behrle, E., Dennehy, K. M., Wicovsky, A., Peters, N., Warnke, C., Pfizenmaier, K. and Wajant, H. (2005). The extracellular domains of FasL and Fas are sufficient for the formation of supramolecular FasL-Fas clusters of high stability. *Journal of Cell Biology* 168(7): 1087-1098.

Hermiston, M. L., Xu, Z. and Weiss, A. (2003). CD45: A critical regulator of signaling thresholds in immune cells. *Annual Reviews of Immunology* 21: 107-137.

Holler, N., Zaru, R., Micheau, O., Thome, M., Attinger, A., Valitutti, S., Bodmer, J.-L., Schneider, P., Seed, B. and Tschopp, J. (2000). Fas triggers an alternative, caspase-8-independent cell death pathway using the kinase RIP as effector molecule. *Nature Immunology* 1(6): 489-495.

Holler, N., Tardivel, A., Kovacsovics-Bankowski, M., Hertig, S., Gaide, O., Martinon, F., Tinel, A., Deperthes, D., Calderara, S., Schulthess, T., Engel, J., Schneider, P. and Tschopp, E. (2003). Two adjacent trimeric Fas ligands are required for Fas signaling and formation of a death-inducing signaling complex. *Molecular and Cellular Biology* 23(4): 1428-1440.

Horak, P., Pils, D., Kaider, A., Pinter, A., Elandt, K., Sax, C., Zielinski, C. C., Horvat, R., Zeillinger, R., Reinthaller, A. and Krainer, M. (2005). Perturbation of the Tumor Necrosis Factor–Related Apoptosis-Inducing Ligand Cascade in Ovarian Cancer: Overexpression of FLIP$_L$ and Deregulation of the Functional Receptors DR4 and DR5. *Clinical Cancer Research* 11(24): 8585-8591.

Hu, P., Han, Z., Couvillon, A. D., Kaufman, R. J. and Exton, J. H. (2006). Autocrine tumor necrosis factor alpha links endoplasmic reticulum stress to the membrane death receptor pathway through IRE1 alpha-mediated NF-kappa B activation and down-regulation of TRAF2 expression. *Molecular and Cellular Biology* 26(8): 3071-3084.

Hu, W.-H., Johnson, H. and Shu, H.-B. (1999). Tumor Necrosis Factor-related Apoptosis-inducing Ligand Receptors Signal NF-kappa B and JNK Activation and Apoptosis through Distinct Pathways. *Journal of Biological Chemistry* 274(43): 30603-30610.

Hughes, M. A., Harper, N., Butterworth, M., Cain, K., Cohen, G. M. and MacFarlane, M. (2009). Reconstitution of the Death-inducing Signaling Complex Reveals a Substrate Switch that Determines CD95-Mediated Death or Survival. *Molecular Cell* 35(3): 265-279.

Hymowitz, S. G., Christinger, H. W., Fuh, G., Ultsch, M., O'Connell, M., Kelley, R. F., Ashkenazi, A. and de Vos, A. M. (1999). Triggering Cell Death: The Crystal Structure of Apo2L/TRAIL in a Complex with Death Receptor 5. *Molecular Cell* 4(4): 563-571.

Hymowitz, S. G., O'Connell, M. P., Ultsch, M. H., Hurst, A., Totpal, K., Ashkenazi, A., de Vos, A. M. and Kelley, R. F. (2000). A Unique Zinc-Binding Site Revealed by a High-Resolution X-ray Structure of Homotrimeric Apo2L/TRAIL. *Biochemistry* 39(4): 633-640.

Jacobson, M. D., Weil, M. and Raff, M. C. (1997). Programmed cell death in animal development. *Cell* 88(3): 347-354.

Janssen, E. M., Droin, N. M., Lemmens, E. E., Pinkoski, M. J., Bensinger, S. J., Ehst, B. D., Griffith, T. S., Green, D. R. and Schoenberger, S. P. (2005). CD4(+) T-cell help controls CD8(+) T-cell memory via TRAIL-mediated activation-induced cell death. *Nature* 434(7029): 88-93.

Jennewein, C., Karl, S., Baumann, B., Micheau, O., Debatin, K. M. and Fulda, S. (2012). Identification of a novel pro-apoptotic role of NF-kappa B in the regulation of TRAIL- and CD95-mediated apoptosis of glioblastoma cells. *Oncogene* 31(11): 1468-1474.

Jin, Z. and El-Deiry, W. S. (2006). Distinct Signaling Pathways in TRAIL- versus Tumor Necrosis Factor-Induced Apoptosis. *Molecular Cell Biology* 26(21): 8136-8148.

Jin, Z. Y., Li, Y., Pitti, R., Lawrence, D., Pham, V. C., Lill, J. R. and Ashkenazi, A. (2009). Cullin3-Based Polyubiquitination and p62-Dependent Aggregation of Caspase-8 Mediate Extrinsic Apoptosis Signaling. *Cell* 137(4): 721-735.

Kavuri, S. M., Geserick, P., Berg, D., Dimitrova, D. P., Feoktistova, M., Siegmund, D., Gollnick, H., Neumann, M., Wajant, H. and Leverkus, M. (2011). Cellular FLICE-inhibitory Protein (cFLIP) Isoforms Block CD95- and TRAIL Death Receptor-induced Gene Induction Irrespective of Processing of Caspase-8 or cFLIP in the Death-inducing Signaling Complex. *Journal of Biological Chemistry* 286(19): 16631-16646.

Kelley, R. F., Totpal, K., Lindstrom, S. H., Mathieu, M., Billeci, K., DeForge, L., Pai, R., Hymowitz, S. G. and Ashkenazi, A. (2005). Receptor-selective Mutants of Apoptosis-inducing Ligand 2/Tumor Necrosis Factor-related Apoptosis-inducing Ligand Reveal a Greater Contribution of Death Receptor (DR) 5 than DR4 to Apoptosis Signaling. *Journal of Biological Chemistry* 280(3): 2205-2212.

Kerr, J. F. R., Wyllie, A. H. and Currie, A. R. (1972). Apoptosis: A basic biological phenomenon with wide-ranging implications in tissue kinetics. *British Journal of Cancer* 26(4): 239-257.

Kimberley, F. C. and Screaton, G. R. (2004). Following a TRAIL: Update on a ligand and its five receptors. *Cell Research* 14(5): 359-372.

Kischkel, F., Hellbardt, S., Behrmann, I., Germer, M., Pawlita, M., Krammer, P. and Peter, M. (1995). Cytotoxicity-dependant APO-1 (Fas/CD95)-associated proteins form a death-inducing signalling complex (DISC) with the receptor. *The EMBO Journal* 14(22): 5579-5588.

Kischkel, F., Lawrence, D., Chuntharapai, A., Schow, P., Kim, K. and Ashkenazi, A. (2000). Apo2L/TRAIL-dependent recruitment of endogenous FADD and caspase-8 to death receptors 4 and 5. *Immunity* 12(6): 611-620.

Kischkel, F. C., Lawrence, D. A., Tinel, A., LeBlanc, H., Virmani, A., Schow, P., Gazdar, A., Blenis, J., Arnott, D. and Ashkenazi, A. (2001). Death Receptor Recruitment of Endogenous Caspase-10 and Apoptosis Initiation in the Absence of Caspase-8. *Journal of Biological Chemistry* 276(49): 46639-46646.

Kontermann, R. E., Scheurich, P. and Pfizenmaier, M. (2009). Antagonists of TNF action: clinical experience and new developments. *Expert Opinion on Drug Discovery* 4(3): 279-292.

Koschny, R., Walczak, H. and Ganten, T. (2007). The promise of TRAIL—potential and risks of a novel anticancer therapy. *Journal of Molecular Medicine* 85(9): 923-935.

Krammer, P. H., Arnold, R. and Lavrik, I. N. (2007). Life and death in peripheral T cells. *Nature Reviews Immunology* 7(7): 532-542.

Kreuz, S., Siegmund, D., Scheurich, P. and Wajant, H. (2001). NF-kappa B inducers upregulate cFLIP, a cycloheximide-sensitive inhibitor of death receptor signaling. *Molecular and Cellular Biology* 21(12): 3964-3973.

Krippner-Heidenreich, A., Tubing, F., Bryde, S., Willi, S., Zimmermann, G. and Scheurich, P. (2002). Control of receptor-induced signaling complex formation by the kinetics of ligand/receptor interaction. *Journal of Biological Chemistry* 277(46): 44155-44163.

Krueger, A., Schmitz, I., Baumann, S., Krammer, P. H. and Kirchhoff, S. (2001). Cellular FLICE-inhibitory Protein Splice Variants Inhibit Different Steps of Caspase-8 Activation at the CD95 Death-inducing Signaling Complex. *Journal of Biological Chemistry* 276(23): 20633-20640.

Kucharczak, J., Simmons, M. J., Fan, Y. J. and Gelinas, C. (2003). To be, or not to be: NF-kappa B is the answer - role of Rel/NF-kappa B in the regulation of apoptosis. *Oncogene* 22(56): 8961-8982.

Lalaoui, N., Morlé, A., Mérino, D., Jacquemin, G., Iessi, E., Morizot, A., Shirley, S., Robert, B., Solary, E., Garrido, C. and Micheau, O. (2011). TRAIL-R4 Promotes Tumor Growth and Resistance to Apoptosis in Cervical Carcinoma HeLa Cells through AKT. *PLoS One* 6(5): e19679.

Lane, D., Matte, I., Rancourt, C. and Piche, A. (2012). Osteoprotegerin (OPG) protects ovarian cancer cells from TRAIL-induced apoptosis but does not contribute to malignant ascites-mediated attenuation of TRAIL-induced apoptosis. *Journal of Ovarian Research* 5: 34.

Langmuir, I. (1916). The constitution and fundamental properties of solids and liquids. Part I. Solids. *Journal of the American Chemical Society* 38(11): 2221-2295.

Lee, H. W., Lee, S. H., Ryu, Y. W., Kwon, M. H. and Kim, Y. S. (2005). Homomeric and heteromeric interactions of the extracellular domains of death receptors and death decoy receptors. *Biochemical and Biophysical Research Communications* 330(4): 1205-1212.

Lemke, J., Noack, A., Adam, D., Tchikov, V., Bertsch, U., Röder, C., Schütze, S., Wajant, H., Kalthoff, H. and Trauzold, A. (2010). TRAIL signaling is mediated by DR4 in pancreatic tumor cells despite the expression of functional DR5. *Journal of Molecular Medicine* 88(7): 729-740.

Lewis, A. K., Valley, C. C. and Sachs, J. N. (2012). TNFR1 Signaling Is Associated with Backbone Conformational Changes of Receptor Dimers Consistent with Overactivation in the R92Q TRAPS Mutant. *Biochemistry* 51(33): 6545-6555.

Li, P., Nijhawan, D., Budihardjo, I., Srinivasula, S. M., Ahmad, M., Alnemri, E. S. and Wang, X. D. (1997). Cytochrome c and dATP-dependent formation of Apaf-1/caspase-9 complex initiates an apoptotic protease cascade. *Cell* 91(4): 479-489.

Lin, Y., Devin, A., Cook, A., Keane, M. M., Kelliher, M., Lipkowitz, S. and Liu, Z.-g. (2000). The Death Domain Kinase RIP Is Essential for TRAIL (Apo2L)-Induced Activation of Ikappa B Kinase and c-Jun N-Terminal Kinase. *Molecular and Cellular Biology* 20(18): 6638-6645.

MacFarlane, M., Ahmad, M., Srinivasula, S. M., Fernandes-Alnemri, T., Cohen, G. M. and Alnemri, E. S. (1997). Identification and Molecular Cloning of Two Novel Receptors for the Cytotoxic Ligand TRAIL. *Journal of Biological Chemistry* 272(41): 25417-25420.

Madhunapantula, S. V., Sharma, A. and Robertson, G. P. (2007). PRAS40 Deregulates Apoptosis in Malignant Melanoma. *Cancer Research* 67(8): 3626-3636.

Mariani, S. and Krammer, P. (1998). Differential regulation of TRAIL and CD95 ligand in transformed cells of the T and B lymphocyte lineage. *European Journal of Immunology* 28(3): 973-982.

Marsters, S. A., Sheridan, J. P., Pitti, R. M., Huang, A., Skubatch, M., Baldwin, D., Yuan, J., Gurney, A., Goddard, A. D., Godowski, P. and Ashkenazi, A. (1997). A novel receptor for Apo2L/TRAIL contains a truncated death domain. *Current Biology* 7(12): 1003-1006.

Martinou, J.-C. and Youle, R. J. (2011). Mitochondria in Apoptosis: Bcl-2 Family Members and Mitochondrial Dynamics. *Developmental Cell* 21(1): 92-101.

Mascarenhas, N. M. and Kästner, J. (2012). Are different stoichiometries feasible for complexes between lymphotoxin-alpha and tumor necrosis factor receptor 1? *BMC Structural Biology* 12(8).

Mérino, D., Lalaoui, N., Morizot, A., Schneider, P., Solary, E. and Micheau, O. (2006). Differential Inhibition of TRAIL-Mediated DR5-DISC Formation by Decoy Receptors 1 and 2. *Molecular and Cellular Biology* 26(19): 7046-7055.

Micheau, O., Lens, S., Gaide, O., Alevizopoulos, K. and Tschopp, J. (2001). NF-κB Signals Induce the Expression of c-FLIP. *Molecular and Cellular Biology* 21(16): 5299-5305.

Micheau, O., Thome, M., Schneider, P., Holler, N., Tschopp, J., Nicholson, D. W., Briand, C. and Grutter, M. G. (2002). The long form of FLIP is an activator of caspase-8 at the fas death-inducing signaling complex. *Journal of Biological Chemistry* 277(47): 45162-45171.

Miyamoto, S., Maki, M., Schmitt, M. J., Hatanaka, M. and Verma, I. M. (1994). Tumor necrosis factor α-induced phosphorylation of IκBα is a signal for its degradation but not dissociation from NF-κB. *Proceedings of the National Academy of Sciences of the United States of America* 91(26): 12740-12744.

Mongkolsapaya, J., Grimes, J. M., Chen, N., Xu, X.-N., Stuart, D. I., Jones, E. Y. and Screaton, G. R. (1999). Structure of the TRAIL-DR5 complex reveals mechanisms conferring specificity in apoptotic initiation. *Nature Structural Biology* 6(11): 1048-1053.

Mukai, Y., Nakamura, T., Yoshikawa, M., Yoshioka, Y., Tsunoda, S., Nakagawa, S., Yamagata, Y. and Tsutsumi, Y. (2010). Solution of the structure of the TNF-TNFR2 complex. *Science Signaling* 3(148): ra83.

Nagata, S. (2000). Apoptotic DNA fragmentation. *Experimental Cell Research* 256(1): 12-18.

Naismith, J. H., Devine, T. Q., Brandhuber, B. J. and Sprang, S. R. (1995). Crystallographic Evidence for Dimerization of Unliganded Tumor Necrosis Factor Receptor. *Journal of Biological Chemistry* 270(22): 13303-13307.

Naismith, J. H., Devine, T. Q., Kohno, T. and Sprang, S. R. (1996). Structures of the extracellular domain of the type I tumor necrosis factor receptor. *Structure* 4(11): 1251-1262.

Nelson, C. A., Warren, J. T., Wang, M. W. H., Teitelbaum, S. L. and Fremont, D. H. (2012). RANKL Employs Distinct Binding Modes to Engage RANK and the Osteoprotegerin Decoy Receptor. *Structure* 20(11): 1971–1982.

Neumann, S., Bidon, T., Branschädel, M., Krippner-Heidenreich, A., Scheurich, P. and Doszczak, M. (2012). The Transmembrane Domains of TNF-Related Apoptosis-Inducing Ligand (TRAIL) Receptors 1 and 2 Co-Regulate Apoptotic Signaling Capacity. *PLoS One* 7(8): e42526.

Nicholson, D. W., Ali, A., Thornberry, N. A., Vaillancourt, J. P., Ding, C. K., Gallant, M., Gareau, Y., Griffin, P. R., Labelle, M., Lazebnik, Y. A., Munday, N. A., Raju, S. M., Smulson, M. E., Yamin, T.-T., Yu, V. L. and Miller, D. K. (1995). Identification and inhibition of the ICE/CED-3 protease necessary for mammalian apoptosis. *Nature* 376(6535): 37-43.

Oberst, A., Pop, C., Tremblay, A. G., Blais, V., Denault, J. B., Salvesen, G. S. and Green, D. R. (2010). Inducible Dimerization and Inducible Cleavage Reveal a Requirement for Both Processes in Caspase-8 Activation. *Journal of Biological Chemistry* 285(22): 16632-16642.

Pan, G., Ni, J., Wei, Y.-F., Yu, G.-l., Gentz, R. and Dixit, V. M. (1997a). An Antagonist Decoy Receptor and a Death Domain-Containing Receptor for TRAIL. *Science* 277(5327): 815-818.

Pan, G., O'Rourke, K., Chinnaiyan, A. M., Gentz, R., Ebner, R., Ni, J. and Dixit, V. M. (1997b). The Receptor for the Cytotoxic Ligand TRAIL. *Science* 276(5309): 111-113.

Pan, G., Ni, J., Yu, G.-L., Wei, Y.-F. and Dixit, V. M. (1998). TRUNDD, a new member of the TRAIL receptor family that antagonizes TRAIL signalling. *FEBS Letters* 424(1-2): 41-45.

Park, H. H., Lo, Y. C., Lin, S. C., Wang, L., Yang, J. K. and Wu, H. (2007a). The death domain superfamily in intracellular signaling of apoptosis and inflammation. Annual Reviews of Immunology. Palo Alto, Annual Reviews. 25: 561-586.

Park, H. H., Logette, E., Raunser, S., Cuenin, S., Walz, T., Tschopp, J. and Wu, H. (2007b). Death domain assembly mechanism revealed by crystal structure of the oligomeric PIDDosome core complex. *Cell* 128(3): 533-546.

Pitti, R. M., Marsters, S. A., Ruppert, S., Donahue, C. J., Moore, A. and Ashkenazi, A. (1996). Induction of Apoptosis by Apo-2 Ligand, a New Member of the Tumor Necrosis Factor Cytokine Family. *Journal of Biological Chemistry* 271(22): 12687-12690.

Plantivaux, A., Szegezdi, E., Samali, A. and Egan, L. (2009). Is There a Role for Nuclear Factor kappa B in Tumor Necrosis Factor-Related Apoptosis-Inducing Ligand Resistance? Natural Compounds and Their Role in Apoptotic Cell Signaling Pathways. M. Diederich. Oxford, Blackwell Publishing. 1171: 38-49.

R Development Core Team. (2012). R: A Language and Environment for Statistical Computing. Retrieved 2013-01-14, from http://www.R-project.org/.

Radhakrishnan, S. K. and Kamalakaran, S. (2006). Pro-apoptotic role of NF-kappa B: Implications for cancer therapy. *Biochimica et Biophysica Acta-Reviews on Cancer* 1766(1): 53-62.

Rossin, A., Derouet, M., Abdel-Sater, F. and Hueber, A. O. (2009). Palmitoylation of the TRAIL receptor DR4 confers an efficient TRAIL-induced cell death signalling. *Biochemical Journal* 419: 185-192.

Rudel, T. and Bokoch, G. M. (1997). Membrane and morphological changes in apoptotic cells regulated by caspase-mediated activation of PAK2. *Science* 276(5318): 1571-1574.

Salvesen, G. S. and Dixit, V. M. (1999). Caspase activation: The induced-proximity model. *Proceedings of the National Academy of Sciences of the United States of America* 96(20): 10964-10967.

Sandu, C., Morisawa, G., Wegorzewska, I., Huang, T., Arechiga, A. F., Hill, J. M., Kim, T., Walsh, C. M. and Werner, M. H. (2006). FADD self-association is required for stable interaction with an activated death receptor. *Cell Death and Differentiation* 13(12): 2052-2061.

Scaffidi, C., Fulda, S., Srinivasan, A., Friesen, C., Li, F., Tomaselli, K. J., Debatin, K. M., Krammer, P. H. and Peter, M. E. (1998). Two CD95 (APO-1/Fas) signaling pathways. *The EMBO Journal* 17(6): 1675-1687.

Scheidereit, C. (2006). I kappa B kinase complexes: gateways to NF-kappa B activation and transcription. *Oncogene* 25(51): 6685-6705.

Schimmer, A. D., Welsh, K., Pinilla, C., Wang, Z., Krajewska, M., Bonneau, M.-J., Pedersen, I. M., Kitada, S., Scott, F. L., Bailly-Maitre, B., Glinsky, G., Scudiero, D., Sausville, E., Salvesen, G., Nefzi, A., Ostresh, J. M., Houghten, R. A. and Reed, J. C. (2004). Small-molecule antagonists of apoptosis suppressor XIAP exhibit broad antitumor activity. *Cancer Cell* 5(1): 25-35.

Schindelin, J., Arganda-Carreras, I., Frise, E., Kaynig, V., Longair, M., Pietzsch, T., Preibisch, S., Rueden, C., Saalfeld, S., Schmid, B., Tinevez, J.-Y., White, D. J., Hartenstein, V., Eliceiri, K., Tomancak, P. and Cardona, A. (2012). Fiji: an open-source platform for biological-image analysis. *Nature Methods* 9(7): 676-682.

Schneeweis, L. A., Willard, D. and Milla, M. E. (2005). Functional Dissection of Osteoprotegerin and Its Interaction with Receptor Activator of NF-κB Ligand. *Journal of Biological Chemistry* 280(50): 41155-41164.

Schneider, B., Münkel, S., Krippner-Heidenreich, A., Grunwald, I., Wels, W. S., Wajant, H., Pfizenmaier, K. and Gerspach, J. (2010). Potent antitumoral activity of TRAIL through generation of tumor-targeted single-chain fusion proteins. *Cell Death and Disease* 1: e68.

Scott, F. L., Denault, J.-B., Riedl, S. J., Shin, H., Renatus, M. and Salvesen, G. S. (2005). XIAP inhibits caspase-3 and -7 using two binding sites: evolutionarily conserved mechanism of IAPs. *The EMBO Journal* 24(3): 645-655.

Scott, F. L., Stec, B., Pop, C., Dobaczewska, M. K., Lee, J. J., Monosov, E., Robinson, H., Salvesen, G. S., Schwarzenbacher, R. and Riedl, S. J. (2008). The Fas-FADD death domain complex structure unravels signalling by receptor clustering. *Nature* 457(7232): 1019-1022.

Secchiero, P., Gonelli, A., Carnevale, E., Milani, D., Pandolfi, A., Zella, D. and Zauli, G. (2003). TRAIL promotes the survival and proliferation of primary human vascular endothelial cells by activating the Akt and ERK pathways. *Circulation* 107(17): 2250-2256.

Sedger, L. M., Shows, D. M., Blanton, R. A., Peschon, J. J., Goodwin, R. G., Cosman, D. and Wiley, S. R. (1999). IFN-γ Mediates a Novel Antiviral Activity Through Dynamic Modulation of TRAIL and TRAIL Receptor Expression. *Journal of Immunology* 163(2): 920-926.

Senes, A., Engel, D. E. and DeGrado, W. F. (2004). Folding of helical membrane proteins: the role of polar, GxxxG-like and proline motifs. *Current Opinion in Structural Biology* 14(4): 465-479.

Shedlock, D. J., Whitmire, J. K., Tan, J., MacDonald, A. S., Ahmed, R. and Shen, H. (2003). Role of CD4 T cell help and costimulation in CD8 T cell responses during listeria monocytogenes infection. *Journal of Immunology* 170(4): 2053-2063.

Shi, Y. (2002). Mechanisms of Caspase Activation and Inhibition during Apoptosis. *Molecular Cell* 9(3): 459-470.

Siegel, R. M., Frederiksen, J. K., Zacharias, D. A., Chan, F. K.-M., Johnson, M., Lynch, D., Tsien, R. Y. and Lenardo, M. J. (2000). Fas Preassociation Required for Apoptosis Signaling and Dominant Inhibition by Pathogenic Mutations. *Science* 288(5475): 2354-2357.

Siegel, R. M., Muppidi, J. R., Sarker, M., Lobito, A., Jen, M., Martin, D., Straus, S. E. and Lenardo, M. J. (2004). SPOTS: Signaling Protein Oligomeric Transduction Structures Are Early Mediators of Death Receptor-Induced Apoptosis at the Plasma Membrane. *Journal of Cell Biology* 167(4): 735-744.

Smulski, C. R., Beyrath, J., Decossas, M., Chekkat, N., Wolff, P., Gionnet, K., Guichard, G., Speiser, D., Schneider, P. and Fournel, S. (2013). Cysteine-rich domain one of CD40 mediates receptor self-assembly. *Journal of Biological Chemistry* in press.

Smyth, M. J., Cretney, E., Takeda, K., Wiltrout, R. H., Sedger, L. M., Kayagaki, N., Yagita, H. and Okumura, K. (2001). Tumor Necrosis Factor–Related Apoptosis-Inducing Ligand (Trail) Contributes to Interferon γ–Dependent Natural Killer Cell Protection from Tumor Metastasis. *Journal of Experimental Medicine* 193(6): 661-670.

Song, J. H., Tse, M. C. L., Bellail, A., Phuphanich, S., Khuri, F., Kneteman, N. M. and Hao, C. (2007). Lipid rafts and nonrafts mediate tumor necrosis factor-related apoptosis-inducing ligand-induced apoptotic and nonapoptotic signals in non-small cell lung carcinoma cells. *Cancer Research* 67(14): 6946-6955.

Springer, J. E., Azbill, R. D., Nottingham, S. A. and Kennedy, S. E. (2000). Calcineurin-Mediated BAD Dephosphorylation Activates the Caspase-3 Apoptotic Cascade in Traumatic Spinal Cord Injury. *The Journal of Neuroscience* 20(19): 7246-7251.

Stepensky, D. (2007). FRETcalc plugin for calculation of FRET in non-continuous intracellular compartments. *Biochemical and Biophysical Research Communications* 359(3): 752-758.

Takahashi, R., Deveraux, Q., Tamm, I., Welsh, K., Assa-Munt, N., Salvesen, G. S. and Reed, J. C. (1998). A Single BIR Domain of XIAP Sufficient for Inhibiting Caspases. *Journal of Biological Chemistry* 273(14): 7787-7790.

Takeda, K., Hayakawa, Y., Smyth, M. J., Kayagaki, N., Yamaguchi, N., Kakuta, S., Iwakura, Y., Yagita, H. and Okumura, K. (2001). Involvement of tumor necrosis factor-related apoptosis-inducing ligand in surveillance of tumor metastasis by liver natural killer cells. *Nature Medicine* 7(1): 94-100.

Tan, Y., Ruan, H., Demeter, M. R. and Comb, M. J. (1999). p90RSK Blocks Bad-mediated Cell Death via a Protein Kinase C-dependent Pathway. *Journal of Biological Chemistry* 274(49): 34859-34867.

Thedieck, K., Polak, P., Kim, M. L., Molle, K. D., Cohen, A., Jeno, P., Arrieumerlou, C. and Hall, M. N. (2007). PRAS40 and PRR5-Like Protein Are New mTOR Interactors that Regulate Apoptosis. *PLoS One* 2(11): e1217.

Truneh, A., Sharma, S., Silverman, C., Khandekar, S., Reddy, M. P., Deen, K. C., McLaughlin, M. M., Srinivasula, S. M., Livi, G. P., Marshall, L. A., Alnemri, E. S., Williams, W. V. and Doyle, M. L. (2000). Temperature-sensitive Differential Affinity of TRAIL for Its Receptors. DR5 is the highest affinity receptor. *Journal of Biological Chemistry* 275(30): 23319-23325.

Valley, C. C., Lewis, A. K., Mudaliar, D. J., Perlmutter, J. D., Braun, A. R., Karim, C. B., Thomas, D. D., Brody, J. R. and Sachs, J. N. (2012). Tumor necrosis factor-related apoptosis-inducing ligand (TRAIL) induces Death Receptor 5 networks that are highly organized. *Journal of Biological Chemistry* 287(25): 21265-21278.

van Geelen, C. M. M., Pennarun, B., Le, P. T. K., de Vries, E. G. E. and de Jong, S. (2011). Modulation of TRAIL resistance in colon carcinoma cells: Different contributions of DR4 and DR5. *BMC Cancer* 11: 39.

Vandenabeele, P., Galluzzi, L., Vanden Berghe, T. and Kroemer, G. (2010). Molecular mechanisms of necroptosis: an ordered cellular explosion. *Nature Reviews Molecular Cell Biology* 11(10): 700-714.

Varfolomeev, E., Maecker, H., Sharp, D., Lawrence, D., Renz, M., Vucic, D. and Ashkenazi, A. (2005). Molecular determinants of kinase pathway activation by Apo2 ligand/tumor necrosis factor-related apoptosis-inducing ligand. *Journal of Biological Chemistry* 280(49): 40599-40608.

Vercammen, D., Beyaert, R., Denecker, G., Goossens, V., Van Loo, G., Declercq, W., Grooten, J., Fiers, W. and Vandenabeele, P. (1998). Inhibition of caspases increases the sensitivity of L929 cells to necrosis mediated by tumor necrosis factor. *Journal of Experimental Medicine* 187(9): 1477-1485.

Verhagen, A. M., Ekert, P. G., Pakusch, M., Silke, J., Connolly, L. M., Reid, G. E., Moritz, R. L., Simpson, R. J. and Vaux, D. L. (2000). Identification of DIABLO, a mammalian protein that promotes apoptosis by binding to and antagonizing IAP proteins. *Cell* 102(1): 43-53.

Verhagen, A. M., Silke, J., Ekert, P. G., Pakusch, M., Kaufmann, H., Connolly, L. M., Day, C. L., Tikoo, A., Burke, R., Wrobel, C., Moritz, R. L., Simpson, R. J. and Vaux, D. L. (2002). HtrA2 Promotes Cell Death through Its Serine Protease Activity and Its Ability to Antagonize Inhibitor of Apoptosis Proteins. *Journal of Biological Chemistry* 277(1): 445-454.

Vucic, D., Dixit, V. M. and Wertz, I. E. (2011). Ubiquitylation in apoptosis: a post-translational modification at the edge of life and death. *Nature Reviews Molecular Cell Biology* 12(7): 439-452.

Wagner, K. W., Punnoose, E. A., Januario, T., Lawrence, D. A., Pitti, R. M., Lancaster, K., Lee, D., von Goetz, M., Yee, S. F., Totpal, K., Huw, L., Katta, V., Cavet, G., Hymowitz, S. G., Amler, L. and Ashkenazi, A. (2007). Death-receptor O-glycosylation controls tumor-cell sensitivity to the proapoptotic ligand Apo2L/TRAIL. *Nature Medicine* 13(9): 1070-1077.

Wajant, H., Haas, E., Schwenzer, R., Muhlenbeck, F., Kreuz, S., Schubert, G., Grell, M., Smith, C. and Scheurich, P. (2000). Inhibition of death receptor-mediated gene induction by a cycloheximide-sensitive factor occurs at the level of or upstream of Fas-associated death domain protein (FADD). *Journal of Biological Chemistry* 275(32): 24357-24366.

Wajant, H., Moosmayer, D., Wüest, T., Bartke, T., Gerlach, E., Schönherr, U., Peters, N., Scheurich, P. and Pfizenmaier, K. (2001). Differential activation of TRAIL-R1 and -2 by soluble and membrane TRAIL allows selective surface antigen-directed activation of TRAIL-R2 by a soluble TRAIL derivative. *Oncogene* 20(30): 4101-4106.

Wajant, H. and Scheurich, P. (2011). TNFR1-induced activation of the classical NF-κB pathway. *FEBS Journal* 278(6): 862-876.

Walczak, H., Degli-Esposti, M., Johnson, R., Smolak, P., Waugh, J., Boiani, N., Timour, M., Gerhart, M., Schooley, K., Smith, C., Goodwin, R. and Rauch, C. (1997). TRAIL-R2: a novel apoptosis-mediating receptor for TRAIL. *The EMBO Journal* 16(17): 5386-5397.

Walczak, H., Miller, R. E., Ariail, K., Gliniak, B., Griffith, T. S., Kubin, M., Chin, W., Jones, J., Woodward, A., Le, T., Smith, C., Smolak, P., Goodwin, R. G., Rauch, C. T., Schuh, J. C. L. and Lynch, D. H. (1999). Tumoricidal activity of tumor necrosis factor-related apoptosis-inducing ligand in vivo. *Nature Medicine* 5(2): 157-163.

Wang, L., Yang, J. K., Kabaleeswaran, V., Rice, A. J., Cruz, A. C., Park, A. Y., Yin, Q., Damko, E., Jang, S. B., Raunser, S., Robinson, C. V., Siegel, R. M., Walz, T. and Wu, H. (2010). The Fas-FADD death domain complex structure reveals the basis of DISC assembly and disease mutations. *Nature Structural & Molecular Biology* 17(11): 1324-1329.

Wassenaar, T. A., Quax, W. J. and Mark, A. E. (2008). The conformation of the extracellular binding domain of Death Receptor 5 in the presence and absence of the activating ligand TRAIL: A molecular dynamics study. *Proteins: Structure, Function, and Bioinformatics* 70(2): 333-343.

Wiley, S. R., Schooley, K., Smolak, P. J., Din, W. S., Huang, C.-P., Nicholl, J. K., Sutherland, G. R., Smith, T. D., Rauch, C., Smith, C. A. and Goodwin, R. G. (1995). Identification and characterization of a new member of the TNF family that induces apoptosis. *Immunity* 3(6): 673-682.

Wilkinson, J. C., Wilkinson, A. S., Galban, S., Csomos, R. A. and Duckett, C. S. (2008). Apoptosis-inducing factor is a target for ubiquitination through interaction with XIAP. *Molecular and Cellular Biology* 28(1): 237-247.

Winkel, C., Neumann, S., Surulescu, C. and Scheurich, P. (2012). A minimal mathematical model for the initial molecular interactions of death receptor signaling. *Mathematical Biosciences and Engineering* 9(3): 663-683.

Würstle, M. L., Laussmann, M. A. and Rehm, M. (2012). The central role of initiator caspase-9 in apoptosis signal transduction and the regulation of its activation and activity on the apoptosome. *Experimental Cell Research* 318(11): 1213-1220.

Yang, E., Zha, J., Jockel, J., Boise, L. H., Thompson, C. B. and Korsmeyer, S. J. (1995). Bad, a heterodimeric partner for Bcl-xL and Bcl-2, displaces bax and promotes cell death. *Cell* 80(2): 285-291.

Youle, R. J. and Strasser, A. (2008). The BCL-2 protein family: opposing activities that mediate cell death. *Nature Reviews Molecular Cell Biology* 9(1): 47-59.

Yuan, J. Y. and Kroemer, G. (2010). Alternative cell death mechanisms in development and beyond. *Genes & Development* 24(23): 2592-2602.

Zauli, G., Sancilio, S., Cataldi, A., Sabatini, N., Bosco, D. and Di Pietro, R. (2005). PI-3K/Akt and NF-kappa B/I kappa B alpha pathways are activated in Jurkat T cells in response to TRAIL treatment. *Journal of Cellular Physiology* 202(3): 900-911.

Zha, J., Harada, H., Yang, E., Jockel, J. and Korsmeyer, S. J. (1996). Serine Phosphorylation of Death Agonist BAD in Response to Survival Factor Results in Binding to 14-3-3 Not BCL-XL. *Cell* 87(4): 619-628.

Zhan, C., Patskovsky, Y., Yan, Q., Li, Z., Ramagopal, U., Cheng, H., Brenowitz, M., Hui, X., Nathenson, S. G. and Almo, S. C. (2011). Decoy Strategies: The Structure of TL1A:DcR3 Complex. *Structure* 19(2): 162-171.

Zhang, S. J., Li, G. Q., Zhao, Y. F., Liu, G. Z., Wang, Y., Ma, X. X., Li, D. X., Wu, Y. and Lu, J. F. (2012). Smac Mimetic SM-164 Potentiates APO2L/TRAIL- and Doxorubicin-Mediated Anticancer Activity in Human Hepatocellular Carcinoma Cells. *PLoS One* 7(12): : e51461.

Zhang, X. R., Zhang, L. Y., Devadas, S., Li, L., Keegan, A. D. and Shi, Y. F. (2003). Reciprocal expression of TRAIL and CD95L in Th1 and Th2 cells: role of apoptosis in T helper subset differentiation. *Cell Death and Differentiation* 10(2): 203-210.

6. Appendix

6.1. Plasmid maps and sequences

<u>pEF PGKpuropA (v18) R1ΔC-3FLAG</u>
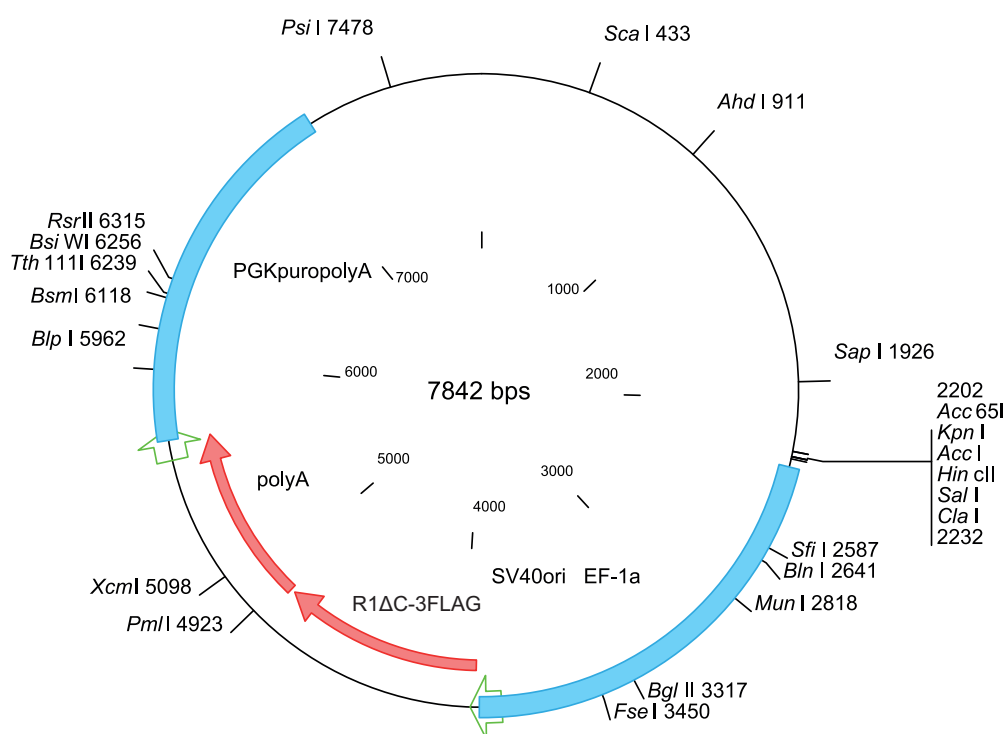
Figure 27: Plasmid map of pEF PGKpuropA (v18) R1ΔC-3FLAG

<u>Amino acid sequence of R1ΔC-3FLAG</u>

```
        10         20         30         40         50         60
MAPPPARVHL GAFLAVTPNP GSAASGTEAA AATPSKVWGS SAGRIEPRGG GRGALPTSMG
        70         80         90        100        110        120
QHGPSARARA GRAPGPRPAR EASPRLRVHK TFKFVVVGVL LQVVPSSAAT IKLHDQSIGT
       130        140        150        160        170        180
QQWEHSPLGE LCPPGSHRSE RPGACNRCTE GVGYTNASNN LFACLPCTAC KSDEEERSPC
       190        200        210        220        230        240
TTTRNTACQC KPGTFRNDNS AEMCRKCSTG CPRGMVKVKD CTPWSDIECV HKESGNGHNI
       250        260        270        280        290        300
WVILVVTLVV PLLLVAVLIV CCCIGSGCGG DPKCMDEFDY KDDDDKDYKD DDDKDYKDDD
```

DK

pEF PGKpuropA (v18) R2ΔC-FLAG
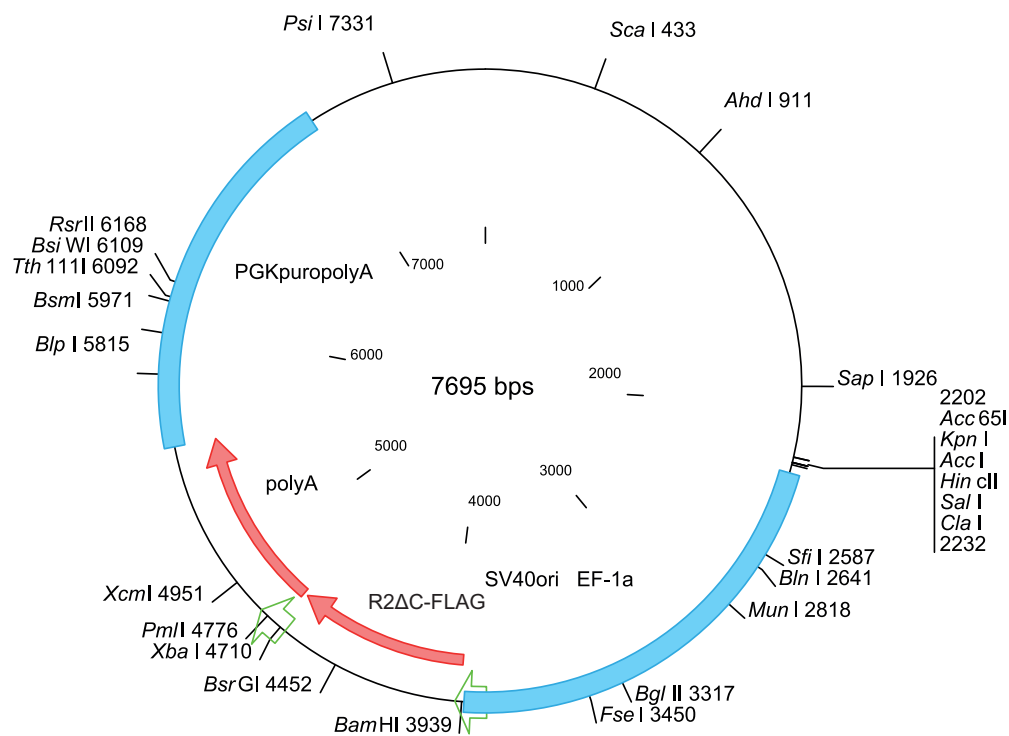
Figure 28: Plasmid map of pEF PGKpuropA (v18) R2ΔC-FLAG

Amino acid sequence of R2ΔC-FLAG

```
          10         20         30         40         50         60
MEQRGQNAPA ASGARKRHGP GPREARGARP GLRVPKTLVL VVAAVLLLVS AESALITQQD
          70         80         90        100        110        120
LAPQQRVAPQ QKRSSPSEGL CPPGHHISED GRDCISCKYG QDYSTHWNDL LFCLRCTRCD
         130        140        150        160        170        180
SGEVELSPCT TTRNTVCQCE EGTFREEDSP EMCRKCRTGC PRGMVKVGDC TPWSDIECVH
         190        200        210        220        230        240
KESGTKHSGE APAVEETVTS SPGTPASPCS LSGIIIGVTV AAVVLIVAVF VCKSLLWKKV
         250
LPYLKGDYKD DDDK
```

pCDNA3.1+ R2ΔC-GFP
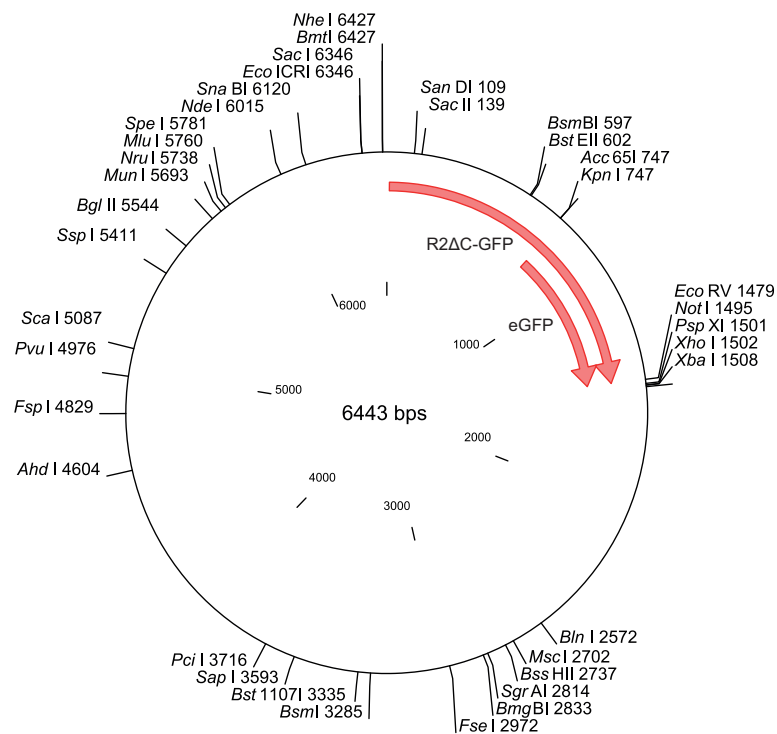
Figure 29: Plasmid map of pCDNA3.1+ R2ΔC-GFP

Amino acid sequence of R2ΔC-GFP

```
        10         20         30         40         50         60
MEQRGQNAPA ASGARKRHGP GPREARGARP GLRVPKTLVL VVAAVLLLVS AESALITQQD

        70         80         90        100        110        120
LAPQQRVAPQ QKRSSPSEGL CPPGHHISED GRDCISCKYG QDYSTHWNDL LFCLRCTRCD

       130        140        150        160        170        180
SGEVELSPCT TTRNTVCQCE EGTFREEDSP EMCRKCRTGC PRGMVKVGDC TPWSDIECVH

       190        200        210        220        230        240
KESGTKHSGE APAVEETVTS SPGTPASPCS LSGIIIGVTV AAVVLIVAVF VCKSLLWKKV

       250        260        270        280        290        300
LPYLKGTKGG VSKGEELFTG VVPILVELDG DVNGHKFSVS GEGEGDATYG KLTLKFICTT

       310        320        330        340        350        360
GKLPVPWPTL VTTLTYGVQC FSRYPDHMKQ HDFFKSAMPE GYVQERTIFF KDDGNYKTRA

       370        380        390        400        410        420
EVKFEGDTLV NRIELKGIDF KEDGNILGHK LEYNYNSHNV YIMADKQKNG IKVNFKIRHN

       430        440        450        460        470        480
IEDGSVQLAD HYQQNTPIGD GPVLLPDNHY LSTQSALSKD PNEKRDHMVL LEFVTAAGIT


LGMDELYK
```

pCDNA3.1+ R4ΔC-GFP
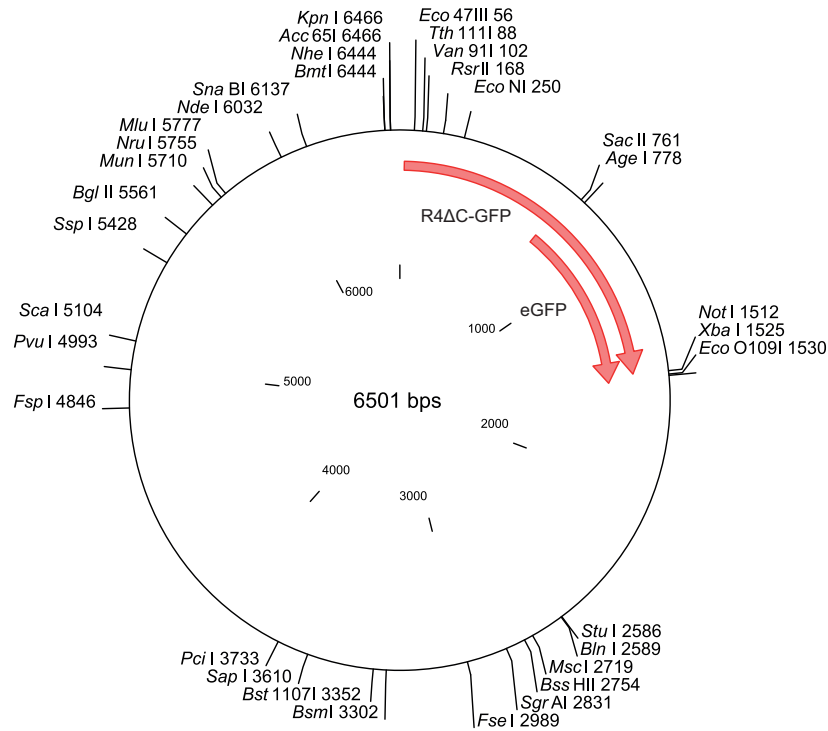
Figure 30: Plasmid map of pCDNA3.1+ R4ΔC-GFP

Amino acid sequence of R4ΔC-GFP

```
           10         20         30         40         50         60
MGLWGQSVPT ASSARAGRYP GARTASGTRP WLLDPKILKF VVFIVAVLLP VRVDSATIPR
           70         80         90        100        110        120
QDEVPQQTVA PQQQRRSLKE EECPAGSHRS EYTGACNPCT EGVDYTIASN NLPSCLLCTV
          130        140        150        160        170        180
CKSGQTNKSS CTTTRDTVCQ CEKGSFQDKN SPEMCRTCRT GCPRGMVKVS NCTPRSDIKC
          190        200        210        220        230        240
KNESAASSTG KTPAAEETVT TILGMLASPY HYLIIIVVLV IILAVVVVGF SCRKKFISYL
          250        260        270        280        290        300
KGICSGGPRA RDPPVATMVS KGEELFTGVV PILVELDGDV NGHKFSVSGE GEGDATYGKL
          310        320        330        340        350        360
TLKFICTTGK LPVPWPTLVT TLTYGVQCFS RYPDHMKQHD FFKSAMPEGY VQERTIFFKD
          370        380        390        400        410        420
DGNYKTRAEV KFEGDTLVNR IELKGIDFKE DGNILGHKLE YNYNSHNVYI MADKQKNGIK
          430        440        450        460        470        480
VNFKIRHNIE DGSVQLADHY QQNTPIGDGP VLLPDNHYLS TQSALSKDPN EKRDHMVLLE
          490
FVTAAGITLG MDELYK
```

pEGFP-N1 R1ΔC

Figure 31: Plasmid map of pEGFP-N1 R1ΔC

Amino acid sequence of R1ΔC-GFP

```
            10          20          30          40          50          60
MAPPPARVHL  GAFLAVTPNP  GSAASGTEAA  AATPSKVWGS  SAGRIEPRGG  GRGALPTSMG

            70          80          90         100         110         120
QHGPSARARA  GRAPGPRPAR  EASPRLRVHK  TFKFVVVGVL  LQVVPSSAAT  IKLHDQSIGT

           130         140         150         160         170         180
QQWEHSPLGE  LCPPGSHRSE  RPGACNRCTE  GVGYTNASNN  LFACLPCTAC  KSDEEERSPC

           190         200         210         220         230         240
TTTRNTACQC  KPGTFRNDNS  AEMCRKCSTG  CPRGMVKVKD  CTPWSDIECV  HKESGNGHNI

           250         260         270         280         290         300
WVILVVTLVV  PLLLVAVLIV  CCCIGSGCGG  DPKCMDRDPP  VATMVSKGEE  LFTGVVPILV

           310         320         330         340         350         360
ELDGDVNGHK  FSVSGEGEGD  ATYGKLTLKF  ICTTGKLPVP  WPTLVTTLTY  GVQCFSRYPD

           370         380         390         400         410         420
HMKQHDFFKS  AMPEGYVQER  TIFFKDDGNY  KTRAEVKFEG  DTLVNRIELK  GIDFKEDGNI

           430         440         450         460         470         480
LGHKLEYNYN  SHNVYIMADK  QKNGIKVNFK  IRHNIEDGSV  QLADHYQQNT  PIGDGPVLLP

           490         500         510         520
DNHYLSTQSA  LSKDPNEKRD  HMVLLEFVTA  AGITLGMDEL  YK
```
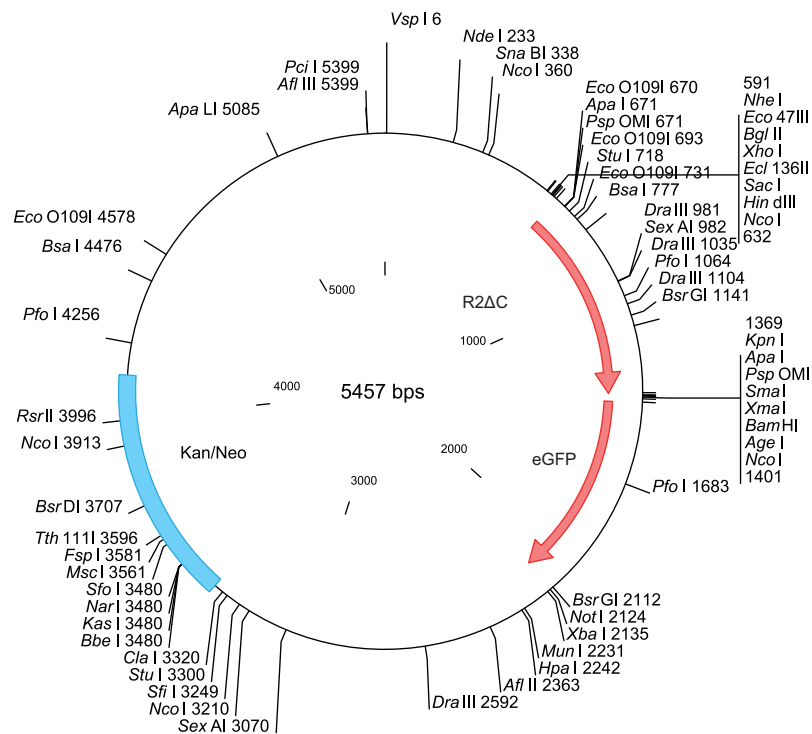
pEGFP-N1 R2ΔC

Figure 32: Plasmid map of pEGFP-N1 R2ΔC

Amino acid sequence of R2ΔC-GFP

```
          10         20         30         40         50         60
MEQRGQNAPA ASGARKRHGP GPREARGARP GLRVPKTLVL VVAAVLLLVS AESALITQQD

          70         80         90        100        110        120
LAPQQRVAPQ QKRSSPSEGL CPPGHHISED GRDCISCKYG QDYSTHWNDL LFCLRCTRCD

         130        140        150        160        170        180
SGEVELSPCT TTRNTVCQCE EGTFREEDSP EMCRKCRTGC PRGMVKVGDC TPWSDIECVH

         190        200        210        220        230        240
KESGTKHSGE APAVEETVTS SPGTPASPCS LSGIIIGVTV AAVVLIVAVF VCKSLLWKKV

         250        260        270        280        290        300
LPYLKGTKGG VSKGEELFTG VVPILVELDG DVNGHKFSVS GEGEGDATYG KLTLKFICTT

         310        320        330        340        350        360
GKLPVPWPTL VTTLTYGVQC FSRYPDHMKQ HDFFKSAMPE GYVQERTIFF KDDGNYKTRA

         370        380        390        400        410        420
EVKFEGDTLV NRIELKGIDF KEDGNILGHK LEYNYNSHNV YIMADKQKNG IKVNFKIRHN

         430        440        450        460        470        480
IEDGSVQLAD HYQQNTPIGD GPVLLPDNHY LSTQSALSKD PNEKRDHMVL LEFVTAAGIT


LGMDELYK
```

pEGFP-N1 R4ΔC

Figure 33: Plasmid map of pEGFP-N1 R4ΔC

Amino acid sequence of R4ΔC-GFP

```
         10         20         30         40         50         60
MGLWGQSVPT ASSARAGRYP GARTASGTRP WLLDPKILKF VVFIVAVLLP VRVDSATIPR

         70         80         90        100        110        120
QDEVPQQTVA PQQQRRSLKE EECPAGSHRS EYTGACNPCT EGVDYTIASN NLPSCLLCTV

        130        140        150        160        170        180
CKSGQTNKSS CTTTRDTVCQ CEKGSFQDKN SPEMCRTCRT GCPRGMVKVS NCTPRSDIKC

        190        200        210        220        230        240
KNESAASSTG KTPAAEETVT TILGMLASPY HYLIIIVVLV IILAVVVVGF SCRKKFISYL

        250        260        270        280        290        300
KGICSGGPRA RDPPVATMVS KGEELFTGVV PILVELDGDV NGHKFSVSGE GEGDATYGKL

        310        320        330        340        350        360
TLKFICTTGK LPVPWPTLVT TLTYGVQCFS RYPDHMKQHD FFKSAMPEGY VQERTIFFKD

        370        380        390        400        410        420
DGNYKTRAEV KFEGDTLVNR IELKGIDFKE DGNILGHKLE YNYNSHNVYI MADKQKNGIK

        430        440        450        460        470        480
VNFKIRHNIE DGSVQLADHY QQNTPIGDGP VLLPDNHYLS TQSALSKDPN EKRDHMVLLE

        490
FVTAAGITLG MDELYK
```

pmCherry-N1 R1ΔC
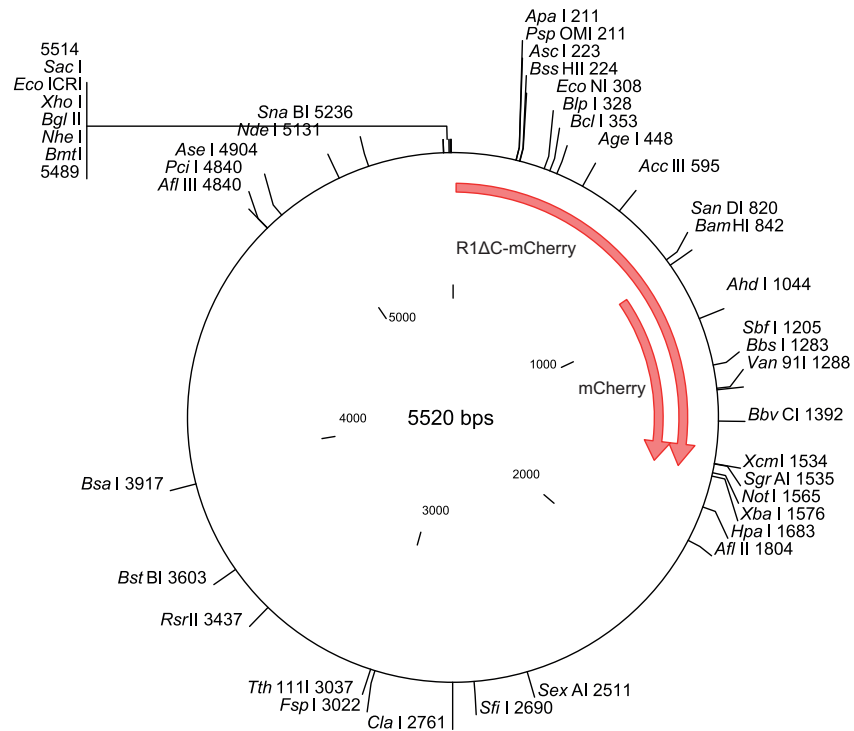
Figure 34: Plasmid map of pmCherry-N1 R1ΔC

Amino acid sequence of R1ΔC-mCherry

```
            10          20          30          40          50          60
MAPPPARVHL  GAFLAVTPNP  GSAASGTEAA  AATPSKVWGS  SAGRIEPRGG  GRGALPTSMG
            70          80          90         100         110         120
QHGPSARARA  GRAPGPRPAR  EASPRLRVHK  TFKFVVVGVL  LQVVPSSAAT  IKLHDQSIGT
           130         140         150         160         170         180
QQWEHSPLGE  LCPPGSHRSE  RPGACNRCTE  GVGYTNASNN  LFACLPCTAC  KSDEEERSPC
           190         200         210         220         230         240
TTTRNTACQC  KPGTFRNDNS  AEMCRKCSTG  CPRGMVKVKD  CTPWSDIECV  HKESGNGHNI
           250         260         270         280         290         300
WVILVVTLVV  PLLLVAVLIV  CCCIGSGCGG  DPKCMDRDPP  VATMVSKGEE  DNMAIIKEFM
           310         320         330         340         350         360
RFKVHMEGSV  NGHEFEIEGE  GEGRPYEGTQ  TAKLKVTKGG  PLPFAWDILS  PQFMYGSKAY
           370         380         390         400         410         420
VKHPADIPDY  LKLSFPEGFK  WERVMNFEDG  GVVTVTQDSS  LQDGEFIYKV  KLRGTNFPSD
           430         440         450         460         470         480
GPVMQKKTMG  WEASSERMYP  EDGALKGEIK  QRLKLKDGGH  YDAEVKTTYK  AKKPVQLPGA
           490         500         510
YNVNIKLDIT  SHNEDYTIVE  QYERAEGRHS  TGGMDELYK
```

pmCherry-N1 R2ΔC
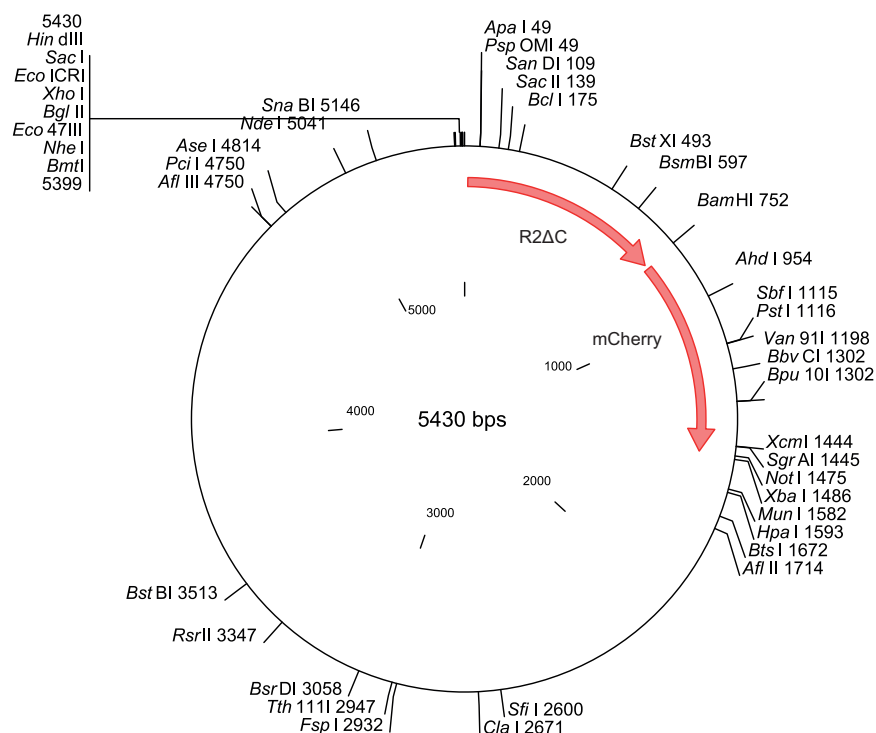
Figure 35: Plasmid map of pmCherry-N1 R2ΔC

Amino acid sequence of R2ΔC-mCherry

```
         10         20         30         40         50         60
MEQRGQNAPA ASGARKRHGP GPREARGARP GLRVPKTLVL VVAAVLLLVS AESALITQQD

         70         80         90        100        110        120
LAPQQRVAPQ QKRSSPSEGL CPPGHHISED GRDCISCKYG QDYSTHWNDL LFCLRCTRCD

        130        140        150        160        170        180
SGEVELSPCT TTRNTVCQCE EGTFREEDSP EMCRKCRTGC PRGMVKVGDC TPWSDIECVH

        190        200        210        220        230        240
KESGTKHSGE APAVEETVTS SPGTPASPCS LSGIIIGVTV AAVVLIVAVF VCKSLLWKKV

        250        260        270        280        290        300
LPYLKGRDPA TMVSKGEEDN MAIIKEFMRF KVHMEGSVNG HEFEIEGEGE GRPYEGTQTA

        310        320        330        340        350        360
KLKVTKGGPL PFAWDILSPQ FMYGSKAYVK HPADIPDYLK LSFPEGFKWE RVMNFEDGGV

        370        380        390        400        410        420
VTVTQDSSLQ DGEFIYKVKL RGTNFPSDGP VMQKKTMGWE ASSERMYPED GALKGEIKQR

        430        440        450        460        470        480
LKLKDGGHYD AEVKTTYKAK KPVQLPGAYN VNIKLDITSH NEDYTIVEQY ERAEGRHSTG


GMDELYK
```

pmCherry-N1 R4ΔC
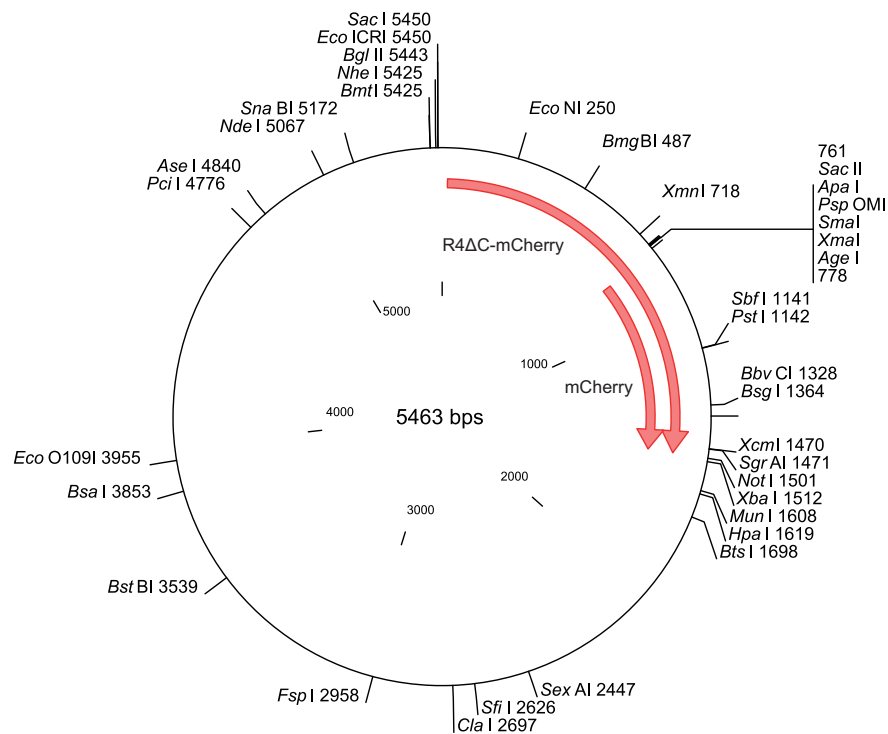
Figure 36: Plasmid map of pmCherry-N1 R4ΔC

Amino acid sequence of R4ΔC-mCherry

```
            10          20          30          40          50          60
MGLWGQSVPT  ASSARAGRYP  GARTASGTRP  WLLDPKILKF  VVFIVAVLLP  VRVDSATIPR
            70          80          90         100         110         120
QDEVPQQTVA  PQQQRRSLKE  EECPAGSHRS  EYTGACNPCT  EGVDYTIASN  NLPSCLLCTV
           130         140         150         160         170         180
CKSGQTNKSS  CTTTRDTVCQ  CEKGSFQDKN  SPEMCRTCRT  GCPRGMVKVS  NCTPRSDIKC
           190         200         210         220         230         240
KNESAASSTG  KTPAAEETVT  TILGMLASPY  HYLIIIVVLV  IILAVVVVGF  SCRKKFISYL
           250         260         270         280         290         300
KGICSGGPRA  RDPPVATMVS  KGEEDNMAII  KEFMRFKVHM  EGSVNGHEFE  IEGEGEGRPY
           310         320         330         340         350         360
EGTQTAKLKV  TKGGPLPFAW  DILSPQFMYG  SKAYVKHPAD  IPDYLKLSFP  EGFKWERVMN
           370         380         390         400         410         420
FEDGGVVTVT  QDSSLQDGEF  IYKVKLRGTN  FPSDGPVMQK  KTMGWEASSE  RMYPEDGALK
           430         440         450         460         470         480
GEIKQRLKLK  DGGHYDAEVK  TTYKAKKPVQ  LPGAYNVNIK  LDITSHNEDY  TIVEQYERAE
           490
GRHSTGGMDE  LYK
```

pIRESpuro3 sTRAILR1
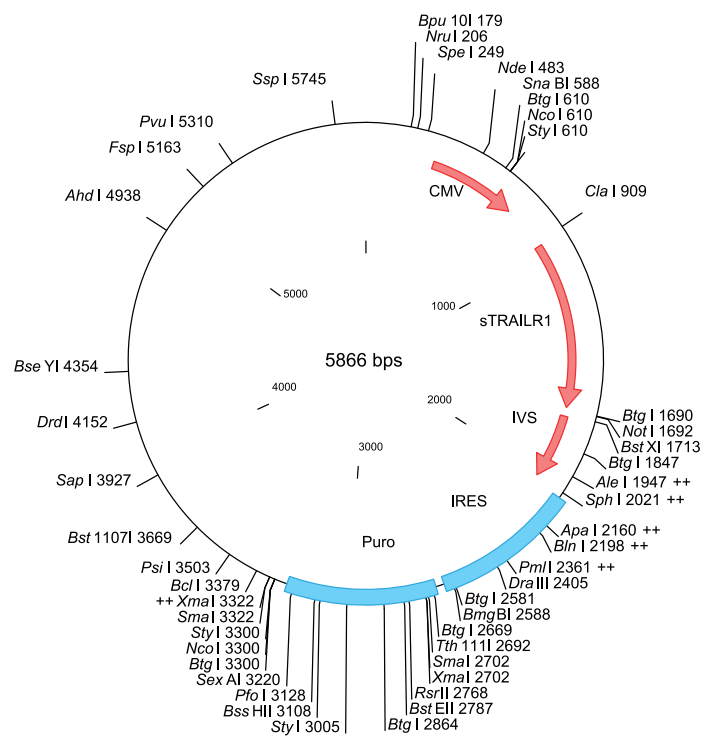
Figure 37: Plasmid map of pIRESpuro3 sTRAILR1

Amino acid sequence of sTRAILR1

```
         10          20          30          40          50          60
MDWTWRVFCL LAVAPGAHSL EASGTEAAAA TPSKVWGSSA GRIEPRGGGR GALPTSMGQH
         70          80          90         100         110         120
GPSARARAGR APGPRPAREA SPRLRVHKTF KFVVVGVLLQ VVPSSAATIK LHDQSIGTQQ
        130         140         150         160         170         180
WEHSPLGELC PPGSHRSERP GACNRCTEGV GYTNASNNLF ACLPCTACKS DEEERSPCTT
        190         200         210         220         230         240
TRNTACQCKP GTFRNDNSAE MCRKCSTGCP RGMVKVKDCT PWSDIECVHK ESGNGDYKDD
        250
DDKIEGRHHH HHH
```

pIRESpuro3 sTRAILR4
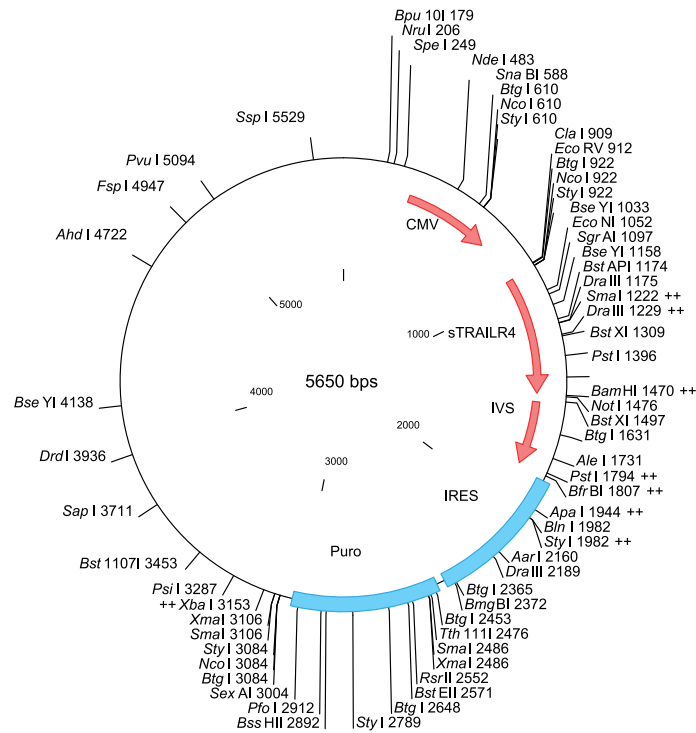
Figure 38: Plasmid map of pIRESpuro3 sTRAILR4

Amino acid sequence of sTRAILR4

```
         10          20          30          40          50          60
MDWTWRVFCL  LAVAPGAHSL  EATIPRQDEV  PQQTVAPQQQ  RRSLKEEECP  AGSHRSEYTG

         70          80          90         100         110         120
ACNPCTEGVD  YTIASNNLPS  CLLCTVCKSG  QTNKSSCTTT  RDTVCQCEKG  SFQDKNSPEM

        130         140         150         160         170         180
CRTCRTGCPR  GMVKVSNCTP  RSDIKCKNES  AASSTGAAAV  DDYKDDDDKE  FIEGRHHHHH

H
```

Danksagung

Zuallererst möchte ich mich bei Peter Scheurich bedanken, für die Bereitstellung des Themas, für die tolle Betreuung und Unterstützung während meiner Promotion. Dafür dass seine Tür immer offen stand und er immer ein offenes Ohr für alle möglichen Probleme und Angelegenheiten hatte. Die interessanten und fruchtbaren Diskussionen haben mir immer geholfen die richtige Sichtweise zu behalten und neue Ideen zu entwickeln.

Bei Malgorzata Doszczak möchte ich mich für ihre Unterstützung und die vielen guten Ideen bedanken.

Mein besonderer Dank gilt Jessica Tepperink für die hervorragende Labororganisation, die Hilfsbereitschaft und für die vielen Tipps und Tricks die mir den Laboralltag oft erleichtert haben.

Vielen Dank an Nadine Pollak für ihre Unterstützung, die vielen guten Ratschläge und die angenehme Zusammenarbeit.

Den vielen Diplom-, Studien-, und Bachelorarbeitern und allen weiteren aktuellen und ehemaligen Laborkollegen möchte ich für die gute Arbeitsatmosphäre im Labor danken. Insbesondere die aktuelle Stammbesatzung, Bea Schmieder, Lubna Siddiq und Andrea Zappe, hat viel zur guten Atmosphäre beigetragen. Bei Bea Schmieder möchte ich mich außerdem für die Organisation des Laborumzuges und die Unterstützung bei der Laborarbeit bedanken.

Besonderer Dank geht an Felix Neugart für die technische und theoretische Unterstützung bei meinen Mikroskopie Experimenten, sowie für die Programmierung des FRET_Plotters. Auch Margarete Witkowski möchte ich für ihre Hilfe an den Mikroskopen danken.

Bei Fabian Richter möchte ich mich für die Einarbeitung am Attana Biosensor bedanken.

Anja Krippner-Heidenreich danke ich dafür dass sie meinen Auslandsaufenthalt möglich gemacht hat und für die Unterstützung in Newcastle upon Tyne.

Meinen Bürokolleginnen und –kollegen (Kornelia Ellwanger, Nadine Pollak, Martin Siegemund und Nicole Weis) möchte ich für die freundliche Aufnahme und die angenehme, ruhige Arbeitsumgebung danken.

Vielen Dank an Gabi Sawall für die Erledigung aller verwaltungsrelevanten Aufgaben und die Unterstützung bei allen möglichen kleineren und größeren Angelegenheiten.

Meinen Eltern, Hiltrud und Hartmut, sowie meiner Schwester Katrin möchte ich für die stetige Unterstützung während meiner Promotion danken.

Ohne die großartige Unterstützung, Motivationsarbeit und manchmal auch gezielte Ablenkung von Martina wäre dies Alles nur schwer möglich gewesen. Vielen Dank!

Curriculum vitae

Persönliche Daten

Simon Paul Neumann, geboren am 23. Juli 1982 in Stuttgart

Schulische Ausbildung

09/1989 - 07/1993	Gustav-Sieber-Grundschule, Tamm
09/1993 - 07/1997	Friedrich-List-Gymnasium, Asperg
09/1997 - 06/2002	Friedrich-Schiller-Gymnasium, Ludwigsburg
	Abschluss: Allgemeine Hochschulreife

Akademische Ausbildung

10/2003 – 09/2009	Universität Stuttgart, Studium der Technischen Biologie, Schwerpunkte: Immunologie (Hauptfach), Bioverfahrenstechnik (Nebenfach), Meeresbiologie (Nebenfach), Biochemie (Wahlpflichtfach) Abschluss: Diplom-Biologe (technisch-orientiert), Dipl.-Biol. (t.o.)
11/2008 – 09/2009	Diplomarbeit am Institut für Zellbiologie und Immunologie, Titel: "Characterization of signaling competence of TRAIL receptors expressed in mouse fibroblasts"
Seit 10/2009	Promotion am Institut für Zellbiologie und Immunologie der Universität Stuttgart, Betreuer: Prof. Dr. rer. nat. Peter Scheurich, Titel der Dissertation: "Analysis of receptor-receptor interactions and their implications on the formation of signaling competent TRAIL receptor clusters"
04/2012 – 07/2012	Forschungsaufenthalt am Institute of Cellular Medicine, Newcastle University, Newcastle upon Tyne, England

Publikationen

Neumann, S., Scheurich, P. and Maier, O. (April 2013). Tumour Necrosis Factors. In: eLS. John Wiley & Sons, Ltd: Chichester., , http://www.els.net/
[DOI: 10.1002/9780470015902.a0000935.pub3]

Neumann, S., Bidon, T., Scheurich, P. and Doszczak, M. (2012) The Transmembrane Domains of TNF-Related Apoptosis-Inducing Ligand (TRAIL) Receptors 1 and 2 coregulate ligand responsiveness. *PLoS One* 7(8): e42526

Winkel, C., Neumann, S., Surulescu, C. and Scheurich P. (2012) A minimal mathematical model for the initial molecular interactions of death receptor signalling. *Mathematical Biosciences and Engineering* 9(3): 663-683

Neumann, S., Reuner, A., Schill, R. O. and Brümmer, F. (2009) DNA damage in storage cells of anhydrobiotic tardigrades. *Comparative Biochemistry and Physiology Part A: Molecular & Integrative Physiology* 153(4):425-429

Stuttgart, im März 2013